# Immersed Finite Elements for a Second Order Elliptic Operator and Their Applications

Qiao Zhuang

Dissertation submitted to the Faculty of the
Virginia Polytechnic Institute and State University
in partial fulfillment of the requirements for the degree of

Doctor of Philosophy
in
Mathematics

Tao Lin, Chair
Slimane Adjerid
Serkan Gugercin
Shu-Ming Sun

April 27, 2020
Blacksburg, Virginia

Keywords: Immersed Finite Element, Second Order Elliptic Operator, Interface Problems, Elliptic Equations, Wave Equations, Diffusion Equations, Error Analysis

# Immersed Finite Elements for a Second Order Elliptic Operator and Their Applications

Qiao Zhuang

(ABSTRACT)

This dissertation studies immersed finite elements (IFE) for a second order elliptic operator and their applications to interface problems of related partial differential equations.

We start with the immersed finite element methods for the second order elliptic operator with a discontinuous coefficient associated with the elliptic interface problems. We introduce an energy norm stronger than the one used in [111]. Then we derive an estimate for the IFE interpolation error with this energy norm using patches of interface elements. We prove both the continuity and coercivity of the bilinear form in a partially penalized IFE (PPIFE) method. These properties allow us to derive an error bound for the PPIFE solution in the energy norm under the standard piecewise $H^2$ regularity assumption instead of the more stringent $H^3$ regularity used in [111]. As an important consequence, this new estimation further enables us to show the optimal convergence in the $L^2$ norm which could not be done by the analysis presented in [111].

Then we consider applications of IFEs developed for the second order elliptic operator to wave propagation and diffusion interface problems. The first application is for the time-harmonic wave interface problem that involves the Helmholtz equation with a discontinuous coefficient. We design PPIFE and DGIFE schemes including the higher degree IFEs for Helmholtz interface problems. We present an error analysis for the symmetric linear/bilinear PPIFE methods. Under the standard piecewise $H^2$ regularity assumption for the exact solution, following Schatz's arguments, we derive optimal error bounds for the PPIFE solutions in both an energy norm and the usual $L^2$ norm provided that the mesh size is sufficiently small.

In the second group of applications, we focus on the error analysis for IFE methods developed for solving typical time-dependent interface problems associated with the second order elliptic operator with a discontinuous coefficient. For hyperbolic interface problems, which are typical wave propagation interface problems, we reanalyze the fully-discrete PPIFE method in [143]. We derive the optimal error bounds for this PPIFE method for both an energy norm and the $L^2$ norm under the standard piecewise $H^2$ regularity assumption in the space variable of the exact solution. Simulations for standing and travelling waves are presented to corroborate the results of the error analysis. For parabolic interface problems, which are typical diffusion interface problems, we reanalyze the PPIFE methods in [113]. We prove that these PPIFE methods have the optimal convergence not only in an energy norm but also in the usual $L^2$ norm under the standard piecewise $H^2$ regularity.

# Immersed Finite Elements for a Second Order Elliptic Operator and Their Applications

Qiao Zhuang

(GENERAL AUDIENCE ABSTRACT)

This dissertation studies immersed finite elements (IFE) for a second order elliptic operator and their applications to a few types of interface problems.

We start with the immersed finite element methods for the second order elliptic operator with a discontinuous coefficient associated with the elliptic interface problem. We can show that the IFE methods for the elliptic interface problems converge optimally when the exact solution has lower regularity than that in the previous publications.

Then we consider applications of IFEs developed for the second order elliptic operator to wave propagation and diffusion interface problems. For interface problems of the Helmholtz equation which models time-Harmonic wave propagations, we design IFE schemes, including higher degree schemes, and derive error estimates for a lower degree scheme. For interface problems of the second order hyperbolic equation which models time dependent wave propagations, we derive better error estimates for the IFE methods and provides numerical simulations for both the standing and traveling waves. For interface problems of the parabolic equation which models the time dependent diffusion, we also derive better error estimates for the IFE methods.

# Acknowledgments

I would like to hereby take this opportunity to sincerely thank people who helped and supported me during my five years' PhD. Study. First of all, I would like to express my heartfelt gratitude to my advisor, Dr. Tao Lin, who led me into the fantastic world of computational mathematics, especially finite element methods. Under his careful guidance and huge supports, I have developed scientific ways to consider and learned scientific approaches to investigate problems pertinent to computational mathematics. His integrity, enthusiasm, professionalism, erudition and patience inspire me to become better as a scholar, an educator, and a person.

I would also like to heartily thank the other members of my PhD. thesis committee Dr. Slimane Adjerid, Dr. Serkan Gugercin, and Dr. Shu-Ming Sun. I have learned a lot from each of them and I am grateful for their insightful comments and precious suggestions on my thesis and research. Special thanks to Dr. Adjerid for his guidance and advices in my study on IFE methods for hyperbolic interface problems.

I would also like to sincerely thank Dr. Yanping Lin and Dr. Ruchi Guo, for their collaboration and help in various research projects. And sincere thanks to Dr. Xiaoming He and Dr. Xu Zhang, for their valuable suggestions and help in my research and growth in the academic career.

I also wish to express my sincerest gratitude to my parents for their continuous love and supports in my path of academic pursuance and journey of this life.

At last, I would like to sincerely thank other people who have helped me during my PhD. study, including but not limited to other faculty members, staffs and fellow graduate students.

# Contents

# List of Figures

# List of Tables

# Chapter 1

# Introduction

Many simulations in science and engineering are carried out in domains consisting of different media separated by curves or surfaces, from which interface problems arise. We begin this introductory chapter with a description of typical second order elliptic interface problems and a brief survey about their applications. Then, we review some numerical methods for interface problems, including immersed finite element (IFE) methods. After that, we describe additional studies of IFEs for a second order elliptic operator and related applications carried out in this thesis. At last, we outline the layout of the thesis.

## 1.1 Second Order Elliptic Interface Problems and Some Applications

We consider a domain $\Omega \subseteq \mathbb{R}^d$ $(d = 1, 2, 3)$ that is divided by an interface $\Gamma$ into two subdomains: $\Omega^-$ and $\Omega^+$. We assume that each of the subdomains is formed by one material such that the diffusion coefficient $\beta$ of $\Omega$ is a piecewise positive constant function:

$$\beta(X) = \begin{cases} \beta^- & \text{for } X \in \Omega^-, \\ \beta^+ & \text{for } X \in \Omega^+. \end{cases} \tag{1.1}$$

In $\Omega$, we consider the following typical second order elliptic boundary value problem (BVP):

$$-\nabla \cdot (\beta \nabla u) = f, \quad \text{in } \Omega = \Omega^- \cup \Omega^+, \tag{1.2a}$$

$$u = g, \quad \text{on } \partial\Omega. \tag{1.2b}$$

Because of the discontinuity in the diffusion coefficient $\beta$, the exact solution $u$ to the boundary value problem is a piecewise function

$$u(X) = \begin{cases} u^- & \text{for } X \in \Omega^-, \\ u^+ & \text{for } X \in \Omega^+, \end{cases}$$

that is assumed to satisfy the following jump conditions across the interface $\Gamma$:

$$[u]_\Gamma \quad := \quad u^+|_\Gamma - u^-|_\Gamma = 0, \tag{1.2c}$$

$$\left[\beta \nabla u \cdot \mathbf{n}\right]_\Gamma \quad := \quad \beta^+ \nabla u^+ \cdot \mathbf{n}|_\Gamma - \beta^- \nabla u^- \cdot \mathbf{n}|_\Gamma = 0, \tag{1.2d}$$

where $\mathbf{n}$ is the unit normal vector to the interface $\Gamma$, and the restriction of a function onto $\Gamma$ is in the sense of its trace. From now on, we call the problem described by (1.2) the second order elliptic interface problem.

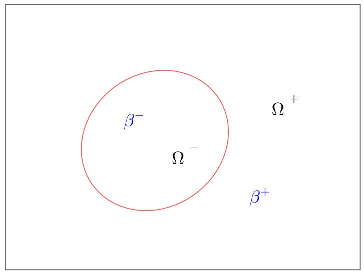


Figure 1.1: The domain of the interface problem

There are many applications that involve this model interface problem. One example is the particle-in-cell method for plasma particle simulation [40, 70, 87, 88, 151] where the electrostatic potential field $u$ is modeled by the interface problem described by (1.2). Another example is to solve some inverse problems associated with the interface problem (1.2) by shape optimization [61, 65, 125, 133, 146] where we need to minimize a cost functional $\mathcal{J}(\Gamma, u(\Gamma))$ subject to the model interface problem (1.2) whose solution yields a value of this cost functional for each interface $\Gamma$. We note that in a shape optimization, a chosen optimization algorithm repeatedly drives the interface from one configuration to another such that the associated interface problem (1.2) has to be solved at each iteration.

## 1.2 An Overview of IFE Methods

To solve the interface problems numerically with optimal convergence by traditional finite element methods, body-fitting meshes are usually employed for discretization [16, 23, 37, 142]. An important requirement of body-fitting mesh is that the mesh has to be tailored to fit the interface: each element is essentially located on one side of the interface. In other words, the mesh suitable for using a traditional finite element method to solve an interface problem is interface dependent. This requirement, however, impedes the efficiency of finite element methods, especially in applications where the interface varies because of physical laws [99, 137] or the set-up of specific algorithms (for instance, those for shape optimization [27, 130]). Under those circumstances, meshes have to be repeatedly regenerated, which can be very time consuming.

To remove the burden of remeshing, numerical methods based on interface independent meshes have been developed, such as immersed interface methods (IIM) [97, 101, 102] and matched interface and boundary method (MIB) [136, 153] in finite difference approach; and difference potentials methods (DPM) based on difference potentials approach [25, 129]. As for methods based on finite element approach, they can be classified into two categories. The methods in the first category modify the weak formulation near the interface, for instances, unfitted finite element methods [18, 66, 69] using Nitsche's penalty along the interface and cut finite element method (CutFEM) [29, 138] adding stabilization terms to control the jump of the finite element functions near the interface. The methods in the second category modify the local shape functions on the interface elements, such as the partition of unity method [15], extended finite element methods (XFEM) [18, 29, 117], and multi-scale finite element methods (MsFEMs) [39, 80]. Immersed finite element (IFE) methods discussed in this thesis also belong to the second category.

We now provide an overview about immersed finite element methods (IFE), which are nontraditional finite element methods developed recently for solving interface problems on meshes independent of the interfaces. The basic idea of IFE methods is, as it is illustrated in Figure 1.2, to use standard polynomials as local IFE shape functions on non-interface elements, but employ Hesie-Clogh-Tocher type macro polynomials [22, 41] as the local IFE shape functions on interface elements which satisfy the jump conditions in some weak sense.

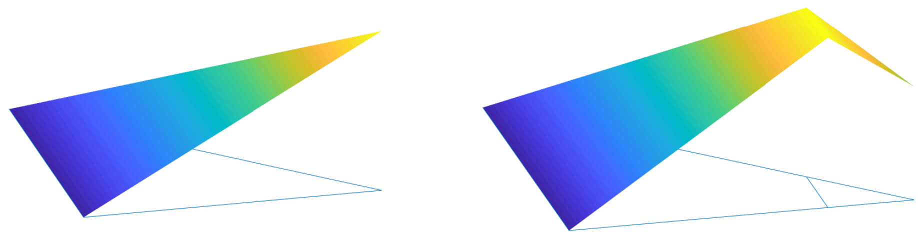

Figure 1.2: IFE shape function on left: non-interface element; right: interface element.

Instead of fitting the interface with the mesh, IFE methods adapt the interface with special finite element functions constructed on the interface elements, which enable IFE methods to solve interface problems on highly structured interface-independent meshes, such as Cartesian meshes.

A key issue in an IFE method is the construction of an IFE space according to the interface jump conditions. We use two dimensional IFE spaces to explain the basic ideas for constructing IFE shape functions in terms of macro polynomials. We start from the construction of lower degree two dimensional IFE spaces, including the linear IFE spaces [54, 94, 100] and the bilinear IFE spaces [70, 71, 107], that relies on an approach such that all the jump conditions are imposed on a line that connects the intersection points of the interface and the boundary of the element (i.e., the linear approximation of the curve $\Gamma$), as shown in Figure 1.3. One reason for this approach is that the IFE shape function on an interface element is supposed to be a piecewise polynomial which does not necessarily satisfy the interface jump condition across the interface curve unless the interface has a simple geometry. The IFE spaces constructed using this approach are proved to have the optimal approximation capabilities [72, 100]. However, the linear approximation of a curve has an intrinsic $O(h^2)$ limitation that hinders the application of this approach to higher degree polynomials. Thus imposing the jump conditions along the interface $\Gamma$ is a viable idea to construct higher degree IFE spaces. For example, in recent works [57, 59, 67], lower order IFE spaces are constructed by imposing jump conditions along the interface, and the optimal orders of approximation capability are proved for those IFE spaces.

But there is still an issue for developing higher degree IFE spaces: the original jump conditions (1.2c) and (1.2d) are not enough to determine the degree of freedom in a higher degree IFE shape function. To settle this issue, in addition to the original jump conditions (1.2c) and (1.2d), normal extended jump conditions (1.3) and Laplacian extended jump conditions (1.4) are proposed [3, 6, 128] for constructing higher degree IFE spaces:

$$\left[\beta \frac{\partial^j u}{\partial \mathbf{n}^j}\right]_\Gamma = 0, \quad j = 2, 3, \cdots p, \tag{1.3}$$

$$\left[\beta \frac{\partial^j \triangle u}{\partial \mathbf{n}^j}\right]_\Gamma = 0, \quad j = 0, 1, 2, \cdots p-2. \tag{1.4}$$

One idea to construct a higher degree IFE shape function is to penalize each interface condition (including the extended ones) through an $L^2$ inner product of a suitably chosen polynomial space on the interface, and this approach has been employed to construct arbitrary $p$-th degree IFE shape functions [5, 154].

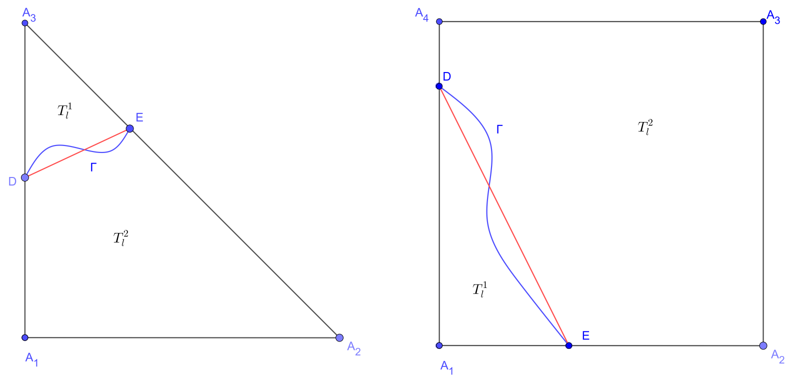


Figure 1.3: left: triangular interface element; right: rectangular interface element.

Another key issue is a suitable variational formulation for using an IFE space to solve interface problems at the desirable convergence rates. IFE methods in the literature are mostly for solving second order elliptic interface problems described by (1.2). The earlier works [70, 71, 100, 104, 107] use the linear or the bilinear IFE space in the classical Galerkin formulation to solve the elliptic interface problems and it has been demonstrated by numerical results that the IFE solutions have the optimal orders of convergence to the exact solutions in $H^1$ and $L^2$ norms. For the purpose of obtaining more stable numerical simulation, interior penalty ideas are utilized in partially penalized IFE (PPIFE) methods, discontinuous Galerkin IFE (DGIFE) methods [58, 70, 73, 77, 111, 112, 152], and enriched IFE methods [8] for solving the elliptic interface problems. It has been proved that these penalized IFE methods can converge optimally in energy norms provided that the exact solution possess a sufficient regularity.

IFE methods developed for second order elliptic interface problems naturally extend to interface problems of other related types of partial differential equations, such as the diffusion interface problems and wave interface problems. For instance, for the diffusion interface problem based on the standard parabolic equation defined by the second order elliptic operator, the authors in [13] investigated IFE methods for semi-linear parabolic interface problems, proving the optimal convergence for semi-discrete and fully-discrete (backward Euler) solution. The authors in [113, 144] designed IFE methods with interior penalties (PPIFE and DGIFE methods) for linear parabolic interface problems, proving the optimal convergence of the solutions in an energy norm provided that the exact solution has the piecewise-$H^3$ regularity in the space variable. The authors in [56, 76] discussed IFE schemes for parabolic interface problems with moving interface. For the second order hyperbolic interface problems, the author in [143] studied PPIFE methods where an optimal error estimate in an energy norm is provided under the assumption that the exact solution has the piecewise-$H^3$ regularity in the space variable.

IFE methods can also be applied to interface problems based on other types of differential operators. For example, IFE methods have been applied to solve the interface problems related to a system of partial differential equations. For interface problems of the time independent planar elasticity system, authors in [52, 53, 103, 145] investigate linear IFE methods. Among these works, it has been observed that the proposed nonconforming IFE methods [52, 103, 145] converge in the $L^\infty$ norm at the rate of $\mathcal{O}(h)$ at least; while the optimal order of convergence $\mathcal{O}(h^2)$ in $L^\infty$ norm is observed for conforming IFE methods in [53]. The authors in [106, 110] also have discussed linear, bilinear and rotated-$Q_1$ IFE methods for planar elasticity interface problems, and numerical examples indicate that these IFE methods can converge optimally in the $L^2$ norm and the semi-$H^1$ norm. The optimal approximation capability of linear, bilinear and rotated-$Q_1$ vector IFE spaces for solving elasticity interface problems is proved in the recent article [60] by a vector multi-point Taylor expansion. The authors in [64] then use linear and a bilinear vector IFE spaces to develop a PPIFE method for the planar elasticity interface problems, and they have proved this

PPIFE method can converge optimally in both an energy norm and the $L^2$ norm. As another extension, an IFE method has been developed for solving the interface problems for the Stokes system in [4, 32] where the authors propose an immersed $Q_1/Q_0$ finite element space according to the location of the interface and the related interface jump conditions. Numerical results generated by this IFE method demonstrates the optimal convergence in the $L^2$ norm and the semi $H^1$ norm. Two dimensional Stokes interface problem with moving interface and axisymmetric three dimensional Stokes interface problem are also solved by IFE methods in [7, 32]. The authors in [2, 120] propose immersed DG (DGIFE) methods for solving interface problems described by a first-order hyperbolic system. In these articles, numerical results demonstrate the optimal orders of convergence and the stability analysis of the numerical scheme is conducted.

## 1.3 Topics of the Thesis

The research to be reported in this thesis is for both the development of IFE methods and their related error analysis. We can put the research projects into two groups.

The first group is about the fundamentals of IFE methods associated with the second order elliptic operator whose coefficient is discontinuous. We will investigate the conditioning issue in a least squares framework for the construction of higher degree IFE spaces for solving the second order elliptic interface problems, which, as we will report later in this thesis, are necessary for solving wave propagation interface problems with a large wave number. Another research goal in this group is to improve the error estimation for the linear PPIFE method for the second order elliptic interface problems so that its optimal error bounds follow from the standard piecewise $H^2$ regularity assumption instead of the fastidious piecewise $H^3$ regularity used in the related literature.

The second group of research projects extend the IFE methods and related analysis to other types of interface problems in which the partial differential equations involve the second order elliptic operator. For a Helmholtz interface problem that models time-harmonic wave propagation in a domain consisting of different materials, we develop a PPIFE method and a DGIFE method and carry out an error analysis for the PPIFE method in a symmetric configuration. For a hyperbolic interface problem, we analyze a PPIFE method discussed in [143] for the interface problems of the second order hyperbolic equation modeling time dependent wave propagation across a domain formed by different materials. Our new analysis shows that this PPIFE method can converge optimally in both an energy norm and the $L^2$ with the standard regularity assumption instead of the stringent piecewise $H^3$ regularity. We then move on to reinvestigate the IFE methods in [113] for a parabolic interface problem which can be considered as the time dependent counterpart of the fundamental second order elliptic interface problem. Again, we prove that these PPIFE methods can actually converge optimally in both an energy norm and the $L^2$ with the standard regularity assumption.

We now provide a little more descriptions for these research projects to be reported in this thesis.

### 1.3.1 Research projects for the fundamentals of IFE methods

**A stabilized construction for higher order IFE spaces**:

Higher degree IFE methods are desirable for accuracy and for their performance in dealing wave propagation with a large wave number. The authors in [5] proposed an approach to construct higher degree IFE spaces based on a least squares framework. In this work, the authors reported an issue that the local linear system to determine the coefficients of IFE shape functions can be very ill-conditioned if one of the subelements partitioned by the interface is very small. As a consequence, the performance of the methods using this higher degree IFE space can deteriorate. To deal with this conditioning issue, we propose a stabilized construction for higher order IFE spaces. This construction method is still based on the original least squares framework, but we will resort to the idea of element extension for a better stability. This idea, such as a patch of an interface element introduced in [39] and a triangular annulus introduced in [67], has been used in numerical investigations of interface problems on non-body fitting meshes [39, 67]. We plan to construct IFE spaces using fictitious elements, which are extensions of the original elements. Using fictitious elements can help avoid the situation that one of the sub-elements is very small, thus improve the conditioning in constructing higher degree IFE spaces.

**An improved error estimation for a linear PPIFE method**:

For the model second order elliptic interface problem (1.2), the authors in [111] employed a piecewise $H^3$ regularity assumption for the exact solution to derive an optimal convergence in an energy norm for the PPIFE solutions. However, given the body force term $f \in L^2(\Omega)$, the exact solution to the interface problem (1.2) only has piecewise $H^2$ regularity [45] in general. This motivates us to investigate whether the PPIFE methods developed in [111] can converge optimally in an energy norm under the standard piecewise $H^2$ regularity assumption instead of the excessive piecewise $H^3$ regularity. In addition, we note that the piecewise $H^3$ regularity assumption in [111] hinders the derivation of the optimal error estimates in $L^2$ norm, although the optimal convergence in $L^2$ norm has been numerically observed. We will prove the optimal convergence of the PPIFE solution for the elliptic interface problem in $L^2$ norm under piecewise $H^2$ regularity assumption of the exact solution.

### 1.3.2 Research projects for extending IFE methods

There are many real-world interface problems related to the second order elliptic operator. Two typical applications are of great interest. The first is the wave propagation and the second is the diffusion process in domains consisting of different materials because partial differential equations defined by the second order elliptic operator can be used in the related mathematical models.

Wave propagation is a ubiquitous phenomenon that involves the travels of waves that appear when an object or a system reacts to a perturbation and transmits it to its neighbors [55]. Interface problems related to wave propagation process can arise in wave diffraction [44, 134], wave scattering [34, 150], and wave reflection/transmission [21, 38] in composite media. Wave propagation processes can be simulated by the time-domain and frequency-domain wave equations, respectively. The second order hyperbolic partial differential equations are typical time-domain wave equations. Applying the Fourier transform to the hyperbolic equations, we can convert them to the frequency-domain wave equations such as the Helmholtz equations. Both the second order hyperbolic equations and Helmholtz equations contain the second order elliptic operator. Therefore, it is natural to explore how to extend the IFE methods developed for the second order elliptic interface problems to interface problems arisen in wave propagation.

Diffusion is the process by which matter is transported from one part of a system to another as a result of random molecular motions [43]. Interface problems related to diffusion process can arise in drug transportation [30], geochemical kinetics [140], and molecular dynamics [116] in heterogeneous media, to name just a few. The diffusion process can be described by the Fick's law, the Fick's first law is used to describe the steady-state diffusion, while the Fick's second law is used to describe the non-steady state diffusion [141]. The Fick's second law leads to a parabolic partial differential equation that defines the change in concentration within a phase due to the process of molecular diffusion [90]. The parabolic equation contains the second order elliptic operator. Therefore, the techniques used to study IFE methods for elliptic interface problems are promising for diffusion interface problems governed by the parabolic equation.

**IFE methods and related error analysis for Helmholtz interface problems**:

The Helmholtz equation

$$-\Delta u - \omega^2 u = f, \tag{1.5}$$

which arises in many areas in physics such as electromagnetism [91], seismology [92], and acoustics [50], can be derived by taking the Fourier transformation of the second order hyperbolic equation which has the following general form

$$\frac{1}{c^2}\frac{\partial^2 \phi(x,t)}{\partial t^2} - \Delta\phi(x,t) = q(x,t). \tag{1.6}$$

The Helmholtz interface problems arise in the process of wave propagation in heterogeneous media. In a suitable physical configuration, the amplitude of the wave can be described by the Helmholtz equation. Across the interface between two different materials, the amplitude is required to satisfy the jump conditions [86, 155] imposed according to pertinent physics, such as the continuity of pressure, the normal velocity or volume flow [21, 38, 86, 149]. These considerations lead us to consider the following interface BVP for the Helmholtz equation [26, 93, 114]: find $u(X)$ that satisfies the Helmholtz equation and the boundary condition

$$-\nabla \cdot (\beta \nabla u) - \omega^2 u = f, \quad \text{in } \Omega^- \cup \Omega^+, \tag{1.7a}$$

$$\beta \frac{\partial u}{\partial \boldsymbol{n}_\Omega} + i\omega u = g, \quad \text{on } \partial\Omega, \tag{1.7b}$$

together with the jump conditions across the interface [21, 26, 38, 86, 93]:

$$[u]_\Gamma := u^+|_\Gamma - u^-|_\Gamma = 0, \tag{1.7c}$$

$$\big[\beta \nabla u \cdot \mathbf{n}\big]_\Gamma := \beta^+ \nabla u^+ \cdot \mathbf{n}|_\Gamma - \beta^- \nabla u^- \cdot \mathbf{n}|_\Gamma = 0. \tag{1.7d}$$

Here the domain $\Omega \subseteq \mathbb{R}^2$ is divided by an interface curve $\Gamma$ into two subdomains $\Omega^-$ and $\Omega^+$, occupied by a different material each, with $\overline{\Omega} = \overline{\Omega^- \cup \Omega^+ \cup \Gamma}$, $i = \sqrt{-1}$, $\omega$ is the wave number, $\mathbf{n}_\Omega$ is the unit outward normal vector to $\partial\Omega$, $u^s = u|_{\Omega^s}$, $s = \pm$, $\mathbf{n}$ is the unit normal vector to the interface $\Gamma$, and the coefficient $\beta$ is a positive piecewise constant function representing different materials such that

$$\beta(X) = \begin{cases} \beta^- & \text{for } X \in \Omega^-, \\ \beta^+ & \text{for } X \in \Omega^+. \end{cases}$$

There are many numerical methods for solving the Helmholtz boundary value problems (BVPs), among them are the classic finite element methods [14, 17, 82, 84]. More sophisticated finite element methods such as the interior penalty Galerkin (IPG) method [28, 47] and discontinuous Galerkin (DG) method (including interior penalty DG, IPDG for abbreviation) [49, 50, 51, 85, 95, 122] have been developed for solving Helmholtz BVPs. Penalty terms in IPG and IPDG methods can enhance the stability, and DG methods allow efficient refinement in either the mesh or the finite element degree [42]. The main challenge for the error analysis for Helmholtz-type problem lies in that the coercivity of the corresponding bilinear form is not necessarily guaranteed, thus the process of the error analysis for the elliptic problem might not be applied to the Helmholtz problem directly. In some earlier works [84, 122, 131], the optimal orders of convergence of numerical solution in the energy norm or broken $H^1$ norm is proved provided that the mesh is fine enough using Schatz's argument. Recently, the authors in [50] show the optimal order of convergence in broken $H^1$ norm and sub-optimal order of convergence in $L^2$ norm without any mesh constraint using DG method. We note that, when applied to interface problems, traditional finite element methods in the literature need to use interface dependent meshes.

In recent years, numerical methods based on interface-independent meshes are also applied to Helmholtz interface problems, such as [150] using IIM and [135, 155] using CutFEM. As another mesh-independent technique for solving interface problems, we will extend IFE methods to Helmholtz interface problem. Since the Helmholtz equation contains the elliptic operator and the interface jump conditions specified in (1.7c) and (1.7d) are the same as those for the elliptic interface problem (1.2); therefore, it is natural for us to develop IFE methods for the Helmholtz interface problems by using the IFE spaces constructed for the second order elliptic interface problems, except for that the IFE solution is complex valued. We will also apply penalizing techniques in the IFE methods for Helmholtz interface problems. We will explore higher degree IFE methods because it is well known that higher degree finite element methods have desirable features for wave propagation problems [10, 20, 132], such as reducing the numerical dispersion and errors in solution due to the pollution effect caused by a large wave number [83, 139], and it was found that employing higher degree finite elements requires less degrees of freedom for numerical solutions to attain a specific accuracy [83].

In the error analysis for finite element methods for Helmholtz interface problems, following the framework of Schatz argument, the authors in [35, 68] analyzed the stability and proved the optimal error bounds for the finite element solution under the assumption that the mesh size is small enough. In this thesis, we aim to conduct error estimation for the proposed PPIFE methods for Helmholtz interface problems with Robin boundary condition. In particular, under suitable regularity assumption of the exact solution [119, 135] and a mesh constraint, we intend to establish optimal error bounds in both an energy norm and the $L^2$ norm for these IFE methods.

**Improved analysis for a PPIFE method for hyperbolic interface problems**:

Hyperbolic interface problems appear in the physical processes of wave propagation in inhomogeneous media [1, 115, 123] in many fields such as acoustics [19, 115], elastodynamics [115], seismology [19] and electromagnetism [11].

In recent years, numerical methods using interface-independent meshes to solve hyperbolic interface problems have appear in the literature, for instance, IIM method [147, 148] and DGIFE [2, 120] method for first-order hyperbolic system. For solving the second order time-domain hyperbolic interface problems directly without transforming them into a coupled first-order system, the authors in [98] investigated a hyperbolic BVP with equivalued surface on a domain with an interface, discussing the existence and uniqueness of the solution. The authors in [19] studied a second order hyperbolic interface problem with conventional finite element methods using body fitting meshes.

Recently, the author in [143] investigated a class of PPIFE methods for solving second order hyperbolic interface problems in the following form: find $u(X, t)$ such that

$$u_{tt} - \nabla \cdot (c^2 \nabla u) = f, \quad \text{in } \Omega^- \cup \Omega^+, t \in [0, T], \tag{1.8a}$$

$$u|_{\partial\Omega} = g(X, t), \quad t \in [0, T], \tag{1.8b}$$

$$u(X, 0) = w_0(X), u_t(X, 0) = w_1(X) \quad X \in \Omega, \tag{1.8c}$$

together with the usual interface jump conditions:

$$[u]_\Gamma := u^+|_\Gamma - u^-|_\Gamma = 0, \tag{1.8d}$$

$$\left[c^2 \nabla u \cdot \mathbf{n}\right]_\Gamma := (c^+)^2 \nabla u^+ \cdot \mathbf{n}|_\Gamma - (c^-)^2 \nabla u^- \cdot \mathbf{n}|_\Gamma = 0, \tag{1.8e}$$

where the domain $\Omega \subseteq \mathbb{R}^2$ is divided by an interface curve $\Gamma$ into two subdomains $\Omega^-$ and $\Omega^+$, with $\overline{\Omega} = \overline{\Omega^- \cup \Omega^+ \cup \Gamma}$, and the coefficient $c$ is a positive piecewise constant function such that

$$c(X) = \begin{cases} c^- & \text{for } X \in \Omega^-, \\ c^+ & \text{for } X \in \Omega^+. \end{cases}$$

In [143], optimal error estimates for these PPIFE methods have been derived in an energy norm under the assumption that the exact solution to the hyperbolic interface problem has a piecewise $H^3$ regularity in space. But, to our best knowledge, the $L^2$ error estimates for these PPIFE methods were not given in any published research works. This motivates us to further study the error analysis for these PPIFE methods. We aim to reanalyze the fully discrete PPIFE method proposed in [143] for the second order hyperbolic interface problems, we will establish optimal error bounds in an energy norm and the $L^2$ norm with less demanding regularity of the exact solution, *i.e.*, $u$ is assumed to be piecewise $H^2$ in space. Also, we intend to discuss the stability of the scheme and present numerical examples for realistic wave propagation with traveling waves including incident, reflected, and transmitted waves. To our best knowledge, those results are generated by IFE methods for second order hyperbolic equations for the first time.

**Improved analysis for PPIFE methods for parabolic interface problems**:

Parabolic equations are used to describe the diffusion phenomenon such as heat conduction, diffusion of vorticity [124], and dynamics of population densities [121]. Parabolic interface problems appear in many real world processes such as chemical diffusion in heterogeneous media [89], channel-flow of a viscous fluid [33], and electrodynamics [46], to name just a few.

IFE methods [13, 76, 105, 108, 109, 113, 144], including penalized IFE methods [113, 144], have been applied to solve parabolic interface problems in the following form:

$$\frac{\partial u}{\partial t} - \nabla \cdot (\beta \nabla u) = f, \quad \text{in } \Omega^- \cup \Omega^+, t \in [0,T], \tag{1.9a}$$

$$u|_{\partial\Omega} = g(X,t), \quad t \in [0,T], \tag{1.9b}$$

$$u|_{t=0} = u_0(X), \quad X \in \partial\Omega, \tag{1.9c}$$

together with the following jump conditions:

$$[u]_\Gamma \;:=\; u^+|_\Gamma - u^-|_\Gamma = 0, \tag{1.9d}$$

$$\big[\beta \nabla u \cdot \mathbf{n}\big]_\Gamma \;:=\; \beta^+ \nabla u^+ \cdot \mathbf{n}|_\Gamma - \beta^- \nabla u^- \cdot \mathbf{n}|_\Gamma = 0, \tag{1.9e}$$

where the domain $\Omega \subseteq \mathbb{R}^2$ is divided by an interface curve $\Gamma$ into two subdomains $\Omega^-$ and $\Omega^+$, with $\overline{\Omega} = \overline{\Omega^- \cup \Omega^+ \cup \Gamma}$ and the coefficient $\beta$ is a piecewise positive constant function such that

$$\beta(X) = \begin{cases} \beta^- & \text{for } X \in \Omega^-, \\ \beta^+ & \text{for } X \in \Omega^+. \end{cases}$$

For the above parabolic interface problem, the authors in [113, 144] considered some PPIFE and DGIFE methods and they proved that these IFE methods could converge optimally in an energy norm under a piecewise $H^3$ regularity assumption for the exact solution. But these articles did not address the optimal convergence in the $L^2$ norm for these IFE methods. Recently, using the patch idea [64], the authors in [63] developed PPIFE method for elliptic interface problems where optimal orders of convergence of the solutions in an energy norm and the $L^2$ norm are guaranteed by only requiring piecewise $H^2$ regularity of the exact solution. Motivated by this work and the patch idea, we will improve the error estimation for IFE methods developed in [113] for parabolic interface problems. We will show optimal orders of convergence in both an energy norm and the $L^2$ norm under piecewise $H^2$ regularity assumption in the space variable.

## 1.4 Outline of the thesis

The outline of the thesis is as follows.

In Chapter 2, we introduce notations, assumptions, and recall the linear/bilinear IFE spaces that will be used throughout this thesis.

In Chapter 3, we introduce a stabilized construction of higher degree IFE spaces based on least squares framework, which will be utilized to solve Helmhotlz interface problems in Chapter 5.

In Chapter 4, we provide an improved error analysis for the linear/bilinear PPIFE methods for second order elliptic interface problems based on the patch idea, which will serve as the theoretical foundation for the error analysis for their related applications (IFE methods for wave propagation and diffusion interface problems in Chapters 5, 6 and 7) in this thesis.

In Chapter 5, we study linear/bilinear and higher degree PPIFE and DGIFE methods for Helmholtz interface problems. The error analysis is conducted for the linear/bilinear PPIFE methods utilizing the framework of Schatz's argument. Numerical examples are presented to demonstrate the features of IFE methods and validate the theoretical results of error analysis.

In Chapter 6, we study the error analysis of a PPIFE method for the hyperbolic interface problems. The optimal error bounds are derived in an energy norm and $L^2$ norm under the assumption that the exact solution has the piecewise $H^2$ regularity in the space variable. Numerical examples are presented including stationary and travelling waves when the linear or curved interface is embedded.

In Chapter 7, we study the error analysis of a group of PPIFE methods for the parabolic interface problems. The optimal error bounds are derived in an energy norm and $L^2$ norm under the assumption that the exact solution has piecewise $H^2$ regularity in the space variable. A Numerical example is presented to corroborate the results of error analysis.

# Chapter 2

# Notations, assumptions, and linear/bilinear IFE spaces

In this chapter, we will introduce notations, assumptions, and IFE spaces that will be used throughout the thesis.

## 2.1 Notations and assumptions

Let $\Omega$ be a bounded domain. For every open set $\tilde{\Omega} \subseteq \Omega$, let $W^{k,p}(\tilde{\Omega})$ be the standard Sobolev space on $\tilde{\Omega}$ with the standard norm $\|\cdot\|_{k,p,\tilde{\Omega}}$ and the semi-norm $|v|_{k,p,\tilde{\Omega}}$. If $\tilde{\Omega}^s := \tilde{\Omega} \cap \Omega^s \neq \emptyset$, $s = \pm$, we let the related Sobolev norms and semi-norms be

$$\|\cdot\|^2_{k,p,\tilde{\Omega}} = \|\cdot\|^2_{k,p,\tilde{\Omega}^-} + \|\cdot\|^2_{k,p,\tilde{\Omega}^+}, \qquad |\cdot|^2_{k,p,\tilde{\Omega}} = |\cdot|^2_{k,p,\tilde{\Omega}^-} + |\cdot|^2_{k,p,\tilde{\Omega}^+}.$$

Furthermore, we introduce the following spaces on $\tilde{\Omega}$ in the case $\tilde{\Omega}^s \neq \emptyset$, $s = \pm$:

$$PW^{k,p}(\tilde{\Omega}) = \Big\{u : u|_{\tilde{\Omega}^s} \in W^{k,p}(\tilde{\Omega}^s),\ s = \pm;\ [u] = 0,\ [\beta \nabla u \cdot \mathbf{n}_\Gamma] = 0 \text{ on } \Gamma \cap \tilde{\Omega}\Big\},\ p \geq 1,$$

$$PC^2(\tilde{\Omega}) = \Big\{u : u|_{\tilde{\Omega}^s} \in C^2(\tilde{\Omega}^s),\ s = \pm;\ [u] = 0,\ [\beta \nabla u \cdot \mathbf{n}_\Gamma] = 0 \text{ on } \Gamma \cap \tilde{\Omega}\Big\},$$

for suitable $k$ and $p$ such that the involved quantities on $\Gamma \cap \tilde{\Omega}$ are well defined. Here, $\mathbf{n}_\Gamma$ is the unit normal vector of $\Gamma$ and we adopt the jump notation such that $[v] = v^+|_\Gamma - v^-|_\Gamma$ for a function $v$ such that $v^s = v|_{\Omega^s},\ s = \pm$. Also, we will omit $p = 2$ from the pertinent norms and semi-norms for $H^k(\tilde{\Omega}) = W^{k,2}(\tilde{\Omega})$ and $PH^k(\tilde{\Omega}) = PW^{k,2}(\tilde{\Omega})$.

We let $\mathcal{T}_h$ be a triangular or a rectangular mesh for the domain $\Omega \subset \mathbb{R}^2$, and, without loss of generality, we assume that $\Omega = \cup_{T \in \mathcal{T}_h} T$. Let $\mathcal{N}_h$ be the collection of the nodes in the mesh $\mathcal{T}_h$. We use $\mathcal{T}_h^i$ and $\mathcal{T}_h^n$ to denote the sets of interface elements and non-interface elements, respectively. We denote the set of interior interface elements as $\mathring{\mathcal{T}}_h^i$, the set of boundary elements (elements who have at least one boundary on the boundary of the domain) as $\mathcal{T}_h^b$, the set of boundary interface elements (interface elements who have at least one edge on the boundary of the domain) as $\mathcal{T}_h^{bi}$. Also, we denote the set of interior edges by $\mathring{\mathcal{E}}_h$, the interface edges by $\mathcal{E}_h^i$, the interior interface edges by $\mathring{\mathcal{E}}_h^i$, and the interior non-interface edges by $\mathring{\mathcal{E}}_h^n$, respectively. In addition, we denote the set of boundary edge as $\mathcal{E}_h^b$, the set of boundary interface edges by $\mathcal{E}_h^{bi}$. As in [5, 70, 71, 74], we make the following assumptions for the mesh $\mathcal{T}_h$:

**(H1)** The interface $\Gamma$ cannot intersect an edge of any element at more than two points unless the edge is part of $\Gamma$.

**(H2)** If $\Gamma$ intersects the boundary of an element at two points, these intersection points must be on different edges of this element.

**(H3)** The interface $\Gamma$ is a piecewise $C^2$ function, and the mesh $\mathcal{T}_h$ is formed such that on every interface element $T \in \mathcal{T}_h^i$, $\Gamma \cap T$ is $C^2$.

**(H4)** The interface $\Gamma$ is smooth enough so that $PC^2(T)$ is dense in $PH^2(T)$ for every interface element $T \in \mathcal{T}_h^i$.

In general, these assumptions can be satisfied when the mesh size is small enough.

We will also adopt the following standard notations for the penalty terms on edges of a mesh $\mathcal{T}_h$. Let $v$ be a piecewise function defined by elements of $\mathcal{T}_h$. Then, on each $e \in \mathring{\mathcal{E}}_h$ shared by two elements $T_1^e$ and $T_2^e$, we let

$$[v]_e = (v|_{T_1^e})|_e - (v|_{T_2^e})|_e \quad \text{and} \quad \{v\}_e = \frac{1}{2}\left((v|_{T_1^e})|_e + (v|_{T_2^e})|_e\right). \tag{2.1}$$

But for $e \in \mathcal{E}_h^b$, we define

$$[v]_e = \{v\}_e = v|_e. \tag{2.2}$$

For each interface element $T$, let $T^s, s = \pm$ be the two subelements of $T$ partitioned by $\Gamma$ and let $v$ be a piecewise function defined on these subelements. Then, we can similarly define the jump and average of $v$ on the interface inside this interface element as follows:

$$[v]_{\Gamma\cap T} = v^+|_{\Gamma\cap T} - v^-|_{\Gamma\cap T} \quad \text{and} \quad \{v\}_{\Gamma\cap T} = \frac{1}{2}\left(v^+|_{\Gamma\cap T} + v^-|_{\Gamma\cap T}\right), \tag{2.3}$$

where $v^s = v|_{T^s}, s = \pm$. And we also recall the following underlying piecewise $H^1$ function spaces:

$$\begin{aligned} V_h(\Omega) = \Big\{v \in L^2(\Omega) : \; v|_T \in H^1(T), \; \nabla v \cdot \boldsymbol{n}|_{\partial T} \in L^2(\partial T), \; \forall T \in \mathcal{T}_h, \\ [v]_e = 0, \; \forall \; e \in \mathring{\mathcal{E}}_h^n\Big\}, \end{aligned} \tag{2.4}$$

and

$$\begin{aligned} V_{h,0}(\Omega) = \Big\{v \in L^2(\Omega) : \; v|_T \in H^1(T), \; \nabla v \cdot \boldsymbol{n}|_{\partial T} \in L^2(\partial T), \; \forall T \in \mathcal{T}_h, \\ [v]_e = 0, \; \forall \; e \in \mathring{\mathcal{E}}_h^n, \; v|_{\partial\Omega\setminus\mathcal{E}_h^{bi}} = 0\Big\}. \end{aligned} \tag{2.5}$$

## 2.2 Local linear and bilinear IFE spaces

For each element $T \in \mathcal{T}_h$, its index set is either $\mathcal{I}_T = \{1, 2, 3\}$ when $T$ is triangular or $\mathcal{I}_T = \{1, 2, 3, 4\}$ when $T$ is rectangular. Let $A_i$, $i \in \mathcal{I}_T$ be the vertices of an element $T \in \mathcal{T}_h$. Then, the interface partitions the index set $\mathcal{I}$ into $\mathcal{I}_T^- = \{i : A_i \in T^-\}$ and $\mathcal{I}_T^+ = \{i : A_i \in T^+\}$. On each element $T \in \mathcal{T}_h$, we consider the standard linear or bilinear Lagrangian shape functions:

$$\psi_{j,T}(A_i) = \delta_{ij}, \quad \forall i, j \in \mathcal{I}_T. \tag{2.6}$$

As usual in IFE methods, we use the polynomial space

$$\mathbb{P}^1(T) = \mathrm{Span}\,\{\psi_{j,T}, j \in \mathcal{I}_T\} \quad \text{or} \quad \mathbb{Q}^1(T) = \mathrm{Span}\,\{\psi_{j,T}, j \in \mathcal{I}_T\} \tag{2.7}$$

as the local IFE space on the non-interface $T$ according to whether $T$ is triangular or rectangular. For simplicity, $\mathbb{P}^1(T)$ and $\mathbb{Q}^1(T)$ are denoted as $\mathbb{P}(T)$ and $\mathbb{Q}(T)$ in this thesis.

On the other hand, on each interface element $T$, we will use the linear and bilinear IFE shape functions [70, 71, 75, 100, 104, 107]. To be specific, let the interface $\Gamma$ intersect the edges of $T$ at the points $D$ and $E$, as shown in Figure 1.3. Let $l$ be the line passing through points $D$ and $E$ with the normal vector $\bar{\mathbf{n}} = (\bar{n}_x, \bar{n}_y)$. This line partitions $T$ into two subelements $T_l^{\pm}$. When this interface element $T$ is triangular, a linear IFE shape function $\phi_T(x, y)$ is a piecewise linear polynomial specified by [75, 100, 104]:

$$\phi_T(x,y) = \begin{cases} \phi_T^-(x,y) = a^-x + b^-y + c^-, & \text{if } (x,y) \in T_l^-, \\ \phi_T^+(x,y) = a^+x + b^+y + c^+, & \text{if } (x,y) \in T_l^+, \\ \phi_T^-(D) = \phi_T^+(D),\ \phi_T^-(E) = \phi_T^+(E), & \\ \beta^+ \frac{\partial \phi_T^+}{\partial \bar{\mathbf{n}}} - \beta^- \frac{\partial \phi_T^-}{\partial \bar{\mathbf{n}}} = 0. & \end{cases} \tag{2.8}$$

When $T$ is a rectangular interface element, a bilinear IFE shape function $\phi_T(x,y)$ is a piecewise bilinear polynomial specified by [71, 75, 107]:

$$\phi_T(x,y) = \begin{cases} \phi_T^-(x,y) = a^-x + b^-y + c^- + d^-xy, & \text{if } (x,y) \in T_l^-, \\ \phi_T^+(x,y) = a^+x + b^+y + c^+ + d^+xy, & \text{if } (x,y) \in T_l^+, \\ \phi_T^-(D) = \phi_T^+(D),\ \phi_T^-(E) = \phi_T^+(E),\ d^- = d^+, & \\ \int_{\overline{DE}} (\beta^+ \frac{\partial \phi_T^+}{\partial \bar{\mathbf{n}}} - \beta^- \frac{\partial \phi_T^-}{\partial \bar{\mathbf{n}}}) ds = 0. & \end{cases} \tag{2.9}$$

It has been shown [70, 71, 100] that there is a unique IFE shape function $\phi_{i,T}(x,y), i \in \mathcal{I}_T$ in the format of (2.8) or (2.9) satisfying the nodal value conditions

$$\phi_{i,T}(A_j) = \delta_{ij}, \quad \forall i,j \in \mathcal{I}_T. \tag{2.10}$$

Then the local IFE space on an interface element $T$ is defined as

$$S_h^1(T) = \begin{cases} \text{Span}\{\psi_{i,T}, i = 1, 2, ..., |\mathcal{I}|\}, & T \in \mathcal{T}_h^n, \\ \text{Span}\{\phi_{i,T}, i = 1, 2, ..., |\mathcal{I}|\}, & T \in \mathcal{T}_h^i. \end{cases} \tag{2.11}$$

For simplicity, the linear/bilinear IFE space $S_h^1(T)$ is denoted as $S_h(T)$ in the thesis.

# Chapter 3

# Stabilized construction of higher degree IFE spaces

## 3.1 Introduction

In this chapter, by following the least squares framework proposed in [5], we will study a stabilized construction of higher degree IFE spaces for solving the second order elliptic interface problems described by (1.2). The stabilization is to overcome the conditioning issue reported in [5] caused by the situation that one of the sub-elements is too small. Using fictitious elements in constructing the IFE spaces can avoid this situation and thus improving the conditioning; therefore, we propose a stabilized construction of higher degree IFE spaces in this chapter with fictitious elements. This chapter consists of four additional sections. In Secton 3.2, we recall a construction method proposed in [5] for local higher degree IFE spaces. In Section 3.3, we present a stabilized construction of higher degree IFE shape functions using fictitious elements. In Section 3.4, we numerically test the approximation capabilities of the proposed higher degree IFE spaces. Finally, we make some brief conclusions in Section 3.5.

## 3.2 A least squares method for constructing higher degree IFE spaces

Here we briefly review the work from [5] for constructing the local higher degree IFE spaces with a least squares framework. Let $\mathcal{T}_h$ be a triangular mesh of the domain $\Omega$ on which the second order elliptic interface problems described by (1.2) are considered. On each element $T \in \mathcal{T}_h$, we first introduce the index set $\mathcal{I} = \{1, 2, \cdots, \frac{(p+1)(p+2)}{2}\}$ for an integer $p \geq 1$, and denote the usual local Lagrange nodes on $T$ by $N_i,\ i \in \mathcal{I}$. Let $\psi_{j,T},\ j \in \mathcal{I}$ be the standard $p$-th degree Lagrange finite element shape functions on $T$ such that

$$\psi_{j,T}(N_i) = \delta_{ij}, \quad \forall i, j \in \mathcal{I}. \tag{3.1}$$

We use the standard $p$-th degree polynomial space

$$\mathbb{P}^p(T) = \text{Span}\left\{\psi_{j,T}, j \in \mathcal{I}\right\} \tag{3.2}$$

as the local IFE space on each non-interface elements $T \in \mathcal{T}_h^n$.

For each interface element $T \in \mathcal{T}_h^i$, the interface $\Gamma$ splits it into two subelements $T^- = \Omega^- \cap T$ and $T^+ = \Omega^+ \cap T$. Consequently, $\Gamma$ also divides the index set $\mathcal{I}$ into two subsets: $\mathcal{I}^- = \{i\ :\ N_i \in T^-\}$ and $\mathcal{I}^+ = \{i\ :\ N_i \in T^+\}$, with $\mathcal{I} = \mathcal{I}^- \cup \mathcal{I}^+$. In [5], the IFE shape functions are chosen from the following space

$$\mathcal{P}^p(T) = \left\{q\ :\ q|_{T^-} \in \mathbb{P}^p(T^-)\ \text{ and }\ q|_{T^+} \in \mathbb{P}^p(T^+)\right\}, \tag{3.3}$$

which is isomorphic to the product polynomial space $\mathcal{S}^p(T) = \left[\mathbb{P}^p(T)\right]^2$, through a map $\mathcal{F}_T : \mathcal{S}^p(T) \to \mathcal{P}^p(T)$, with $\mathcal{F}_T v|_{T^i} = v_i$, $i = \pm$, $\forall v = (v_1, v_2) \in \mathcal{S}^p(T)$. This isomorphism enables one to develop the IFE shape functions by working on $\mathcal{S}^p(T) = \left[\mathbb{P}^p(T)\right]^2$ instead of $\mathcal{P}^p(T)$. Based on this configuration, the fundamental idea in [5] is to partition $\mathcal{S}^p(T)$ into two subspaces

$$\mathcal{V}_1 = \mathrm{Span}\left\{\xi_{i,T} \in \mathcal{S}^p(T) \,:\, i \in \mathcal{I}\right\}, \quad \mathcal{V}_2 = \mathrm{Span}\left\{\eta_{i,T} \in \mathcal{S}^p(T) \,:\, i \in \mathcal{I}\right\}, \tag{3.4}$$

where

$$\xi_{i,T} = \begin{cases} (\psi_{i,T},\, 0), & \text{if } i \in \mathcal{I}^-, \\ (0,\, \psi_{i,T}), & \text{if } i \in \mathcal{I}^+, \end{cases} \quad \text{and} \quad \eta_{i,T} = \begin{cases} (0,\, \psi_{i,T}), & \text{if } i \in \mathcal{I}^-, \\ (\psi_{i,T},\, 0), & \text{if } i \in \mathcal{I}^+, \end{cases} \tag{3.5}$$

in which the subspace $\mathcal{V}_1$ is used to handle the nodal degrees of freedom imposed on shape functions and $\mathcal{V}_2$ is utilized to handle the jump conditions. In addition, $\mathcal{S}^p(T)$ is the direct sum of $\mathcal{V}_1$ and $\mathcal{V}_2$, i.e., $\mathcal{S}^p(T) = \mathcal{V}_1 \bigoplus \mathcal{V}_2$. Furthermore, for any $\widetilde{\Gamma} \subseteq \Gamma$, we consider a linear operator $[[\cdot]]_{\widetilde{\Gamma}}$ defined on $\mathcal{S}^p(T)$:

$$[[v]]_{\widetilde{\Gamma}} := v_1|_{\widetilde{\Gamma}} - v_2|_{\widetilde{\Gamma}}, \quad \forall v = (v_1, v_2) \in \mathcal{S}^p(T). \tag{3.6}$$

According to the two types of extended jump conditions (1.3) and (1.4), the authors in [5] considered two bilinear forms $\mathcal{J}_k : \mathcal{S}^p(T) \times \mathcal{S}^p(T) \to \mathbb{R}$, $k = 1, 2$ defined on a portion of interface $\Gamma_T$ satisfying $\Gamma \cap T \subset \Gamma_T$: for the normal extended jump conditions (1.3),

$$\mathcal{J}_1(v, w) = \omega_0 \int_{\Gamma_T} [[v]]_{\Gamma_T} \, [[w]]_{\Gamma_T} ds + \sum_{j=1}^{p} \omega_j \int_{\Gamma_T} \left[\left[\beta \frac{\partial^j v}{\partial \mathbf{n}^j}\right]\right]_{\Gamma_T} \left[\left[\beta \frac{\partial^j w}{\partial \mathbf{n}^j}\right]\right]_{\Gamma_T} ds; \tag{3.7}$$

and for the Laplacian extended jump conditions (1.4),

$$
\begin{aligned}
\mathcal{J}_2(v,w) =&\omega_0 \int_{\Gamma_T} [[v]]_{\Gamma_T}\, [[w]]_{\Gamma_T} ds + \int_{\Gamma_T} \omega_1 \left[\left[\beta \frac{\partial v}{\partial \mathbf{n}}\right]\right]_{\Gamma_T} \left[\left[\beta \frac{\partial w}{\partial \mathbf{n}}\right]\right]_{\Gamma_T} ds \\
&+ \sum_{j=0}^{p-2} \omega_{j+2} \int_{\Gamma_T} \left[\left[\beta \frac{\partial^j \triangle v}{\partial \mathbf{n}^j}\right]\right]_{\Gamma_T} \left[\left[\beta \frac{\partial^j \triangle w}{\partial \mathbf{n}^j}\right]\right]_{\Gamma_T} ds,
\end{aligned} \tag{3.8}
$$

where $\omega_0 = \max\{\beta^-,\beta^+\}^2$ and $\omega_j = |\Gamma \cap T|^{2j}$, $j \geqslant 1$. Under the isomorphism $\mathcal{F}_T$, given a component $\xi_T = \sum_{i\in\mathcal{I}} v_i \xi_{i,T} \in \mathcal{V}_1$ determined by the nodal degrees of freedom $v_i$, $i \in \mathcal{I}$, each IFE shape function, expressed by $\xi_T + \eta_T$ with $\eta_T = \sum_{i\in\mathcal{I}} c_i \eta_{i,T}$, is defined as a minimizer over $\xi_T + \mathcal{V}_2$ in terms of the semi-norms $|\cdot|_{\mathcal{J}_k}$ induced from the bilinear forms $\mathcal{J}_k$, $k = 1, 2$. The minimizer is solved from the least squares formulation by letting $J_k(\xi_T + \eta_T, \eta_{i,T})$=0, $i \in \mathcal{I}$, which satisfies the linear system

$$
\mathbf{A}^{(k)}\mathbf{c} = \mathbf{b}, \tag{3.9}
$$

with $\mathbf{b} = -\mathbf{B}^{(k)}\mathbf{v}$, $\boldsymbol{v} = (v_1, v_2, ..., v_{|I|})^T$ and $\boldsymbol{c} = (c_1, c_2, ..., c_{|I|})^T$, where

$$
\mathbf{A}^{(k)} = \left(\mathcal{J}_k(\eta_{i,T}, \eta_{j,T})\right)_{i,j\in\mathcal{I}} \in \mathbb{R}^{|\mathcal{I}|\times|\mathcal{I}|}, \tag{3.10}
$$

$$
\mathbf{B}^{(k)} = \left(\mathcal{J}_k(\xi_{i,T}, \eta_{j,T})\right)_{i,j\in\mathcal{I}} \in \mathbb{R}^{|\mathcal{I}|\times|\mathcal{I}|}. \tag{3.11}
$$

The existence of solutions to (3.9) is guaranteed by Theorem 2.1 in [5]. The authors in [5] also provided some conditions of the uniqueness of the minimizer. Then the IFE function associated with the nodal value vector $\mathbf{v}$ is defined as

$$
\phi_T = \begin{cases} \phi_T^- = \sum_{i\in\mathcal{I}^-} v_i\, \psi_{i,T} + \sum_{i\in\mathcal{I}^+} c_i\, \psi_{i,T}, & \text{on } T^-, \\ \phi_T^+ = \sum_{i\in\mathcal{I}^+} v_i\, \psi_{i,T} + \sum_{i\in\mathcal{I}^-} c_i\, \psi_{i,T}, & \text{on } T^+. \end{cases} \tag{3.12}
$$

Specifically, choosing $\mathbf{v} = \mathbf{e}_i$, with $\mathbf{e}_i = (0, \cdots, 1 \cdots, 0)^T$, $i =, 1, 2, ..., |\mathcal{I}|$, the $\phi_T$ in (3.12) becomes a local IFE shape function $\phi_{i,T}$ on the interface element $T$.

In summary, the local IFE space on an element $T \in \mathcal{T}_h$, which is either an interface element or a non-interface element, can be defined as

$$S^p_{k,h}(T) = \begin{cases} \text{Span}\left\{\phi_{i,T},\ i = 1, 2, \cdots, |\mathcal{I}|\right\}, & \text{for } \ T \in \mathcal{T}^i_h, \\ \text{Span}\left\{\psi_{i,T},\ i = 1, 2, \cdots, |\mathcal{I}|\right\}, & \text{for } \ T \in \mathcal{T}^n_h, \end{cases} \tag{3.13}$$

where $k = 1, 2$ according to the given jump condition. Again we refer readers to [5] for more details in this formulation.

The similar idea is also used in CutFEM [29] which minimizes an energy globally involving the Nitsche's penalty on the interface. In that method, if one of the subelements is too small, the whole scheme becomes unstable and some special weights related to the area of the subelements need to be added in the penalty for stablization. Similar phenomena is also observed in [5] that $\mathbf{A}^{(k)}$ in the linear system (3.9) becomes extremely ill-conditioned when $T^-$ or $T^+$ is too small. So instead of imposing the bilinear forms on $\Gamma \cap T$, the authors in [5] considered an extended interface $\Gamma_T$ out of the interface element. By such a strategy, the conditioning can be improved, but still not satisfactory in some extreme cases that the condition number can be as bad as $10^{16}$ according to the example given in [5].

## 3.3 IFE shape functions by a fictitious element

To further improve the conditioning of the linear system (3.9), we propose not only to extend the local interface, but also extend the element, i.e., for the purpose of constructing IFE shape functions on an interface element, we consider a fictitious element associated with this interface element. The motivation behind this idea is that the subelements on a fictitious element can not have an extremely small size.

### 3.3.1 Construction of fictitious elements

In this subsection, we describe the construction of fictitious elements by a similarity transformation. Specifically, for each interface element $T = \triangle A_1A_2A_3$ whose center of gravity is denoted by $G$, we define its fictitious element as $T_\lambda = \Delta A_1'A_2'A_3'$ such that $A_i'$ is on the line determined by $\overline{GA_i}$ with $|\overline{A_i'A_i}|/|\overline{GA_i}| = \lambda$, where $\lambda$ is a non-negative parameter, see the illustration in Figure 3.1. Here $\lambda$ is used to control the size of $T_\lambda$ and we call it the extension ratio. It is obvious that the constructed fictitious element $T_\lambda$ is similar to the interface element $T$ such that

$$\frac{|\overline{A_i'A_j'}|}{|\overline{A_iA_j}|} = 1 + \lambda, \quad i, j \in \{1, 2, 3\},\ i \neq j. \tag{3.14}$$

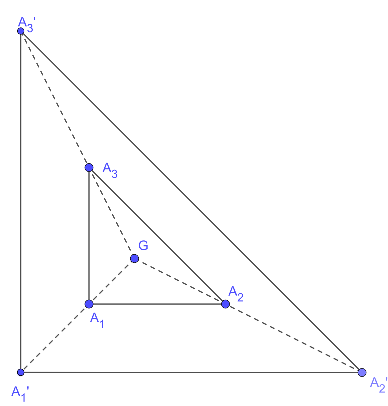


Figure 3.1: sketch of the construction of the fictitious element

On an interface element $T$, an unfavorable case may happen that one of the subelements $T^-$ and $T^+$ is too small, which may make the linear system (3.9) ill conditioned. To investigate how small a subelement can be compared to the whole element, given any measurable set $\widetilde{\Omega}$ such that $\widetilde{\Omega} \cap \Gamma \neq \emptyset$, we define

$$r(\tilde{\Omega}) = \min_{s=-,+} \left\{ \frac{|\tilde{\Omega}^s|}{|\tilde{\Omega}|} \right\}. \tag{3.15}$$

Obviously $r(\tilde{\Omega}) \leqslant 1$. In the following, we show that it is possible to choose a suitable extension ratio such that both of the two subelements in the fictitious element $T_\lambda$ are not too small so that $r(T_\lambda)$ is lower bounded by a certain positive constant.

**Lemma 3.1.** *For $\lambda \in [0, 3]$, assume that $\Gamma$ is a straight line inside the fictitious element $T_\lambda$ of an interface element $T$, then the following holds:*

$$r(T_\lambda) \geqslant \frac{4\lambda^2}{9(\lambda+1)^2}. \tag{3.16}$$

*Proof.* Without loss of generality, we assume $\Gamma$ cuts the edges $A_1A_3$ and $A_2A_3$. Consider an auxiliary element $\tilde{T}_\lambda$ with the same vertices as $T_\lambda$ and an auxiliary linear interface $\tilde{\Gamma}$ such that $\tilde{\Gamma}$ is parallel to $\Gamma$ but goes through the vertex $A_3$. It is clearly that $r(T_\lambda) \geqslant r(\tilde{T}_\lambda)$. In addition, we shall note that the function $r$ is invariable under linear transformation. Therefore, without loss of generality, we only consider the case that the fictitious element $T_\lambda$ is the reference element, i.e., $A_1' = (0,0), A_2' = (1,0), A_3' = (0,1)$ and $\Gamma$ cuts through the vertex $A_3$. In the following, we let the equation of the linear interface be $y = kx + b$ and separate our discussion into three cases.

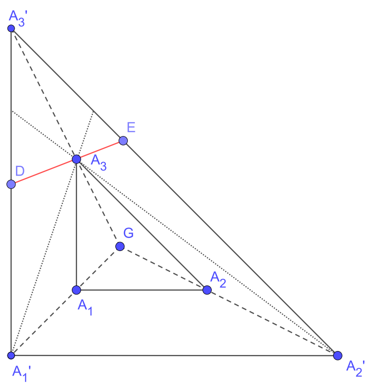


Figure 3.2: case 1

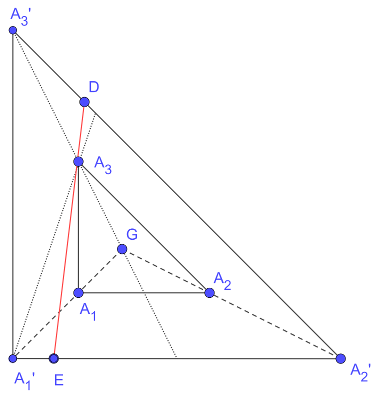


Figure 3.3: case 2

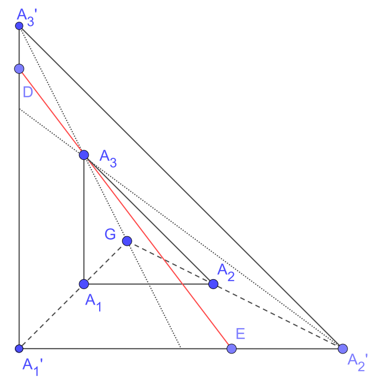


Figure 3.4: case 3

**Case 1**: the interface $\Gamma$ cuts the edges $A_1'A_3'$ and $A_3'A_2'$, as shown in Figure 3.2. In this case, the interface can only vary above the two rays $A_3A_1'$ and $A_3A_2'$ which have the slope $1+\frac{3}{\lambda}$ and $-\frac{3+\lambda}{3+2\lambda}$, respectively. Hence we have $k \in [-\frac{3+\lambda}{3+2\lambda}, 1+\frac{3}{\lambda}]$. Then, by direct computation, we have

$$\frac{|\Delta DEA_3'|}{|\Delta A_1'A_2'A_3'|} = \frac{\lambda^2(k+2)^2}{9(1+\lambda)^2(k+1)} := f(k).$$

One can directly verify that the minimal and maximal values of $f(k)$ over $k \in [-\frac{3+\lambda}{3+2\lambda}, 1+\frac{3}{\lambda}]$ are given by

$$f_{min} = f(0) = \frac{4\lambda^2}{9(\lambda+1)^2}, \qquad f_{max} = f\left(1+\frac{3}{\lambda}\right) = f\left(-\frac{3+\lambda}{3+2\lambda}\right) = \frac{\lambda}{3+2\lambda}.$$

Therefore

$$r(T_\lambda) \geqslant \min\{f_{min}, 1-f_{max}\} = \frac{4\lambda^2}{9(\lambda+1)^2}. \tag{3.17}$$

**Case 2**: the interface $\Gamma$ cuts the edges $A_2'A_3'$ and $A_2'A_1'$, as shown in Figure 3.3. By an argument similar to above, we have $k \in (-\infty, -2] \cup [\frac{\lambda+3}{\lambda}, \infty)$ and

$$\frac{|\Delta DEA_2'|}{|\Delta A_1'A_2'A_3'|} = \frac{(3+\lambda+3k+2\lambda k)^2}{9(1+\lambda)^2 k(k+1)} := f(k).$$

It can be directly verified that for $k \in (-\infty, -2] \cup [\frac{\lambda+3}{\lambda}, \infty)$, $\lambda \leqslant 3$,

$$f_{\min} = f(-2) = \frac{1}{2}, \qquad f_{\max} = f\left(\frac{\lambda+3}{\lambda}\right) = \frac{3+\lambda}{3+2\lambda}.$$

Therefore, for this case we have

$$r(T_\lambda) \geqslant \min\{f_{\min}, 1 - f_{\max}\} = \frac{\lambda}{3+2\lambda}. \tag{3.18}$$

**Case 3**: $\Gamma$ cuts the edges $A_3'A_1'$ and $A_1'A_2'$, as it is shown in Figure 3.4. In this case, the slope $k$ can only vary over $[-2, -\frac{\lambda+3}{2\lambda+3}]$ and we have

$$\frac{|\Delta D A_1' E|}{|\Delta A_1' A_2' A_3'|} = \frac{(\lambda - \lambda k + 3)^2}{-9k(1+\lambda)^2} := f(k).$$

For $k \in [-2, -\frac{\lambda+3}{2\lambda+3}]$, the straightforward calculation yields

$$f_{\min} = f(-2) = \frac{1}{2}, \qquad f_{\max} = f\left(-\frac{\lambda+3}{2\lambda+3}\right) = \frac{3+\lambda}{3+2\lambda}.$$

Hence, we have

$$r(T_\lambda) \geqslant \min\{r_{\min}, 1 - r_{\max}\} = \frac{\lambda}{3+2\lambda}. \tag{3.19}$$

Then the desired result (3.16) follows from the estimates (3.17), (3.18) and (3.19).

□

Utilizing the above lemma, we can derive the following theorem that can provide a lower bound for $r(T_\lambda)$ when $\Gamma$ is a generic curve and when mesh size $h$ is sufficiently small.

**Theorem 3.1.** *For $\lambda \in [0, 3]$, there exists a constant $C$ independent of the interface location* *such that the following holds for an interface independent mesh $\mathcal{T}_h$ with $h$ small enough:*

$$r(T_\lambda) \geqslant \frac{4\lambda^2}{9(1+\lambda)^2} - Ch, \quad \forall T \in \mathcal{T}_h^i \tag{3.20}$$

*Proof.* According to the assumptions **(H1)** and **(H2)**, we can let $D$ and $E$ be the intersection points of $\Gamma$ with $\partial T$. Assume the line $\overline{DE}$ partitions the fictitious element $T_\lambda$ into $\overline{T}_\lambda^-$ and $\overline{T}_\lambda^+$. Lemma 3.1 shows that

$$\min_{s=-,+} \left\{ \frac{|\overline{T}_\lambda^s|}{|T_\lambda|} \right\} \geqslant \frac{4\lambda^2}{9(1+\lambda)^2}. \tag{3.21}$$

Consider the region $\omega_\lambda = (\overline{T}_\lambda^- \cap T_\lambda^+) \cup (\overline{T}_\lambda^+ \cap T_\lambda^-)$ which is the subelement of $T_\lambda$ bounded by the segment $\overline{DE}$ and the interface $\Gamma$. From [100], there exists a constant $C$ independent of the interface location such that $|\omega_\lambda| \leqslant Ch^3$. Using (3.21) and the fact $|T_\lambda| = \mathcal{O}(h^2)$, we have

$$\min_{s=-,+} \left\{ \frac{|T_\lambda^s|}{|T_\lambda|} \right\} \geqslant \min_{s=-,+} \left\{ \frac{|\overline{T}_\lambda^s| - |\omega_\lambda|}{|T_\lambda|} \right\} \geqslant \frac{4\lambda^2}{9(1+\lambda)^2} - Ch. \tag{3.22}$$

□

Theorem 3.1 suggests that, for a mesh fine enough, the subelements of fictitious elements partitioned by the interface curve can not be extremely small for a suitably chose $\lambda > 0$. As an example, provided that the mesh is fine enough ($h$ is small enough), when $\lambda = 0.5$ and $\lambda = 1$, the most unfavorable situation is that the smaller $T_\lambda{}^s$ $(s = -, +)$ will account for about $1/20$ and $1/10$ of the total area of $T_\lambda$, respectively. We believe the fundamental geometric estimation in Theorem 3.1 might be useful for establishing theoretical analysis of the conditioning of (3.9) related to fictitious elements.

### 3.3.2 Local IFE shape functions on interface elements

Now we discuss the construction of local IFE spaces on interface elements through their fictitious elements. For simplicity of presentation, in the following discussion, we denote $\mathcal{J}_k^\lambda$, $k = 1, 2$ as the bilinear forms $\mathcal{J}_k$ in (3.8) defined on $\Gamma_T = \Gamma \cap T_\lambda$, $\lambda \geqslant 0$. In particular, $\mathcal{J}_k^0$ is defined on the portion of interface inside the original interface element, i.e., $\Gamma_T = \Gamma \cap T$. After choosing a suitable extension ratio $\lambda$, we can use the following procedure to construct the proposed local IFE shape functions on every interface element $T \in \mathcal{T}_h^i$:

**Algorithm 3.1** Construction of local IFE shape functions

**step 1**: construct a fictitious element $T_\lambda$ associated with $T$, then generate the local basis functions $\xi_{i,T_\lambda}$ and $\eta_{i,T_\lambda}$ on $T_\lambda$;

**step 2**: form the bilinear forms $J_k^\lambda$, $k = 1, 2$ in (3.7) and (3.8) according to the given extended jump conditions on $\Gamma_T = \Gamma \cap T_\lambda$;

**step 3**: form the matrices $\mathbf{A}_\lambda^{(k)} = (\mathcal{J}_k^\lambda(\eta_{i,T_\lambda}, \eta_{j,T_\lambda}))_{i,j\in\mathcal{I}}$ and $\mathbf{B}_\lambda^{(k)} = (\mathcal{J}_k^\lambda(\xi_{i,T_\lambda}, \eta_{j,T_\lambda}))_{i,j\in\mathcal{I}}$, and solve for the coefficients $\mathbf{c}_i$ from $\mathbf{A}_\lambda^{(k)}\mathbf{c}_i = -\mathbf{B}_\lambda^{(k)}\mathbf{e}_i$ with $\mathbf{e}_i = (0, \cdots, 1 \cdots, 0)^T$ being the $i$-th unit vector;

**step 4**: use $\mathbf{c} = \mathbf{c}_i$, $i \in \mathcal{I}$, in step 3 to form $\phi_{i.T_\lambda}$ as a piecewise polynomial on $T_\lambda^-$ and $T_\lambda^+$ by (3.12), then generate the shape functions on the interface element $T$ by restricting $\phi_{i.T_\lambda}$ to $T$:

$$\phi_{i,T} = \phi_{i,T_\lambda}|_T. \tag{3.23}$$

Then using (3.23), the new local IFE space $S_{k,h}^p(T)$ on the interface element $T \in \mathcal{T}_h^i$ is defined as

$$S_{k,h}^p(T) = \mathrm{Span}\left\{\phi_{i,T},\ i = 1, 2, \cdots, |\mathcal{I}|\right\}, \quad k = 1, 2. \tag{3.24}$$

Compared to the original construction approach in [5], in the proposed approach in Algorithm 3.1, the computations in the least squares framework for constructing the $p$-th degree IFE shape functions are carried out on the fictitious element $T_\lambda$ instead of the interface element $T$ itself such that the involved matrices are

$$\mathbf{A}_\lambda^{(k)} = (\mathcal{J}_k^\lambda(\eta_{i,T_\lambda}, \eta_{j,T_\lambda}))_{i,j\in\mathcal{I}}, \quad \text{and} \quad \mathbf{B}_\lambda^{(k)} = (\mathcal{J}_k^\lambda(\xi_{i,T_\lambda}, \eta_{j,T_\lambda}))_{i,j\in\mathcal{I}}.$$

We note that these matrices are not only generated by the bilinear forms defined on a relatively larger interface portion $\Gamma_T = \Gamma \cap T_\lambda$, but also formed by the Lagrange polynomials $\xi_{i,T_\lambda}$ and $\eta_{i,T_\lambda}$ associated with a relatively larger element $T_\lambda$. Furthermore, according to Theorem 2.1 in [5], the local IFE shape functions also always exist in this approach.

To demonstrate the effectiveness of the proposed construction method based on the fictitious element, we apply the method to a particular interface element $T$ with vertices $(-0.6, 0)$, $(-0.4, 0)$, $(-0.6, 0.2)$ and its fictitious elements $T_\lambda$ with $\lambda = 0.5$, 1 and 1.5. We assume to use the Laplacian extended jump conditions, i.e., using the bilinear form $\mathcal{J}_2^\lambda$ and we present numerical results to show the effects on the condition numbers of the corresponding matrices $\mathbf{A}_\lambda^{(2)}$. In these numerical results, we consider a series of circular interfaces $\Gamma : x^2 + y^2 - r^2 = 0$ with $r = 0.42,\ 0.41,\ 0.405$ and $0.401$. The interface element (fictitious element) is cut by the interface curve $\Gamma$ into the left sub-element $T^+$ ($T_\lambda^+$) and the right sub-element $T^-$ ($T_\lambda^-$). An extreme case was shown in Figure 3.5 with $r = 0.401$ where we can see the original right sub-element $T^-$ is very small while the right sub-elements $T_\lambda^-$ of fictitious ones are relatively larger.

In addition, we fix $\beta^- = 1$, let $\beta^+ = 10$ or 50 and compute the condition numbers of $\mathbf{A}_\lambda^{(2)}$ for the quadratic and cubic polynomials associated with the original element $T$, see Table 3.1, and the fictitious elements, see Tables 3.2-3.4. The numerical results clearly confirm our expectation that the conditioning of $\mathbf{A}_\lambda^{(2)}$, $\lambda = 0.5, 1, 1.5$, is significantly better than the conditioning of $\mathbf{A}_0^{(2)}$, especially for the cases that $T^-$ is extremely small. In particular, the results show the pattern that the condition numbers will stay around a certain magnitude depending on the ratio $\beta^+/\beta^-$ and the polynomial degree, as $\lambda$ increases beyond some value. This observation suggests that it is not necessary to choose $\lambda$ to be very large in real computation.

We also have carried out numerical experiments for computing the condition numbers of $\mathbf{A}_\lambda^{(1)}$ (the normal extended jump conditions) with various $\lambda$, $\beta^-$ and $\beta^+$, and we have observed similar phenomena. The improved conditioning of the linear system to determine the coefficients of IFE shape functions by using fictitious elements inspires us to discuss the approximation capabilities of the constructed higher degree IFE spaces, which will be presented in the next section.

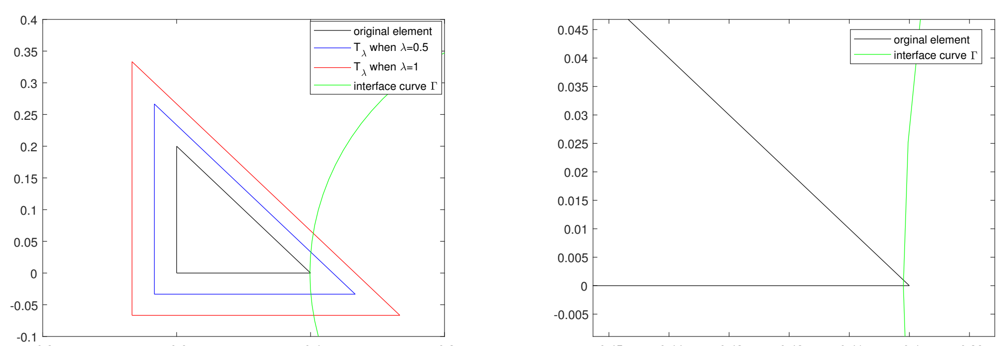


Figure 3.5: left: the interface curve $\Gamma$ intersects the original element $T$ and its fictitious elements $T_\lambda$ for different $\lambda$; right: the zoom-in view of $\Gamma$ intersecting original element $T$.

| | $\beta_2 = 10, p = 2$ | $\beta_2 = 10, p = 3$ | $\beta_2 = 50, p = 2$ | $\beta_2 = 50, p = 3$ |
|---|---|---|---|---|
| $r = 0.42$ | 9.3408E+06 | 1.7619E+12 | 2.1177E+08 | 4.4394E+13 |
| $r = 0.41$ | 1.9990E+08 | 5.4211E+14 | 4.5242E+09 | 1.3255E+16 |
| $r = 0.405$ | 3.8133E+09 | 1.5957E+17 | 8.6070E+10 | 1.2160E+18 |
| $r = 0.401$ | 2.7868E+12 | 2.8297E+18 | 6.2597E+13 | 7.5143E+19 |

Table 3.1: Condition number of $\mathbf{A}^{(2)}$ on the original interface element $T$.

| | $\beta_2 = 10, p = 2$ | $\beta_2 = 10, p = 3$ | $\beta_2 = 50, p = 2$ | $\beta_2 = 50, p = 3$ |
|---|---|---|---|---|
| $r = 0.42$ | 6.0635E+04 | 1.2803E+08 | 1.2778E+06 | 2.7307E+09 |
| $r = 0.41$ | 1.0988E+05 | 2.8910E+08 | 2.3339E+06 | 7.3167E+09 |
| $r = 0.405$ | 1.5183E+05 | 4.7575E+08 | 3.2372E+06 | 1.2299E+10 |
| $r = 0.401$ | 1.9962E+05 | 7.5319E+08 | 4.2688E+06 | 1.9469E+10 |

Table 3.2: Condition number of $\mathbf{A}_\lambda^{(2)}$ on $T_\lambda$ when $\lambda = 0.5$.

| | $\beta_2 = 10, p = 2$ | $\beta_2 = 10, p = 3$ | $\beta_2 = 50, p = 2$ | $\beta_2 = 50, p = 3$ |
|---|---|---|---|---|
| $r = 0.42$ | 1.3469E+04 | 8.0643E+07 | 2.4519E+05 | 1.7465E+09 |
| $r = 0.41$ | 1.8638E+04 | 1.3409E+08 | 3.4575E+05 | 2.8925E+09 |
| $r = 0.405$ | 2.2237E+04 | 2.7091E+07 | 4.1502E+05 | 5.0375E+08 |
| $r = 0.401$ | 2.5759E+04 | 3.3369E+07 | 4.8269E+05 | 6.2290E+08 |

Table 3.3: Condition number of $\mathbf{A}_\lambda^{(2)}$ on $T_\lambda$ when $\lambda = 1$.

| | $\beta_2 = 10, p = 2$ | $\beta_2 = 10, p = 3$ | $\beta_2 = 50, p = 2$ | $\beta_2 = 50, p = 3$ |
|---|---|---|---|---|
| $r = 0.42$ | 6.6256E+03 | 2.4006E+07 | 9.9996E+04 | 4.4647E+08 |
| $r = 0.41$ | 7.9543E+03 | 3.6492E+07 | 1.2334E+05 | 6.9655E+08 |
| $r = 0.405$ | 8.7862E+03 | 4.4968E+07 | 1.3817E+05 | 8.5857E+08 |
| $r = 0.401$ | 9.5606E+03 | 5.3157E+07 | 1.5194E+05 | 1.0142E+09 |

Table 3.4: Condition number of $\mathbf{A}_\lambda^{(2)}$ on $T_\lambda$ when $\lambda = 1.5$.

## 3.4 Approximation capabilities

We can use the local IFE space constructed by the least squares method with fictitious elements to construct a global $p$-th degree IFE space as follows:

$$S_{k,h}^p(\Omega) = \left\{ v \in L^2(\Omega) \ : \ v|_T \in S_{k,h}^p(T) \ \ \forall T \in \mathcal{T}_h \right\}, \tag{3.25}$$

where $k = 1, 2$ according to the given extended jump conditions. We use the $L^2$ projection to demonstrate that this IFE space has the optimal approximation capability. Specifically, for a function $u$ smooth enough, we define its $p$-th degree local IFE projection on each element $T \in \mathcal{T}_h$ as $P_{h,T}u \in S_{k,h}^p(T)$ such that

$$(u - P_{h,T}u, v)_T = 0, \quad \forall v \in S_{k,h}^p(T), \tag{3.26}$$

where $(\cdot,\cdot)_T$ is the standard $L^2$ inner product on each element $T \in \mathcal{T}_h$. Accordingly, we can define the $p$-th degree global IFE projection of $u$ as $P_h u \in S_{k,h}^p(\Omega)$ such that

$$(P_h u)|_T = P_{h,T}u, \quad \forall T \in \mathcal{T}_h. \tag{3.27}$$

We perform the computations of projection errors on the domain $\Omega = (-1,1)\times(-1,1)$ with the circular interface $\Gamma : x^2 + y^2 - r_0^2 = 0$, $r_0 = \pi/6.28$ and the subdomains

$$\Omega^- = \left\{(x,y) : x^2 + y^2 < r_0^2\right\}, \quad \Omega^+ = \Omega \backslash \overline{\Omega^-}.$$

We consider the following function $u$:

$$u(x,y) = \begin{cases} \frac{1}{\beta^-} r^\alpha, & (x,y) \in \Omega^-, \\ \frac{1}{\beta^+} r^\alpha + \left(\frac{1}{\beta^-} - \frac{1}{\beta^+}\right) r_0^\alpha, & (x,y) \in \Omega^+, \end{cases} \tag{3.28}$$

where $r = \sqrt{x^2+y^2}$, $\alpha = 7$, $\beta^- = 1$, $\beta^+ = 5$ or 50. We note that this function (3.28) satisfies both types of the extended jump conditions.

The computations are carried out on a sequence of triangular Cartesian meshes, with the size specified in Table 3.5 . We use $\lambda = 0.5$ for the fictitious elements in the construction of the local IFE spaces on interface elements. The convergence rates are generated by the projection errors on two consecutive meshes.

Clearly, the numerical results demonstrate that with the stabilization using fictitious elements, IFE spaces constructed with either the normal or the Laplacian extended jump conditions show the optimal approximation capabilities in terms of the $L^2$ norm and $H^1$ semi-norm. We have also carried computations with other choices of $\lambda$, $\beta^\pm$, and similar behaviors can be observed.

| $\beta$, $h$ | | normal | | | | Laplacian | | | |
|---|---|---|---|---|---|---|---|---|---|
| $\beta^+$ | $h$ | $\|u-P_hu\|_{0,\Omega}$ | rate | $\|u-P_hu\|_{1,\Omega}$ | rate | $\|u-P_hu\|_{0,\Omega}$ | rate | $\|u-P_hu\|_{1,\Omega}$ | rate |
| 5 | 1/10 | 1.8506e-04 | NA | 7.9069e-02 | NA | 1.8329e-04 | NA | 7.9002e-02 | NA |
| | 1/20 | 1.0445e-05 | 4.1471 | 1.0027e-02 | 2.9793 | 1.0329e-05 | 4.1493 | 1.0023e-02 | 2.9786 |
| | 1/40 | 6.3384e-07 | 4.0425 | 1.2590e-03 | 2.9934 | 6.2787e-07 | 4.0401 | 1.2588e-03 | 2.9932 |
| | 1/80 | 3.8887e-08 | 4.0268 | 1.5765e-04 | 2.9975 | 3.8578e-08 | 4.0246 | 1.5762e-04 | 2.9975 |
| | 1/160 | 2.3968e-09 | 4.0201 | 2.9991e-05 | 2.9991 | 2.3871e-09 | 4.0144 | 1.9717e-05 | 2.9989 |
| 50 | 1/10 | 4.7679e-05 | NA | 1.0041e-02 | NA | 4.2242e-05 | NA | 9.8978e-03 | NA |
| | 1/20 | 2.8530e-06 | 4.0628 | 1.6140e-03 | 2.6372 | 2.7934e-06 | 3.9186 | 1.6081e-03 | 2.6218 |
| | 1/40 | 1.6521e-07 | 4.1101 | 2.1477e-04 | 2.9098 | 1.6131e-07 | 4.1141 | 2.1435e-04 | 2.9073 |
| | 1/80 | 9.6341e-09 | 4.1000 | 2.7995e-05 | 2.9396 | 9.4858e-09 | 4.0879 | 2.7979e-05 | 2.9376 |
| | 1/160 | 5.6426e-10 | 4.0937 | 3.5774e-06 | 2.9681 | 5.6644e-10 | 4.0658 | 3.5841e-06 | 2.9646 |

Table 3.5: Projection errors and convergence rates for cubic IFE spaces using normal and Laplacian extended jump conditions, $\beta^- = 1$, $\beta^+ = 5$ and 50, $\lambda = 0.5$.

## 3.5 Conclusion

Using the fictitious finite elements, we propose a stabilized construction of higher degree IFE spaces based on the least squares framework proposed in [5]. Significant improvement of conditioning in constructing the local IFE shape functions is observed through numerical experiments. And we have also observed the optimal approximation capability of the constructed higher degree IFE spaces in the numerical experiments.

# Chapter 4

# Improved error estimation for some IFE methods for elliptic interface problems

## 4.1 Introduction

In this chapter, we study the error estimation for IFE methods for the model elliptic interface problem (1.2) under piecewise $H^2$ regularity of the exact solution. Our study will focus on the following fundamental elliptic interface problems:

$$-\nabla \cdot (\beta \nabla u) = f, \quad \text{in } \Omega = \Omega^- \cup \Omega^+, \tag{4.1a}$$

$$u = g, \quad \text{on } \partial\Omega, \tag{4.1b}$$

where the domain $\Omega \subseteq \mathbb{R}^2$ is divided by an interface curve $\Gamma$ into two subdomains $\Omega^-$ and $\Omega^+$ on which the coefficient $\beta$ is a positive piecewise constant function defined as

$$\beta(X) = \begin{cases} \beta^- & \text{for } X \in \Omega^-, \\ \beta^+ & \text{for } X \in \Omega^+, \end{cases} \tag{4.1c}$$

with the following jump conditions

$$[u]_\Gamma \;:=\; u^+|_\Gamma - u^-|_\Gamma = 0, \tag{4.1d}$$

$$\left[\beta\nabla u\cdot\mathbf{n}\right]_\Gamma \;:=\; \beta^+\nabla u^+\cdot\mathbf{n}|_\Gamma - \beta^-\nabla u^-\cdot\mathbf{n}|_\Gamma = 0, \tag{4.1e}$$

where $\mathbf{n}$ is the unit normal vector to the interface $\Gamma$.

In the error estimation to be presented, we first introduce a new energy norm stronger than the one used in [111]. Inspired by [67], we derive an estimate for the IFE interpolation error gauged by this energy norm by using the patches of interface elements. Furthermore, under this energy norm, the continuity and coercivity both hold for the bilinear form in the PPIFE method developed in [111]. Thanks to these properties, we are able to derive an error bound for the PPIFE solution in the energy norm under the standard piecewise $H^2$ regularity assumption. The improved estimation further enables us to show the optimal convergence in the $L^2$ norm, which, to our best knowledge, has not been reported in the literature for this PPIFE method. This chapter consists of four additional sections. In Secton 4.2, we re-derive the PPIFE method for the elliptic interface problems. In Section 4.3, we introduce the patches for the interface elements and discuss the approximation capabilities of IFE spaces on these patches. In Section 4.4 we show the optimal convergence of the PPIFE solution. Finally, we make some conclusions in Section 4.5.

## 4.2 PPIFE methods for elliptic interface problems

Here, we re-derive the PPIFE methods discussed in [111] in a slightly more general configuration that allows the interface to intersect with the boundary of the domain (i.e. $\Gamma \cap \partial\Omega \neq \emptyset$). As usual, multiply equation (4.1a) by a function $v \in V_{h,0}(\Omega)$ and integrate on each element $T \in \mathcal{T}_h$, where $\mathcal{T}_h$ is either a triangular mesh or a rectangular mesh on the domain $\Omega$. Then, by Green's formula and the interface jump condition (4.1e), it follows:

$$\int_T \beta \nabla u \nabla v dX - \int_{\partial T} \beta \nabla u \cdot \boldsymbol{n_T} v ds - \int_{\Gamma \cap T} \{\beta \nabla u \cdot \boldsymbol{n_\Gamma}\}[v] ds = \int_T f v dX, \tag{4.2}$$

where the third term on the left hand side of (4.2) disappears because $v|_T \in H^1(T)$, $\forall T \in \mathcal{T}_h$. We recall some set notations about the edges in Chapter 2: the set of interior edges is $\mathring{\mathcal{E}}_h$, the set of interface edges is $\mathcal{E}_h^i$, the set of interior interface edges is $\mathring{\mathcal{E}}_h^i$, the set of boundary edges is $\mathcal{E}_h^b$, the set of boundary interface edges is $\mathcal{E}_h^{bi}$. Then, summing (4.2) over all $T \in \mathcal{T}_h$ leads to

$$\sum_{T \in \mathcal{T}_h} \int_T \beta \nabla u \nabla v dX - \sum_{e \in \mathring{\mathcal{E}}_h} \int_e \{\beta \nabla u \cdot \boldsymbol{n_e}\}[v] ds - \sum_{e \in \mathcal{E}_h^b} \int_e \beta \nabla u \cdot \boldsymbol{n_e} v ds = \int_\Omega f v dX. \tag{4.3}$$

By assuming that $u$ is in $PH^2(\Omega)$ so that $[u]_e = 0$, $\forall e \in \mathring{\mathcal{E}}_h$ , we have

$$\epsilon \sum_{e \in \mathring{\mathcal{E}}_h^i} \int_e \{\beta \nabla v \cdot \mathbf{n}_e\}_e [u]_e ds = 0, \quad \sum_{e \in \mathring{\mathcal{E}}_h^i} \frac{\sigma_e^0}{|e|} \int_e [u]_e \, [v]_e ds = 0, \tag{4.4}$$

with parameters $\epsilon$, and $\sigma_e^0 \geq 0$. Add these two terms in (4.4) to the left side of (4.3). Also add the terms $\epsilon \sum_{e \in \mathcal{E}_h^{bi}} \int_e \{\beta \nabla v \cdot \mathbf{n}_e\}_e [u]_e ds$ and $\sum_{e \in \mathcal{E}_h^{bi}} \frac{\sigma_e^0}{|e|} \int_e [u]_e \, [v]_e ds$ on both sides of (4.3), then we can see that the solution $u$ to the elliptic interface problem (4.1) satisfies the following weak form:

$$a_h(u, v) = L_f(v), \qquad \forall v \in V_{h,0}(\Omega), \tag{4.5}$$

where the bilinear form $a_h(\cdot, \cdot) : V_h(\Omega) \times V_h(\Omega) \to \mathbb{R}$ and the linear form $L_f : V_h(\Omega) \to \mathbb{R}$

are given by

$$\begin{aligned}
a_h(u,v) \;&=\; \sum_{T\in\mathcal{T}_h}\int_T \beta\nabla u\cdot\nabla v dX - \sum_{e\in\mathring{\mathcal{E}}_h^i}\int_e \{\beta\nabla u\cdot\mathbf{n}_e\}_e[v]_e ds \\
&+\epsilon\sum_{e\in\mathring{\mathcal{E}}_h^i}\int_e \{\beta\nabla v\cdot\mathbf{n}_e\}_e[u]_e ds + \sum_{e\in\mathring{\mathcal{E}}_h^i}\frac{\sigma_e^0}{|e|}\int_e [u]_e\,[v]_e ds \qquad (4.6)\\
&-\sum_{e\in\mathcal{E}_h^{bi}}\int_e \beta\nabla u\cdot\mathbf{n}_e v ds + \epsilon\sum_{e\in\mathcal{E}_h^{bi}}\int_e \beta\nabla v\cdot\mathbf{n}_e u ds + \sum_{e\in\mathcal{E}_h^{bi}}\frac{\sigma_e^0}{|e|}\int_e u\,v ds,\\
L_f(v) \;&=\; \int_\Omega f v dX + \sum_{e\in\mathcal{E}_h^{bi}}\frac{\sigma_e^0}{|e|}\int_e v g ds + \epsilon\sum_{e\in\mathcal{E}_h^{bi}}\int_e \beta\nabla v\cdot\mathbf{n}_e g ds. \qquad (4.7)
\end{aligned}$$

By enforcing the continuity on the mesh nodes, we can define the global IFE space as

$$\begin{aligned}
S_h(\Omega) =&\Big\{v\in L^2(\Omega)\ :\ v|_T\in S_h(T),\ \forall T\in\mathcal{T}_h, v \text{ is continuous at each } A_i\in\mathcal{N}_h\Big\},\\
S_{h,0}(\Omega) =&\Big\{v\in L^2(\Omega)\ :\ v\in S_h(\Omega),\ \ v|_{\partial\Omega\setminus\mathcal{E}_h^{bi}}=0\Big\},
\end{aligned} \qquad (4.8)$$

where $S_h(T)$ is the local IFE space on the element $T\in\mathcal{T}_h$ defined by (2.11). Then, as in [111], the weak form (4.5) suggests us to consider the following PPIFE schemes for the interface problem (4.1): find $u_h\in S_h(\Omega)$ such that

$$a_h(u_h,v_h) = L_f(v_h),\quad \forall v_h\in S_{h,0}(\Omega). \qquad (4.9)$$

We follow [111, 127] to consider the PPIFE methods associated with three common choices $\epsilon = 0,-1,1$, respectively, and we call the corresponding PPIFE method the incomplete PPIFE (IPPIFE), the symmetric PPIFE (SPPIFE), and the non-symmetric PPIFE (NPPIFE) method, respectively.

## 4.3 Approximation capabilities on a patch

In this section, following similar ideas in [63, 64, 67], we consider the approximation capability of the IFE spaces locally around an interface element. We recall some notations about the set of elements defined in Chapter 2 that will be used in the later discussion: the set of interface elements $\mathcal{T}_h^i$, the set of interior interface elements $\mathring{\mathcal{T}}_h^i$, and the set of boundary interface elements $\mathcal{T}_h^{bi}$. For each interface element $T \in \mathcal{T}_h^i$ , we consider a patch around it defined as follows [63, 64]:

**Definition 4.1.** *(Patch of an interface element) For each interface element $T \in \mathcal{T}_h^i$, its patch is defined as the union of the neighbor elements:*

$$\omega_T = \cup \left\{ T' \in \mathcal{T}_h : \overline{T'} \cap \overline{T} \neq \phi \right\}. \tag{4.10}$$

Figure 4.1 and Figure 4.2 illustrate the patch of an interior interface element and a boundary interface element, respectively. In the analysis presented later, we make the following assumption on these patches [63]:

**Patch Assumption**: As it is shown in Figure 4.1 and Figure 4.2, for every interface element $T$ and its patch $\omega_T$, let $e$ be an interface edge of $T$. We assume that for $s = \pm$, there exists a triangle $T_e^s \subset \Omega^s \cap \omega_T$ and two constants $C_1$, $C_2$ independent of the interface location such that $e \cap T^s$ is one edge of $T_e^s$ and

$$C_1 |e \cap T^s| h \leq |T_e^s| \leq C_2 |e \cap T^s| h, \quad s = -, +. \tag{4.11}$$

For example, for the interface element $T = \triangle A_1 A_2 A_3$ and the interface edge $e = \overline{A_1 A_2}$ in

Figure 4.1 and Figure 4.2, it is easy to see that

$$T_e^+ = \triangle A_1 DP, \quad T_e^- = \triangle A_2 DQ$$

can be used to fulfill the Patch Assumption for this interface element $T$, here, $D \in e$ is the intersection point of the interface $\Gamma$ and $\partial T$, $P \in \omega_T$ and $Q \in \omega_T$ are points whose distance to the line passing $A_1$ and $A_2$ is about $h$. Basically, the inequality (4.11) to be satisfied in the Patch Assumption means that: the auxiliary triangle $T_e^s$ corresponding to the edge $e \cap T^s$ has a height $\mathcal{O}(h)$. We then summarize the conditions for the Patch Assumption to be satisfied in the following two remarks:

**Remark 4.1.** *As it is shown in Figure 4.1 for the interior interface elements $T \in \mathring{\mathcal{T}}_h^i$, when the mesh size $h$ is sufficient small so that the interface is locally flat enough, the Patch Assumption can be satisfied.*

**Remark 4.2.** *As it is shown in Figure 4.2 and Figure 4.3 for the boundary interface elements $T \in \mathcal{T}_h^{bi}$, the Patch Assumption can be satisfied under the following conditions (i) The mesh size $h$ is sufficient small so that the interface is locally flat enough. (ii) The mesh is sufficiently fine such that the interface $\Gamma$ does not cut the corner of the domain, i.e., only one edge of a boundary interface element is on the boundary of the domain. (iii) There is a constant $m$ independent of $\mathcal{T}_h$, such that $\min\{\overline{A_1D}, \overline{DA_2}\} \geq mh$; (iv) Let the acute angle between the interface and the boundary is $\alpha$, and $\tan(\alpha) \geq m/2$ (This condition is derived based on $\overline{MN} \geq mh$ in Figure 4.3).*

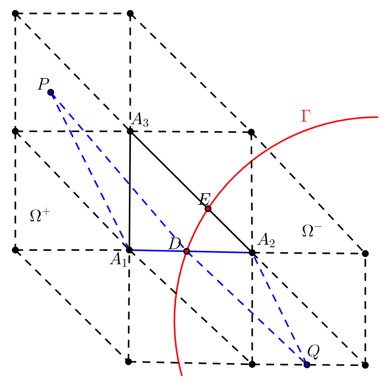


Figure 4.1: The patch of a triangular interior interface element

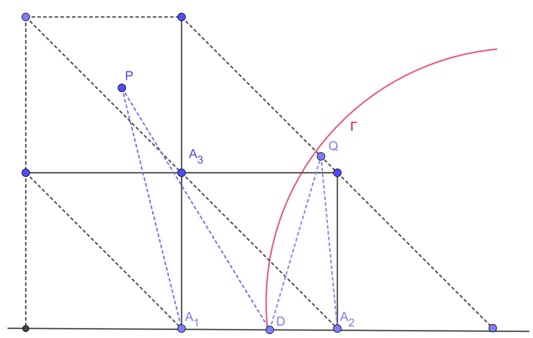


Figure 4.2: The patch of a triangular boundary interface element

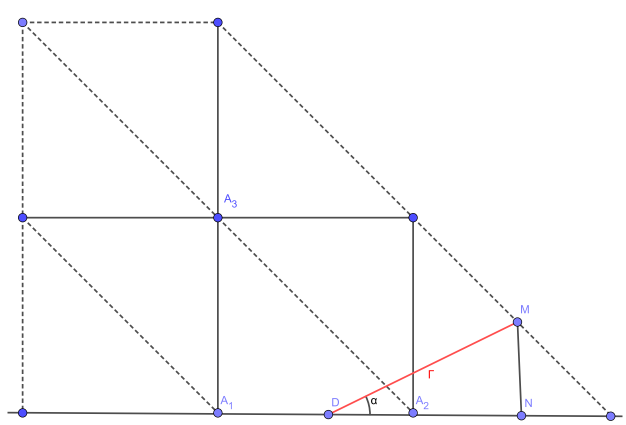


Figure 4.3: The patch of a triangular boundary interface element and the acute angle between the interface and the boundary

We now proceed to investigate the approximation capability of the IFE space on the patch of each interface element. As a preparation, we first consider a few subsets formed according to the interface geometry inside the patch of an interface element. Let $T$ be an interface element. We recall $l$ is the line that passes through the two intersection points of $\Gamma$ and $\partial T$. The interface $\Gamma$ and the line $l$ split the patch $\omega_T$ into the sub-patches $\omega_T^s$ and $\hat{\omega}_T^s$ ($s = \pm$), respectively. Let $\tilde{\omega}_T^s = \omega_T^s \cup \hat{\omega}_T^s$, $s = \pm$, and we can see that $\tilde{\omega}_T = (\tilde{\omega}_T^+ \cap \omega_T^-) \cup (\tilde{\omega}_T^- \cap \omega_T^+)$ is the sub-patch sandwiched between $l$ and $\Gamma$. Following [59, 60], we consider the sub-set

$$\omega_T^{int} = \cup \left\{ l_t \cap \omega_T : l_t \text{ is a tangent line to } \Gamma \cap \omega_T \right\}. \tag{4.12}$$

For every vertex $A_i$ of $T$, $i \in \mathcal{I}_T$, and each point $X \in \omega_T \backslash \omega_T^{int}$, the line segment $\overline{A_i X}$ has either zero or one intersection point with $\Gamma \cap \omega_T$. When there is no intersection point, $A_i$ and $X$ have to be on the same side of $\Gamma \cap \omega_T$; while when there is one intersection point, $A_i$ and $X$ are on the different sides of $\Gamma \cap \omega_T$. We further denote $\omega_T^{*,s} = (\hat{\omega}_T^s \cap \omega_T^s) \backslash \omega_T^{int}$, $s = \pm$, and $\omega_T^* = \omega_T \backslash (\omega_T^{*,-} \cup \omega_T^{*,+})$. By Lemma 3.4 of [60], when the mesh size is small enough, there holds

$$|\omega_T^*| \leq Ch^3. \tag{4.13}$$

For every $X \in \omega_T^{*,s}$, we let $Y_i(t, X) = tA_i + (1-t)X$. When $X$ and $A_i$ are on different sides of $\Gamma$, we let $\tilde{t}_i = \tilde{t}_i(X) \in [0, 1]$ such that $\tilde{Y}_i = Y_i(\tilde{t}_i, X)$ is on the curve $\Gamma \cap T$. Let $\mathbf{n}(\tilde{X}) = (\tilde{n}_x(\tilde{X}), \tilde{n}_y(\tilde{X}))$ be the normal vector to $\Gamma$ at every point $\tilde{X} \in \Gamma \cap \omega_T$. Recall $\bar{\mathbf{n}} = (\bar{n}_x, \bar{n}_y)$ be the normal vector to $l$ and denote $\tilde{X}^\perp$ as the projection of a point $\tilde{X}$ onto $l$. It can be shown, by the similar discussion as the Lemmas 3.1 and 3.2 in [57], that, for any $\tilde{X} \in \Gamma \cap \omega_T$, there holds

$$\|\tilde{X} - \tilde{X}^\perp\| \leq Ch^2, \quad \|\mathbf{n}(\tilde{X}) - \bar{\mathbf{n}}\| \leq Ch. \tag{4.14}$$

As in [71, 100], for a function $u \in H^2(\Omega^- \cup \Omega^+)$, we let $I_h u \in S_h(\Omega)$ be its IFE interpolation defined by

$$I_h u|_T = I_{h,T} u, \quad \text{with} \quad \begin{cases} I_{h,T} u(X) = \sum_{i \in \mathcal{I}_T} u(A_i) \phi_{i,T}(X), & \forall X \in T, \quad \forall T \in \mathcal{T}_h^i, \\ I_{h,T} u(X) = \sum_{i \in \mathcal{I}_T} u(A_i) \psi_{i,T}(X), & \forall X \in T, \quad \forall T \in \mathcal{T}_h^n. \end{cases}$$

On each interface element $T$, every IFE shape function $\phi_{i,T}(X), i \in \mathcal{I}_T$ can be naturally considered as a piecewise polynomial defined on the patch $\omega_T$ according to the sub-patches $\hat{\omega}_T^s, s = -, +$. Therefore, for a function $u \in H^2(\Omega^- \cup \Omega^+)$, we can consider its local IFE interpolation $I_{h,T} u(X)$ on an interface element $T$ as a piecewise polynomial defined on the patch $\omega_T$ according to sub-patches $\hat{\omega}_T^s, s = \pm$, and we proceed to the analysis of its accuracy in the rest of this section. In the discussions below, we denote $s = \pm, s' = \mp$, namely, $s$ and $s'$ take opposite signs whenever a formula have them both. Also, we adopt the following notations: $X = (x, y)$ and $x_1 = x, x_2 = y$.

Following the same arguments in [57], we have the following expansions for $I_h u - u$:

$$\begin{aligned} \partial_{x_d}(I_{h,T} u(X) - u(X)) = & \sum_{i \in \mathcal{I}^{s'}} (E_i^s + F_i^s) \partial_{x_d} \phi_{i,T}(X) \\ & + \sum_{i \in \mathcal{I}} R_i^s \partial_{x_d} \phi_{i,T}(X), \quad \forall X \in \omega_T^{*,s}, \quad s = \pm, \end{aligned} \tag{4.15}$$

$$\begin{aligned} \partial_{x_d x_{d'}} I_{h,T} u(X) = & \sum_{i \in \mathcal{I}^{s'}} (E_i^s + F_i^s) \partial_{x_d x_{d'}} \phi_{i,T}(X) \\ & + \sum_{i \in \mathcal{I}} R_i^s \partial_{x_d x_{d'}} \phi_{i,T}(X), \quad \forall X \in \omega_T^{*,s}, \quad s = \pm, \end{aligned} \tag{4.16}$$

$$\partial_{x_d} I_{h,T} u = \sum_{i \in \mathcal{I}} \tilde{R}_i \partial_{x_d} \phi_{i,T}(X), \quad \forall X \in \omega_T^*, \tag{4.17}$$

$$\partial_{x_d x_{d'}} I_{h,T} u = \sum_{i \in \mathcal{I}} \tilde{R}_i \partial_{x_d x_{d'}} \phi_{i,T}(X), \quad \forall X \in \omega_T^*, \tag{4.18}$$

where $d, d' = 1, 2$ and

$$R_i^s(X) = R_{i1}^s(X) + R_{i2}^s(X) + R_{i3}^s(X), i \in \mathcal{I}^{s'}, \quad X \in \omega_T^{*,s}, \quad \text{with} \tag{4.19}$$

$$\begin{cases} R_{i1}^s(X) = \displaystyle\int_0^{\tilde{t}_i} (1-t) \frac{d^2 u^s}{dt^2} \left(Y_i(t,X)\right) dt, \\ R_{i2}^s(X) = \displaystyle\int_{\tilde{t}_i}^1 (1-t) \frac{d^2 u^{s'}}{dt^2} \left(Y_i(t,X)\right) dt, \\ R_{i3}^s(X) = (1-\tilde{t}_i) \displaystyle\int_0^{\tilde{t}_i} \frac{d}{dt} \Big( \Big( M^s(\tilde{Y}_i) - I \Big) \nabla u^s(Y_i(t,X)) \cdot (A_i - X) \Big) dt, \end{cases} \tag{4.20}$$

$$E_i^s = \left( \left( M^s(\tilde{Y}_i) - \overline{M}^s \right) \nabla u^s(X) \right) \left( A_i - \tilde{Y}_i \right), \quad i \in \mathcal{I}^{s'}, \tag{4.21}$$

$$F_i^s = - \left( \left( \overline{M}^s - I \right) \nabla u^s(X) \right) \left( \tilde{Y}_i - \tilde{Y}_i^{\perp} \right), \quad i \in \mathcal{I}^{s'}, \tag{4.22}$$

$$\tilde{R}_i(X) = \int_0^1 \frac{d}{dt} u \left(Y_i(t,X)\right) dt, \quad i \in \mathcal{I}, \tag{4.23}$$

in which $M^- = (N^+)^{-1} N^-$, $M^+ = (N^-)^{-1} N^+$, $\overline{M}^- = (\overline{N}^+)^{-1} \overline{N}^-$, $\overline{M}^+ = (\overline{N}^-)^{-1} \overline{N}^+$, with

$$N^s = N^s(\tilde{X}) = \begin{pmatrix} \tilde{n}_y(\tilde{X}) & -\tilde{n}_x(\tilde{X}) \\ \beta^s \tilde{n}_x(\tilde{X}) & \beta^s \tilde{n}_y(\tilde{X}) \end{pmatrix} \text{ and } \bar{N}^s = \begin{pmatrix} \bar{n}_y & -\bar{n}_x \\ \beta^s \bar{n}_x & \beta^s \bar{n}_y \end{pmatrix}, \quad s = \pm. \tag{4.24}$$

Now we show the optimal approximation capabilities for the IFE spaces in terms of the interpolation errors on the patch $\omega_T$ for each interface element $T$. This result is stated in the following theorem and it is complementary to that given in [57, 71, 100].

**Theorem 4.1.** *Assume that the mesh $\mathcal{T}_h$ is sufficiently fine, then there exists a constant $C$*

*independent of the interface location such that the following estimate holds on each patch $\omega_T$ associated with every interface element $T$:*

$$
\begin{aligned}
&\|\nabla(I_{h,T}u - u)\|_{L^2(\omega_T)} + h\left\|\nabla^2(I_{h,T}u - u)\right\|_{L^2(\omega_T)} \\
\leq & Ch\left(\|u\|_{PH^2(\omega_T)} + \|u\|_{PW^{1,6}(\omega_T)}\right), \quad \forall u \in PH^2(\omega_T).
\end{aligned} \tag{4.25}
$$

*Proof.* Using Lemma 4.1 in [57] and the fact $\|A_i - X\| \leq Ch$ for $i \in \mathcal{I}, X \in \omega_T$, we directly have

$$
\begin{aligned}
&\|R_i^s\|_{L^2(\omega_T^{*,s})} \\
=&\left(\int_{\omega_T^{*,s}}\left(\int_0^1 (1-t)(A_i - X)^T H_u^s(Y_i(t,X))(A_i - X)dt\right)^2 dX\right)^{1/2} \\
\leq & Ch^2\int_0^1\left(\int_{\omega_T^{*,s}}(1-t)^2\sum_{k,l=1}^{2}\left|\partial_{x_k}\partial_{x_l}u^s(Y_i,t)\right|^2 dX\right)^{1/2} dt \\
\leq & Ch^2\|u\|_{PH^2(\omega_T)},
\end{aligned} \tag{4.26}
$$

where $H_u^s$ is the Hessian matrix given by

$$
H_u^s(Y_i(t,X)) = \begin{pmatrix} u_{xx}^s(Y_i(t,X)) & u_{xy}^s(Y_i(t,X)) \\ u_{yx}^s(Y_i(t,X)) & u_{yy}^s(Y_i(t,X))) \end{pmatrix}. \tag{4.27}
$$

Note that (4.14) implies the $\|M^s(\tilde{Y}_i) - \overline{M}^s\| \leq Ch$, $s = \pm$. Then, because of (4.21), we further have

$$
\begin{aligned}
\|E_i^s\|_{L^2(\omega_T^{*,s})} \leq & \|M^s(\tilde{Y}_i) - \overline{M}^s\|\|\nabla u^s\|_{L^2(\omega_T^{*,s})}\|A_i - \tilde{Y}_j\| \\
\leq & Ch\|M^s(\tilde{Y}_i) - \overline{M}^s\|\|\nabla u^s\|_{L^2(\omega_T^{*,s})} \\
\leq & Ch^2\|u\|_{PH^2(\omega_T)}.
\end{aligned} \tag{4.28}
$$

Next, (4.14) yields

$$\begin{aligned} \|F_i^s\|_{L^2(\omega_T^{*,s})} \leq & \|\overline{M}^s - I\| \|\nabla u^s\|_{L^2(\omega_T^{*,s})} \|\tilde{Y}_i - \tilde{Y}_i^{\perp}\| \\ \leq & Ch^2 \|u\|_{PH^2(\omega_T)}. \end{aligned} \tag{4.29}$$

In addition, using $|\omega_T^*| \leq Ch^3$ from (4.13) and the similar argument as the one used in Lemma 3.2 in [59], we have

$$\begin{aligned} \|\tilde{R}_i\|_{L^2(\omega_T^*)} \leq Ch^2 \|u\|_{PW^{1,6}(\omega_T)}, \\ \|\partial_{x_d} u\|_{L^2(\omega_T^*)} \leq Ch \|u\|_{PW^{1,6}(\omega_T)}, \end{aligned} \tag{4.30}$$

where $d = 1, 2$. Note that the IFE shape functions have the following bounds [57, 71, 100]

$$|\phi_{i,T}|_{W^{k,\infty}(\omega_T)} \leq Ch^{-k}, k = 1, 2. \tag{4.31}$$

Based on the estimations above, it follows from the expansions (4.15)-(4.18) that

$$\begin{aligned} & \|\partial_{x_d}(I_{h,T}u - u)\|_{L^2(\omega_T^{*,s})} \\ \leq & Ch^{-1} \left( \sum_{i \in \mathcal{I}^{s\prime}} \left( \|E_i^s\|_{L^2(\omega_T^{*,s})} + \|F_i^s\|_{L^2(\omega_T^{*,s})} \right) + \sum_{i \in \mathcal{I}} \|R_i^s\|_{L^2(\omega_T^{*,s})} \right) \\ \leq & Ch \left\| u \right\|_{PH^2(\omega_T)}, \end{aligned} \tag{4.32}$$

$$\begin{aligned} & \left\|\partial_{x_d x_{d'}}(I_{h,T}u - u)\right\|_{L^2(\omega_T^{*,s})} \\ \leq & Ch^{-2} \left( \sum_{i \in \mathcal{I}^{s\prime}} \left( \|E_i^s\|_{L^2(\omega_T^{*,s})} + \|F_i^s\|_{L^2(\omega_T^{*,s})} \right) + \sum_{i \in \mathcal{I}} \|R_i^s\|_{L^2(\omega_T^{*,s})} \right) + \|\partial_{x_d x_{d'}} u\|_{L^2(\omega_T^{*,s})} \\ \leq & C \left\| u \right\|_{PH^2(\omega_T)}, \end{aligned} \tag{4.33}$$

$$\begin{aligned} &\|\partial_{x_d}(I_{h,T}u - u)\|_{L^2(\omega_T^*)} \\ \leq & Ch^{-1}\sum_{i\in\mathcal{I}} \|\tilde{R}_i\|_{L^2(\omega_T^*)} + \|\partial_{x_d}u\|_{L^2(\omega_T^*)} \leq Ch\|u\|_{PW^{1,6}(\omega_T)}, \end{aligned} \tag{4.34}$$

$$\begin{aligned} &\|\partial_{x_d x_{d'}}(I_{h,T}u - u)\|_{L^2(\omega_T^*)} \\ \leq & Ch^{-2}\sum_{i\in\mathcal{I}} \|\tilde{R}_i\|_{L^2(\omega_T^*)} + \|\partial_{x_d x_{d'}}u\|_{L^2(\omega_T^*)} \leq C\left(\|u\|_{PW^{1,6}(\omega_T)} + \|u\|_{PH^2(\omega_T)}\right), \end{aligned} \tag{4.35}$$

where $d, d' = 1, 2$. Note that $\omega_T = \omega_T^* \cup \omega_T^{*,-} \cup \omega_T^{*,+}$, thus (4.25) follows from (4.32)-(4.35). □

## 4.4 Error estimation for the PPIFE methods

In this section, we will derive optimal estimates for the errors of PPIFE solutions under the usual piecewise $H^2$ regularity assumption for the exact solution. As usual in the error analysis and without loss of generality, we assume that the interface problem has a homogeneous Dirichlet boundary condition, *i.e.*, $g = 0$ in (4.1b). We use the following quantities to gauge the errors of PPIFE solutions:

$$\|v\|_h^2 = \sum_{T\in\mathcal{T}_h}\int_T \beta\|\nabla v\|^2 dX + \sum_{e\in\mathcal{E}_h^i}\sigma_e^0\int_e \left\||e|^{-1/2}[v]\right\|^2 ds, \quad \forall v \in V_h(\Omega), \tag{4.36}$$

$$|||v|||_h^2 = \|v\|_h^2 + \sum_{e\in\mathcal{E}_h^i}(\sigma_e^0)^{-1}\int_e \||e|^{1/2}\left\{\beta\nabla v\cdot\mathbf{n}_e\right\}\|^2 ds, \quad \forall v \in V_h(\Omega). \tag{4.37}$$

In fact, the following lemma shows the quantities defined in (4.36) and (4.37) are indeed energy norms on the underlying space $V_h(\Omega)$.

**Lemma 4.1.** *$\|\cdot\|_h$ and $|||\cdot|||_h$ are both norms on $V_h(\Omega)$.*

*Proof.* We only present the proof for $|||\cdot|||_h$ and the argument for $\|\cdot\|_h$ is similar. Suppose $|||v|||_h = 0$ for some $v \in V_h(\Omega)$. Due to the construction in (4.36), it is easy to see that $v$ is a piecewise constant on each element and sub-elements of interface elements. Besides, from $|||\cdot|||_h = 0$, it follows easily that $v = 0$ on $\mathcal{E}_h^{bi}$ and $v$ is continuous across $\mathcal{E}_h^{bi}$. Thus $v = 0$ on $T \in \mathcal{T}_h^{bi}$. $v$ is continuous across all the non-interface edges, we have $v = 0$ on $\cup_{T\in\mathcal{T}_h^n} T$. In addition, the second term in (4.36) vanishing implies that $v$ is actually continuous over all the interface edges, and thus, $v = 0$ on $\cup_{T\in\mathcal{T}_h^i} T$. Hence, $v = 0$ on the whole $\Omega$. Since it is easy to verify that $|||\cdot|||_h$ is a semi-norm, we conclude that $|||\cdot|||_h$ is a norm. □

We note that the energy norm (4.36) was already used for the analysis in [111]. It is easy to see that

$$\|v\|_h \leqslant |||v|||_h, \quad v \in V_h(\Omega). \tag{4.38}$$

The following lemma shows the norms respectively defined by (4.36) and (4.37) are actually equivalent when restricted on the IFE space $S_h(\Omega)$.

**Lemma 4.2.** *For sufficiently large $\sigma_e^0$, there exists a constant $C$ independent of the interface location such that $|||v|||_h \leqslant C\|v\|_h$, $\forall v \in S_h(\Omega)$.*

*Proof.* For each $e \in \mathring{\mathcal{E}}_h^i$, let $T_1^e$ and $T_2^e$ be the two elements sharing the same edge $e$. By the trace inequality given by Lemmas 3.2 and 3.5 in [111], there exists a constant $C$ independent of the interface location on both $T_1^e$ and $T_2^e$, such that for each $v \in S_h(\Omega)$, there holds for $e \in \mathring{\mathcal{E}}_h^i$

$$\begin{aligned}\int_e \left\| |e|^{1/2}\{\beta\nabla v\cdot\mathbf{n_e}\}\right\|^2 ds &\leqslant Ch\left(\left\|\beta\nabla v|_{T_1^e}\cdot\mathbf{n_e}\right\|^2_{L^2(e)} + \left\|\beta\nabla v|_{T_2^e}\cdot\mathbf{n_e}\right\|^2_{L^2(e)}\right)\\ &\leqslant C\left\|\sqrt{\beta}\nabla v\right\|^2_{L^2(T_1^e\cup T_2^e)},\end{aligned} \tag{4.39}$$

for $e \in \mathcal{E}_h^{bi}$

$$\int_e \left\||e|^{1/2}\{\beta\nabla v\cdot\mathbf{n_e}\}\right\|^2 ds \leqslant Ch\left(\|\beta\nabla v\cdot\mathbf{n_e}\|^2_{L^2(e)}\right) \leq C\left\|\sqrt{\beta}\nabla v\right\|^2_{L^2(T)}. \tag{4.40}$$

Therefore, for $e \in \mathcal{E}_h^i$, adding and subtracting the term $\sum_{e\in\mathcal{E}_h^i}(\sigma_e^0)^{-1}\int_e \left\||e|^{1/2}\{\beta\nabla v\cdot\mathbf{n_e}\}\right\|^2 ds$ in $\|\cdot\|_h$ yields

$$\begin{aligned}\|v\|_h^2 \geqslant \left(1-\frac{3C}{\sigma_e^0}\right)\sum_{T\in\mathcal{T}_h}\int_T \beta\left\|\nabla v\right\|^2 dX + \sum_{e\in\mathcal{E}_h^i}\sigma_e^0\int_e \left\||e|^{-1/2}[v_h]\right\|^2 ds \\ + \sum_{e\in\mathcal{E}_h^i}(\sigma_e^0)^{-1}\int_e \left\||e|^{1/2}\{\beta\nabla v\cdot\mathbf{n_e}\}\right\|^2 ds,\end{aligned} \tag{4.41}$$

where the constant $C$ is from (4.40). It is easy to see that the desired result follows from taking $\sigma_e^0$ large enough in (4.41). □

The following theorem derives an optimal bound for the error in the flux of the IFE interpolation of a piecewise $H^2$ function on interface edges.

**Theorem 4.2.** *Assume that the mesh $\mathcal{T}_h$ is sufficiently fine and satisfies the Patch Assumption. Then there exists a constant $C$ independent of the interface location such that:*

$$\sum_{e\in\mathcal{E}_h^i}\|\{\beta\nabla(u-I_hu)\cdot\mathbf{n}_e\}\|^2_{L^2(e)} \leq Ch\|u\|^2_{PH^2(\Omega)}, \quad \forall u\in PH^2(\Omega). \tag{4.42}$$

*Proof.* For each interface element $T \in \mathcal{T}_h^i$, let $e \in \mathcal{E}_h^i$ be one of its edges and let $e^s = e\cap\Omega^s$, $s=\pm$. According to the Patch Assumption, there exists an auxiliary triangle $T_e^s \subset \omega_T$, possessing $e^s$ as one of its edges, such that $T_e^s \subset \Omega^s$ and $|e^s|/|T_e^s| \leq Ch^{-1}$, $s=\pm$. Letting $\beta_{max} = \max\{\beta^-,\beta^+\}$, applying the standard trace inequality on $T_e^s$ and using the estimation in (4.25), we have

$$
\begin{aligned}
&\|\beta\nabla(u-I_hu)\cdot\mathbf{n}_e\|_{L^2(e)}\\
\leq&\beta_{max}\left(\|\nabla(I_{h,T}u-u)\|_{L^2(e^-)}+\|\nabla(I_{h,T}u-u)\|_{L^2(e^+)}\right)\\
\leq&C\sum_{s=-,+}(|e^s|/|T_e^s|)^{1/2}\left(\|\nabla(I_{h,T}u-u)\|_{L^2(T_e^s)}+h\left\|\nabla^2(I_{h,T}u-u)\right\|_{L^2(T_e^s)}\right)\\
\leq&Ch^{1/2}\left(\|u\|_{PH^2(\omega_T)}+\|u\|_{PW^{1,6}(\omega_T)}\right).
\end{aligned}
\tag{4.43}
$$

For each interface edge $e\in\mathring{\mathcal{E}}_h^i$, let $T_1^e$ and $T_2^e$ be the two neighbor elements. Then (4.43) implies

$$
\begin{aligned}
&\sum_{e\in\mathring{\mathcal{E}}_h^i}\|\{\beta\nabla(u-I_hu)\cdot\mathbf{n}_e\}\|_{L^2(e)}^2\\
\leqslant&C\sum_{e\in\mathring{\mathcal{E}}_h^i}\left(\left\|\beta\nabla(u-I_{h,T_1^e}u)\cdot\mathbf{n}_e\right\|_{L^2(e)}^2+\left\|\beta\nabla(u-I_{h,T_2^e}u)\cdot\mathbf{n}_e\right\|_{L^2(e)}^2\right)\\
\leqslant&Ch\sum_{T\in\mathcal{T}_h^i}\left(\|u\|_{PH^2(\omega_T)}^2+\|u\|_{PW^{1,6}(\omega_T)}^2\right).
\end{aligned}
\tag{4.44}
$$

For each interface edge $e\in\mathcal{E}_h^{bi}$ and the corresponding boundary interface element $T\in\mathcal{T}_h^{bi}$,

$$
\begin{aligned}
&\sum_{e\in\mathcal{E}_h^{bi}}\|\{\beta\nabla(u-I_hu)\cdot\mathbf{n}_e\}\|_{L^2(e)}^2\\
\leqslant&C\sum_{e\in\mathcal{E}_h^{bi}}\left(\|\beta\nabla(u-I_{h,T}u)\cdot\mathbf{n}_e\|_{L^2(e)}^2+\|\beta\nabla(u-I_{h,T}u)\cdot\mathbf{n}_e\|_{L^2(e)}^2\right)\\
\leqslant&Ch\sum_{T\in\mathcal{T}_h^i}\left(\|u\|_{PH^2(\omega_T)}^2+\|u\|_{PW^{1,6}(\omega_T)}^2\right).
\end{aligned}
\tag{4.45}
$$

Then from (4.44) and (4.45) we have:

$$
\sum_{e\in\mathcal{E}_h^i}\|\{\beta\nabla(u-I_hu)\cdot\mathbf{n}_e\}\|_{L^2(e)}^2\leqslant Ch\left(\|u\|_{PH^2(\Omega)}^2+\|u\|_{PW^{1,6}(\Omega)}^2\right),
\tag{4.46}
$$

where we have utilized the finite-overlapping property of the patches $\omega_T$, $T \in \mathcal{T}_h^i$. Then (4.42) is obtained by applying the standard embedding inequality [126] $\|w\|_{1,6,\Omega^s} \le C\|w\|_{2,\Omega^s}$, $s = \pm$ to (4.46). $\square$

**Remark 4.3.** *Note that, in Theorem 4.2 and the rest parts of the thesis, $\mathcal{T}_h$ is sufficiently fine means that: for some fixed parameter $\epsilon \in (0, \sqrt{2}/2)$ and $\overline{\kappa} \in (0, 1]$, the mesh size $h$ is such that [57]:*

$$h < \min\left\{ \frac{\sqrt{\overline{\kappa}}}{\sqrt{2}(1 + (1 - 2\epsilon^2)^{-3/2})\kappa}, \frac{\epsilon}{\kappa} \right\},$$

*where $\kappa$ is the curvature of the interface $\Gamma$.*

The following theorem is about the approximation capabilities of the IFE spaces in the energy norms on the whole domain $\Omega$.

**Theorem 4.3.** *Assume that the mesh $\mathcal{T}_h$ is sufficiently fine and satisfies the Patch Assumption. Then there exists a constant $C$ independent of the interface location such that*

$$\|I_h u - u\|_h \le Ch\|u\|_{PH^2(\Omega)}, \quad \forall u \in PH^2(\Omega) \tag{4.47}$$

*and*

$$|||I_h u - u|||_h \le Ch\|u\|_{PH^2(\Omega)}, \quad \forall u \in PH^2(\Omega). \tag{4.48}$$

*Proof.* By (4.38), estimate (4.47) follows from (4.48). Estimate (4.48) simply comes from the estimate (4.42) and the definition (4.37) together with the global optimal approximation capabilities of the linear and bilinear IFE spaces given in [71, 100]. $\square$

Now we prove the coercivity and continuity for the bilinear form $a_h(\cdot, \cdot)$ defined in (4.6) in terms of the energy norm $|||\cdot|||_h$.

**Theorem 4.4.** *For $a_h(\cdot,\cdot)$ defined in (4.6), if $\sigma_e^0$ is sufficiently large, then there exists a constant $\kappa$ such that*

$$a_h(v_h, v_h) \geq \kappa \|\|\|v_h\|\|\|_h^2, \quad \forall v_h \in S_h(\Omega). \tag{4.49}$$

*Proof.* Note that

$$\begin{aligned} a_h(v_h, v_h) =& \sum_{T\in\mathcal{T}_h} \int_T \beta\nabla v_h \cdot \nabla v_h dX \\ &+ (\epsilon - 1) \sum_{e\in\mathcal{E}_h^i} \int_e \{\beta\nabla v_h \cdot \mathbf{n}_e\}_e [v_h]_e ds + \sum_{e\in\mathcal{E}_h^i} \frac{\sigma_e^0}{|e|} \int_e [v_h]_e \, [v_h]_e ds. \end{aligned} \tag{4.50}$$

For an interior interface edge $e \in \mathring{\mathcal{E}}_h^i$, we have

$$\begin{aligned} \sum_{e\in\mathring{\mathcal{E}}_h^i} \int_e \{\beta\nabla v_h \cdot \mathbf{n_e}\}[v_h] ds &\leqslant C \sum_{e\in\mathring{\mathcal{E}}_h^i} \left\|\sqrt{\beta}\nabla v_h\right\|_{L^2(T_1^e\cup T_2^e)} \frac{1}{\|e\|^{1/2}} \|v_h\|_{L^2(e)} \\ &\leqslant \frac{\delta}{2} \sum_{T\in\mathcal{T}_h} \left\|\sqrt{\beta}\nabla v_h\right\|_{L^2(T)}^2 + \frac{C}{2\delta} \sum_{e\in\mathring{\mathcal{E}}_h^i} \frac{1}{|e|} \|[v_h]\|_{L^2(e)}^2, \end{aligned} \tag{4.51}$$

for a boundary interface edge $e \in \mathcal{E}_h^{bi}$ and its corresponding boundary interface element $T \in \mathcal{T}_h^{bi}$

$$\begin{aligned} \sum_{e\in\mathcal{E}_h^{bi}} \int_e \{\beta\nabla v_h \cdot \mathbf{n_e}\}[v_h] ds &\leqslant C \sum_{e\in\mathcal{E}_h^{bi}} \left\|\sqrt{\beta}\nabla v_h\right\|_{L^2(T)} \frac{1}{|e|^{1/2}} \|v_h\|_{L^2(e)} \\ &\leqslant \frac{\delta}{2} \sum_{T\in\mathcal{T}_h^{bi}} \left\|\sqrt{\beta}\nabla v_h\right\|_{L^2(T)}^2 + \frac{C}{2\delta} \sum_{e\in\mathcal{E}_h^{bi}} \frac{1}{|e|} \|[v_h]\|_{L^2(e)}^2. \end{aligned} \tag{4.52}$$

Therefore

$$a_h(v_h, v_h) \geq \sum_{T\in\mathcal{T}_h} \int_T \beta\nabla v_h \cdot \nabla v_h dX + \sum_{e\in\mathcal{E}_h^i} \frac{\sigma_e^0}{|e|} \|[v_h]_e\|_{L^2(e)}$$

$$
\begin{aligned}
&+ (\epsilon - 1)\left(\delta \sum_{T\in\mathcal{T}_h} \left\|\sqrt{\beta}\nabla v_h\right\|^2_{L^2(T)} + \frac{C}{2\delta}\sum_{e\in\mathcal{E}_h^i}\frac{1}{|e|}\left\|[v_h]\right\|^2_{L^2(e)}\right) \\
&\geq (1+\delta(\epsilon-1))\sum_{T\in\mathcal{T}_h}\left\|\sqrt{\beta}\nabla v_h\right\|^2_{L^2(T)} + \left(1+\frac{C(\epsilon-1)}{2\delta\sigma_e^0}\right)\sum_{e\in\mathcal{E}_h^i}\frac{\sigma_e^0}{|e|}\left\|[v_h]\right\|^2_{L^2(e)}.
\end{aligned}
\tag{4.53}
$$

Consider the least favorable situation ($\epsilon$ is smallest) where $\epsilon = -1$, by choosing $\delta = \frac{1}{4}$ and $\sigma_e^0 = 5C$, we have:

$$
a_h(v_h, v_h) \geq \kappa |||v_h|||_h^2, \quad \forall v \in S_h(\Omega). \tag{4.54}
$$

The proof for other values of $\epsilon$ follows similarly. $\square$

**Theorem 4.5.** *For $a_h(\cdot,\cdot)$ defined in (4.6), there exists a constant $C$ such that*

$$
a_h(w, v) \leq C|||w|||_h |||v|||_h, \quad \forall w, v \in V_h(\Omega). \tag{4.55}
$$

*Proof.* Note that

$$
\begin{aligned}
|a(w,v)| \leq &\left|\sum_{T\in\mathcal{T}_h}\int_T \beta\nabla w\nabla v dX\right| + \left|\sum_{e\in\mathcal{E}_h^i}\int_e\{\beta\nabla w\cdot\mathbf{n}_e\}[v]ds\right| \\
&+ \left|\sum_{e\in\mathcal{E}_h^i}\int_e\{\beta\nabla v\cdot\mathbf{n}_e\}[w]\right| + \left|\sum_{e\in\mathcal{E}_h^i}\int_e\frac{\sigma_e^0}{|e|^\alpha}[w][v]ds\right|.
\end{aligned}
\tag{4.56}
$$

Denote each term on the right in (4.56) as $Q_i (i = 1, 2, 3, 4)$. Applying Hölder inequality on $Q_i$, we have

$$
|Q_1| \leq C\|w\|_{L^2(T)}\|v\|_{L^2(T)} \leq C|||w|||_h |||v|||_h, \tag{4.57}
$$

$$
\begin{aligned}
|Q_2| &\leq \sum_{e\in\mathcal{E}_h^i} \|\{\beta\nabla w\cdot\mathbf{n}_e\}\|_{L^2(e)} \|[v]\|_{L^2(e)} \\
&\leq \left(\sum_{e\in\mathcal{E}_h^i} (\sigma_e^0)^{-1} \left\||e|^{1/2}\{\beta\nabla w\cdot\mathbf{n}_e\}\right\|_{L^2(e)}^2\right)^{1/2} \left(\sum_{e\in\mathcal{E}_h^i} \sigma_e^0 \left\||e|^{-1/2}[v]\right\|_{L^2(e)}^2\right)^{1/2} \\
&\leq |||w|||_h |||v|||_h.
\end{aligned} \tag{4.58}
$$

Using the similar argument above, we obtain

$$|Q_3| \leq |||w|||_h |||v|||_h, \tag{4.59}$$

$$|Q_4| \leq |||w|||_h |||v|||_h. \tag{4.60}$$

Thus, (4.55) follows from applying (4.57)-(4.60) to (4.56). □

We note the estimate for $\|I_h u - u\|_h$ given in (4.47) was also established in [111], but we prove it here by alternative arguments such that (4.47) follows from (4.48), which is the optimal approximation capability of the IFE space in the stronger energy norm $|||\cdot|||_h$. More importantly, adopting the stronger norm $|||\cdot|||_h$ in the error estimation allows us to establish both the coercivity and continuity for the bilinear form $a_h(\cdot,\cdot)$ employed in the PPIFE methods, which are critical components in obtaining the optimal error estimates for the PPIFE solutions with the standard $PH^2(\Omega)$ regularity in the following theorems.

**Theorem 4.6.** *Assume that the exact solution $u$ to the interface problem (4.1) is in $PH^2(\Omega)$ and $u_h$ is the related PPIFE solution with $\sigma_e^0$ in $a_h(\cdot,\cdot)$ large enough on a mesh $\mathcal{T}_h$ fine enough. Then there exists a constant $C$ such that*

$$|||u-u_h|||_h \leq Ch\|u\|_{PH^2(\Omega)}. \tag{4.61}$$

*Proof.* From (4.5) and (4.9) we have

$$a_h(u_h - I_h u, v) = a_h(u - I_h u, v), \quad \forall v \in S_h(\Omega). \tag{4.62}$$

Letting $v = u_h - I_h u$ and using both the coercivity and the continuity of $a_h(\cdot,\cdot)$, we have

$$\begin{aligned} \kappa |||u_h - I_h u|||_h^2 \le a_h(u_h - I_h u, u_h - I_h u) =& a_h(u - I_h u, u_h - I_h u) \\ \le& C|||u - I_h u|||_h |||u_h - I_h u|||_h. \end{aligned} \tag{4.63}$$

Thus, $|||u_h - I_h u|||_h \le C|||u - I_h u|||_h$. Then, by (4.48), we have

$$|||u - u_h|||_h \le |||u - I_h u|||_h + |||u_h - I_h u|||_h \le (1 + C)|||u - I_h u|||_h \le Ch\|u\|_{PH^2(\Omega)},$$

which proves (4.61). □

Because of (4.38), the estimate given by (4.61) leads to

$$\|u - u_h\|_h \le Ch\|u\|_{PH^2(\Omega)}, \tag{4.64}$$

which is not only an optimal error estimate for the PPIFE solution $u_h$ in the energy norm $\|\cdot\|_h$ but also a better estimate than the one given in Theorem 4.3 of [111] because (4.64) requires a standard and less stringent regularity assumption for the exact solution $u$.

Furthermore, using the standard regularity assumption in the error analysis allows us to derive an optimal error estimate in the $L^2$ norm in the following theorem, which could not be accomplished by the analysis approaches employed in [111] that relied on the excessive $PH^3(\Omega)$ regularity.

**Theorem 4.7.** *Under the conditions of Theorem 4.6, there exists a constant $C$ such that*

$$\|u-u_h\|_{L^2(\Omega)} \le Ch^2\|u\|_{PH^2(\Omega)}. \tag{4.65}$$

*Proof.* The proof is based on the standard duality argument. Let $w \in PH^2(\Omega)$ be the auxiliary function that is the solution to (4.1) with $f$ at the right hand side replaced by $u-u_h$. Then, following standard arguments we have

$$\|u-u_h\|^2_{L^2(\Omega)} = a_h(w, u-u_h). \tag{4.66}$$

Let $I_h w$ be the interpolent of $w$ in IFE space. Since $I_h w \in S_h(\Omega)$, by (4.5) and (4.9) we have $a_h(I_h w, u-u_h) = 0$ which leads to $a_h(w, u-u_h) = a_h(w - I_h w, u-u_h)$. Then, by (4.66) and the continuity of $a_h(\cdot,\cdot)$, we have

$$\|u-u_h\|^2_{L^2(\Omega)} = a_h(w-I_h w, u-u_h) \le C|||w-I_h w|||_h |||u-u_h|||_h. \tag{4.67}$$

According to (4.48) and the regularity for the elliptic interface problem [45], we have

$$|||w-I_h w|||_h \le Ch\|w\|_{PH^2(\Omega)} \le Ch\|u-u_h\|_{L^2(\Omega)}. \tag{4.68}$$

Putting (4.68) to (4.67) leads to

$$\|u-u_h\|_{L^2(\Omega)} \le Ch|||u-u_h|||_h, \tag{4.69}$$

which yields (4.65) by applying (4.61). □

To finish this section, we present a numerical example to corroborate the optimal error estimates obtained in Theorems 4.6 and 4.7. Consider the domain $\Omega = (-1,1)\times(-1,1)$

that is separated by the circular interface $\Gamma : x^2 + y^2 - r_0^2 = 0$, $r_0 = \pi/6.28$ into two subdomains

$$\Omega^- = \left\{(x,y) : x^2 + y^2 < r_0^2\right\}, \quad \Omega^+ = \Omega \backslash \overline{\Omega^-}.$$

On $\Omega$, we choose functions $f$ and $g$ such that the interface problem (4.1) has the following exact solution:

$$u(x,y) = \begin{cases} \dfrac{1}{\beta^-} r^\alpha, & (x,y) \in \Omega^-, \\ \dfrac{1}{\beta^+} r^\alpha + \left(\dfrac{1}{\beta^-} - \dfrac{1}{\beta^+}\right) r_0^\alpha, & (x,y) \in \Omega^+, \end{cases} \tag{4.70}$$

in which $\alpha = 1.5, r = \sqrt{x^2 + y^2}, \beta^- = 1$, and $\beta^+ = 10$. It can be verified that $u \in PH^2(\Omega) \backslash PH^3(\Omega)$. Table 4.1 presents errors of the PPIFE solution $u_h$ generated on a sequence of uniform triangular meshes $\mathcal{T}_h$ of $\Omega$ in which $h = 2/N$ with the integer $N$ listed in the first column in Table 4.1. The data in this table clearly demonstrates that the PPIFE solutions converge optimally in both the $L^2$ and $H^1$ norms to the exact solution $u$ that is a function in the Sobolev space $PH^2(\Omega)$ but not in $PH^3(\Omega)$.

| $N$ | $\|u - u_h\|_{0,\Omega}$ | rate | $\|u - u_h\|_{1,\Omega}$ | rate |
|---|---|---|---|---|
| 10 | 2.9428e-03 | NA | 3.2747e-02 | NA |
| 20 | 8.4280e-04 | 1.8039 | 1.5430e-02 | 1.0856 |
| 40 | 1.9635e-04 | 2.1018 | 7.8261e-03 | 0.9793 |
| 80 | 4.5931e-05 | 2.0958 | 3.9244e-03 | 0.9958 |
| 160 | 1.1242e-05 | 2.0305 | 1.9596e-03 | 1.0019 |
| 320 | 2.9990e-06 | 1.9064 | 9.7966e-04 | 1.0002 |
| 640 | 7.7099e-07 | 1.9597 | 4.8967e-04 | 1.0005 |
| 1280 | 1.9814e-07 | 1.9602 | 2.4490e-04 | 0.9996 |

Table 4.1: Errors of SPPIFE solutions, $\beta^- = 1$, $\beta^+ = 10$, $\alpha = 1.5$.

## 4.5 Conclusions

In this chapter, we have employed a new analysis framework to derive the error bounds for the PPIFE methods developed in [111]. This new framework uses an energy norm $|||\cdot|||_h$ which is stronger than $\|\cdot\|_h$ norm originally used [111]. There are two key-components in this analysis framework. First, it employs a patch technique to show the optimal approximation capability on interface edges for the flux of the IFE interpolation of a function with the standard piecewise $H^2$ regularity. Second, it shows that the bilinear form $a_h(\cdot,\cdot)$ in the PPIFE methods is both coercive and continuous in terms of the stronger energy norm $|||\cdot|||_h$. Benefitted from these two key-components, not only can we show that the IFE space has the optimal approximation capability gauged by the energy norm $|||\cdot|||_h$, but also we can show the PPIFE solution converges optimally in both $|||\cdot|||_h$ and $\|\cdot\|_h$ with the standard piecewise $H^2$ regularity for the exact solution. As a very important consequence of the standard piecewise $H^2$ regularity assumption, we can further show that the PPIFE solution converges optimally in the $L^2$ norm, which the analysis techniques used in [111] could not achieve. The error analysis for IFE for the second order elliptic operator based on the patch will serve as the theoretical foundation for the analysis of the IFE methods for Helmholtz, hyperbolic and parabolic interface problems in the coming chapters.

# Chapter 5

# IFE methods for Helmholtz interface problems

## 5.1 Introduction

In this chapter, we present our exploration for applying IFE methods to solve the Helmholtz interface problem described by (1.7), which we recall here for easy reference: find $u(X)$ that satisfies the Helmholtz equation and the boundary condition

$$-\nabla \cdot (\beta \nabla u) - \omega^2 u = f, \quad \text{in } \Omega^- \cup \Omega^+, \tag{5.1a}$$

$$\beta \frac{\partial u}{\partial \boldsymbol{n}_\Omega} + i\omega u = g, \quad \text{on } \partial\Omega, \tag{5.1b}$$

together with the jump conditions across the interface [21, 26, 38, 86, 93]:

$$[u]_\Gamma := u^+|_\Gamma - u^-|_\Gamma = 0, \tag{5.1c}$$

$$\left[\beta \nabla u \cdot \mathbf{n}\right]_\Gamma := \beta^+ \nabla u^+ \cdot \mathbf{n}|_\Gamma - \beta^- \nabla u^- \cdot \mathbf{n}|_\Gamma = 0. \tag{5.1d}$$

Here the domain $\Omega \subseteq \mathbb{R}^2$ is divided by an interface curve $\Gamma$ into two subdomains $\Omega^-$ and $\Omega^+$, occupied by a different material each, with $\overline{\Omega} = \overline{\Omega^- \cup \Omega^+ \cup \Gamma}$, $i = \sqrt{-1}$, $\omega$ is the wave number, $\mathbf{n}_\Omega$ is the unit outward normal vector to $\partial\Omega$, $u^s = u|_{\Omega^s}$, $s = \pm$, $\mathbf{n}$ is the unit outward normal vector to the interface $\Gamma$, and the coefficient $\beta$ is a positive piecewise constant function representing different materials such that

$$\beta(X) = \begin{cases} \beta^- & \text{for } X \in \Omega^-, \\ \beta^+ & \text{for } X \in \Omega^+. \end{cases}$$

Both the PPIFE methods and the DGIFE methods, including the higher degree schemes, will be developed to solve the Helmholtz interface problems. As for the error estimation, we follow the framework of Schatz's argument to carry out the error analysis for the linear and bilinear symmetric PPIFE methods. To be specific, we utilize the coercivity and continuity of the bilinear form corresponding to the elliptic operator [63, 111] to establish Gårding's inequality and continuity of the bilinear form in these PPIFE methods which are key ingredients in Schatz's argument. We also derive a special trace inequality that is valid for IFE functions which are not $H^1$ functions in general. Consequently, under suitable assumptions about the regularity of the exact solution and the mesh size, we are able to establish the optimal error bounds in both an energy norm and the standard $L^2$ norm for these PPIFE methods for solving the Helmholtz interface problems.

The layout of this section is as follows: In Section 5.2, PPIFE and DGIFE methods are derived for the Helmholtz interface problem (5.1). In Section 5.3, optimal error bounds are derived for the linear/bilinear symmetric PPIFE method in both the energy norm and $L^2$ norm with Schatz's argument [62]. We present numerical examples to show the features of the proposed IFE methods in Section 5.4. Some concise conclusions and remarks are given in Section 5.5.

## 5.2 IFE methods for Helmholtz interface problems

All the IFE methods developed for the elliptic interface problems such as those in [3, 73, 100, 104, 111, 112] are expected to be extended to Helmholtz interface problems since they share the same second order elliptic operator. We will herein focus on the PPIFE methods and DGIFE methods because it has been observed that these methods have the enhanced stability and accuracy with the added penalty terms in the schemes.

To describe the IFE spaces to be used to solve Helmhotlz interface problems, we specify the collection of the nodes $\mathcal{N}_h$ for a mesh $\mathcal{T}_h$ of $\Omega$ as follows:

$$\mathcal{N}_h = \begin{cases} \bigcup\limits_{T\in\mathcal{T}_h} \{X_{i,T}, 1 \le i \le (p+1)(p+2)/2\} & \text{when } \mathcal{T}_h \text{ is a triangular mesh,} \\ \\ \bigcup\limits_{T\in\mathcal{T}_h} \{A_{i,T}, 1 \le i \le 4\} & \text{when } \mathcal{T}_h \text{ is a rectangular mesh,} \end{cases}$$

where $X_{i,T}, 1 \le i \le (p+1)(p+2)/2$ are the local nodes associated with the standard $p$-th degree Lagrange finite element shape functions in a triangular element $T$ and $A_{i,T}, 1 \le i \le 4$ are vertices of a rectangular element $T$.

Then the complex local IFE space to be used is

$$S_h^p(T) = \left\{ v = v_1 + iv_2 : v_1, v_2 \in \tilde{S}_h^p(T) \right\}, \quad \forall T \in \mathcal{T}_h, \tag{5.2}$$

where the real linear/bilinear local IFE space $\tilde{S}_h^1(T)$ is the same as $S_h^1(T)$ in (2.11), and the real higher order IFE space $\tilde{S}_h^p(T)$ $(p \ge 2)$ is the same as $S_{1,h}^p(T)$ in (3.13) (we only consider normal extended jump condition herein when constructing higher degree IFE spaces). Accordingly, the complex global IFE space used in the PPIFE method for Helmholtz interface problems is defined as:

$$S_h^p(\Omega) = \Big\{ v \in L^2(\Omega) \ : \ v|_T \in S_h^p(T), \quad \forall T \in \mathcal{T}_h, \ v \text{ is continuous at each } X \in \mathcal{N}_h \Big\}, \tag{5.3}$$

while the complex global IFE space for the DGIFE method is defined as:

$$DS_h^p(\Omega) = \Big\{ v \in L^2(\Omega) \ : \ v|_T \in S_h^p(T), \quad \forall T \in \mathcal{T}_h \Big\}. \tag{5.4}$$

We note that $v_h \in S_h^p(\Omega)$ is either a piecewise $p$-th degree polynomial or a piecewise bilinear polynomial. The continuity of $v_h \in S_h^p(\Omega)$ at every $X \in \mathcal{N}_h$ implies that $v_h$ is continuous across every non-interface edge $e \in \mathring{\mathcal{E}}_h^n$, but, in general, $v_h \in S_h^p(\Omega)$ can be discontinuous across each interface edge $e \in \mathring{\mathcal{E}}_h^i$, see [73, 100] for more related explanations. As usual, each function $v_h \in DS_h^p(\Omega)$ can be discontinuous across all edges of the mesh.

Furthermore, for each function $v_h \in S_h^p(\Omega)$ or $DS_h^p(\Omega)$, it can be shown that $v_h|_T \in H^1(T)$ for $p = 1$ because $v_h|_T$ is continuous across $l = \overline{DE}$, see Figure 1.3, and $v_h|_T \notin H^1(T)$ for $p \geq 2$ because the piecewise polynomial $v_h$ cannot be continuous across an interface curve $\Gamma$ in general.

### 5.2.1 PPIFE methods for Helmholtz interface problems

First we derive the PPIFE scheme. For simplicity, we assume that $\Gamma \cap \partial\Omega = \emptyset$. Multiply equation (5.1a) by the complex conjugate of a function $v_h \in S_h^p(\Omega)$ and integrate on each element $T \in \mathcal{T}_h$. Then, by Green's formula and the interface jump condition (5.1d), it follows:

$$\begin{aligned}&\int_T \beta\nabla u\nabla\overline{v_h}dX-\int_{\partial T}\beta\nabla u\cdot\boldsymbol{n_T}\overline{v_h}ds-\int_{\Gamma\cap T}\{\beta\nabla u\cdot\boldsymbol{n_\Gamma}\}[\overline{v_h}]ds-\omega^2\int_T u\overline{v_h}dX\\ =&\int_T f\overline{v_h}dX,\end{aligned} \tag{5.5}$$

where the third term on the left of (5.5) disappears when $T\in\mathcal{T}_h^n$.

Here we recall some set notations from Chapter 2 for sets of edges and elements to be used in the later discussions: the set of interior edges is $\mathring{\mathcal{E}}_h$, the set of interface edges is $\mathcal{E}_h^i$, the set of interior interface edges is $\mathring{\mathcal{E}}_h^i$, the set of boundary edges is $\mathcal{E}_h^b$, the set of boundary interface edges is $\mathcal{E}_h^{bi}$; the set of interface elements $\mathcal{T}_h^i$, the set of interior interface elements $\mathring{\mathcal{T}}_h^i$, and the set of boundary interface elements $\mathcal{T}_h^{bi}$.

Summing (5.5) over all $T\in\mathcal{T}_h$ leads to

$$\begin{aligned}&\sum_{T\in\mathcal{T}_h}\int_T\beta\nabla u\nabla\overline{v_h}dX-\sum_{e\in\mathring{\mathcal{E}}_h}\int_e\{\beta\nabla u\cdot\boldsymbol{n_e}\}[\overline{v_h}]ds-\sum_{e\in\mathcal{E}_h^b}\int_e\beta\nabla u\cdot\boldsymbol{n_e}\overline{v_h}ds\\&-\sum_{T\in\mathcal{T}_h^i}\int_{\Gamma\cap T}\{\beta\nabla u\cdot\boldsymbol{n_\Gamma}\}[\overline{v_h}]ds-\omega^2\int_\Omega u\overline{v_h}dX=\int_\Omega f\overline{v_h}dX.\end{aligned} \tag{5.6}$$

Because of the continuity of $\overline{v_h}\in S_h^p(\Omega)$ across non-interface edges, we can write (5.6) as

$$\begin{aligned}&\sum_{T\in\mathcal{T}_h}\int_T\beta\nabla u\nabla\overline{v_h}dX-\sum_{e\in\mathring{\mathcal{E}}_h^i}\int_e\{\beta\nabla u\cdot\boldsymbol{n_e}\}[\overline{v_h}]ds-\sum_{e\in\mathcal{E}_h^b}\int_e\beta\nabla u\cdot\boldsymbol{n_e}\overline{v_h}ds\\&-\sum_{T\in\mathcal{T}_h^i}\int_{\Gamma\cap T}\{\beta\nabla u\cdot\boldsymbol{n_\Gamma}\}[\overline{v_h}]ds-\omega^2\int_\Omega u\overline{v_h}dX=\int_\Omega f\overline{v_h}dX.\end{aligned}$$

Applying the boundary condition (5.1b), we can reduce the above equation to

$$\begin{aligned}\sum_{T\in\mathcal{T}_h}\int_T \beta\nabla u\nabla\overline{v_h}dX - \sum_{e\in\mathring{\mathcal{E}}_h^i}\int_e\{\beta\nabla u\cdot\boldsymbol{n_e}\}[\overline{v_h}]ds + i\omega\sum_{e\in\mathcal{E}_h^b}\int_e u\overline{v_h}ds\\ -\sum_{T\in\mathcal{T}_h^i}\int_\Gamma\{\beta\nabla u\cdot\boldsymbol{n_\Gamma}\}[\overline{v_h}]ds - \omega^2\int_\Omega u\overline{v_h}dX = \int_\Omega f\overline{v_h}dX + \sum_{e\in\mathcal{E}_h^b}\int_e g\overline{v_h}ds.\end{aligned} \tag{5.7}$$

By assuming that $u$ is in $PH^2(\Omega)$ so that $[u]_e = 0,\ \forall e\in\mathring{\mathcal{E}}_h$ and applying the interface jump condition (5.1c), we obtain

$$\begin{aligned}\epsilon\sum_{e\in\mathring{\mathcal{E}}_h^i}\int_e\{\beta\nabla\overline{v_h}\cdot\mathbf{n}_e\}_e[u]_e ds = 0,\quad i\sum_{e\in\mathring{\mathcal{E}}_h^i}\frac{\sigma_e^0}{|e|}\int_e[u]_e\,[\overline{v_h}]_e ds = 0,\\ \epsilon\sum_{T\in\mathcal{T}_h^i}\int_{\Gamma\cap T}\{\beta\nabla\overline{v_h}\cdot\mathbf{n}_\Gamma\}_\Gamma[u]_\Gamma ds = 0,\quad i\sum_{T\in\mathcal{T}_h^i}\frac{\sigma_e^0}{|e|}\int_{\Gamma\cap T}[u]_\Gamma\,[\overline{v_h}]_\Gamma ds = 0,\end{aligned} \tag{5.8}$$

with parameters $\epsilon$, and $\sigma_e^0 \geq 0$. Adding these four terms to the left hand side of (5.7), we can see that the solution $u$ to the Helmholtz interface problem (5.1) satisfies the following weak form:

$$\begin{aligned}&b_h^{PP}(u,v_h) = L_f(v_h),\qquad \forall v_h\in S_h^p(\Omega),\\ \text{with}\qquad &b_h^{PP}(u,v_h) = a_h^{PP}(u,v_h) + i\omega(u,v_h)_{\partial\Omega} - \omega^2(u,v_h)_{L^2(\Omega)}\end{aligned} \tag{5.9}$$

where the bilinear form $a_h^{PP}(\cdot,\cdot) : PH^2(\Omega)\times S_h^p(\Omega)\to\mathbb{C}$ and the linear form $L_f(\cdot) : S_h^p(\Omega)\to\mathbb{C}$ are defined as:

$$\begin{aligned}a_h^{PP}(u,v_h) \;=\; &\sum_{T\in\mathcal{T}_h}\int_T\beta\nabla u\cdot\nabla\overline{v_h}dX - \sum_{e\in\mathring{\mathcal{E}}_h^i}\int_e\{\beta\nabla u\cdot\mathbf{n}_e\}_e[\overline{v_h}]_e ds + \epsilon\sum_{e\in\mathring{\mathcal{E}}_h^i}\int_e\{\beta\nabla\overline{v_h}\cdot\mathbf{n}_e\}_e[u]_e ds\\ &+i\omega\sum_{e\in\mathcal{E}_h^b}\int_e u\overline{v_h}ds + i\sum_{e\in\mathring{\mathcal{E}}_h^i}\frac{\sigma_e^0}{|e|}\int_e[u]_e\,[\overline{v_h}]_e ds - \sum_{T\in\mathcal{T}_h^i}\int_{\Gamma\cap T}\{\beta\nabla u\cdot\mathbf{n}_\Gamma\}[\overline{v_h}]_\Gamma ds\end{aligned}$$

$$+\epsilon \sum_{T\in\mathcal{T}_h^i} \int_{\Gamma\cap T} \{\beta\nabla\overline{v_h}\cdot\mathbf{n}_\Gamma\}_\Gamma [u]_\Gamma ds + i \sum_{T\in\mathcal{T}_h^i} \frac{\sigma_e^0}{|e|} \int_{\Gamma\cap T} [u]_\Gamma\, [\overline{v_h}]_\Gamma ds, \tag{5.10}$$

$$L_f(v_h) \;=\; \int_\Omega f\overline{v_h} dX + \sum_{e\in\mathcal{E}_h^b} \int_e g\overline{v_h} ds. \tag{5.11}$$

The weak form (5.9) suggests the PPIFE method for the Helmholtz interface problem (5.1): find $u_h \in S_h^p(\Omega)$, $p \geq 1$ such that

$$b_h^{PP}(u_h, v_h) = L_f(v_h), \qquad \forall v_h \in S_h^p(\Omega). \tag{5.12}$$

**Remark 5.1.** *The continuity of $v_h|_T$, $\forall T \in \mathcal{T}_h$ for every $v_h \in S_h^1(\Omega)$ implies that the last three terms in the bilinear form $a_h^{PP}(\cdot,\cdot)$ defined in (5.10) can be ignored in the PPIFE method based on the linear and bilinear IFE spaces.*

We will proceed to derive the DGIFE method for the Helmholtz interface problems in the next subsection

### 5.2.2 DGIFE methods for the Helmholtz interface problems

For the DGIFE methods, we begin with (5.6) by using $v_h \in DS_h^p(\Omega)$ instead of $v_h \in S_h^p(\Omega)$. Then, similar to the derivation of PPIFE scheme for Helmholtz interface problems, by assuming that $u$ is in $PH^2(\Omega)$ so that $[u]_e = 0$, $\forall e \in \mathring{\mathcal{E}}_h$ and applying the interface jump condition (5.1c), we have

$$\begin{gathered} \epsilon \sum_{e\in\mathring{\mathcal{E}}_h} \int_e \{\beta\nabla\overline{v_h}\cdot\mathbf{n}_e\}_e [u]_e ds = 0, \quad i \sum_{e\in\mathring{\mathcal{E}}_h} \frac{\sigma_e^0}{|e|} \int_e [u]_e\, [\overline{v_h}]_e ds = 0, \\ \epsilon \int_\Gamma \{\beta\nabla\overline{v_h}\cdot\mathbf{n}_\Gamma\}_\Gamma [u]_\Gamma ds = 0, \quad i\frac{\sigma_e^0}{|e|} \int_\Gamma [u]_\Gamma\, [\overline{v_h}]_\Gamma ds = 0. \end{gathered} \tag{5.13}$$

Similar to the derivation of the PPIFE scheme, we add the four terms above to the left hand side of (5.7), then we can see that the solution $u$ to the Helmholtz interface problem (5.1) satisfies the following weak form:

$$\begin{aligned} &b_h^{DG}(u, v_h) = L_f(v_h), \quad \forall v_h \in DS_h^p(\Omega), \\ \text{with} \quad &b_h^{DG}(u, v_h) = a_h^{DG}(u, v_h) + i\omega(u, v_h)_{\partial\Omega} - \omega^2(u, v_h)_{\Omega}, \end{aligned} \tag{5.14}$$

where the bilinear form $a_h^{DG}(\cdot,\cdot) : PH^2(\Omega) \times DS_h^p(\Omega) \to \mathbb{C}$ and the linear functional $L_f(\cdot) : DS_h^p(\Omega) \to \mathbb{C}$ are defined by

$$\begin{aligned} a_h^{DG}(u, v_h) &= \sum_{T\in\mathcal{T}_h} \int_T \beta\nabla u \cdot \nabla\overline{v_h} dX - \sum_{e\in\mathring{\mathcal{E}}_h} \int_e \{\beta\nabla u \cdot \mathbf{n}_e\}_e [\overline{v_h}]_e ds + \epsilon \sum_{e\in\mathring{\mathcal{E}}_h} \int_e \{\beta\nabla\overline{v_h} \cdot \mathbf{n}_e\}_e [u]_e ds \\ &\quad + i\omega \sum_{e\in\mathcal{E}_h^b} \int_e u\overline{v_h} ds + i \sum_{e\in\mathring{\mathcal{E}}_h} \frac{\sigma_e^0}{|e|} \int_e [u]_e \, [\overline{v_h}]_e ds - \int_\Gamma \{\beta\nabla u \cdot \boldsymbol{n}_\Gamma\} [\overline{v_h}]_\Gamma ds \qquad (5.15) \\ &\quad + \epsilon \int_\Gamma \{\beta\nabla\overline{v_h} \cdot \mathbf{n}_\Gamma\}_\Gamma [u]_\Gamma ds + i\frac{\sigma_e^0}{|e|} \int_\Gamma [u]_\Gamma \, [\overline{v_h}]_\Gamma ds, \\ L_f(v_h) &= \int_\Omega f\overline{v_h} dX + \sum_{e\in\mathcal{E}_h^b} \int_e g\overline{v_h} ds \qquad (5.16) \end{aligned}$$

The weak form (5.14) suggests the DGIFE method for the Helmholtz interface problem: find $u_h \in DS_h^p(\Omega)$, $p \geq 1$ such that

$$b_h^{DG}(u_h, v_h) = L_f(v_h), \quad \forall v_h \in DS_h^p(\Omega). \tag{5.17}$$

**Remark 5.2.** *Similar to the PPIFE method, the continuity of $v_h|_T$, $\forall T \in \mathcal{T}_h$ for every $v_h \in DS_h^1(\Omega)$ implies that the last three terms in the bilinear form $a_h^{DG}(\cdot,\cdot)$ defined in (5.15) can be ignored in the DGIFE method based on the linear and bilinear IFE spaces.*

The following section will provide the error analysis for the linear/bilinear PPIFE methods for Helmholtz interface problems.

## 5.3 Error analysis of symmetric linear/bilinear PPIFE methods

The error estimation to be presented here is for the symmetric linear/bilinear PPIFE methods described by (5.12) (when $p = 1$ and $\epsilon = -1$). In addition to the energy norm $\|\cdot\|_h$ and $|||\cdot|||_h$ defined in (4.36) and (4.37), we will also use the following new energy norm and broken $H^1$ norm for functions $v \in V_h(\Omega)$ ($V_h(\Omega)$ is defined in (2.4)):

$$|||v|||_{\mathcal{H}}^2 = |||v|||_h^2 + \omega^2 \|v\|_{L^2(\Omega)}^2, \tag{5.18}$$

$$\|v\|_{1,\Omega}^2 = \sum_{T\in\mathcal{T}_h} \|v\|_{1,T}^2, \quad |v|_{1,\Omega}^2 = \sum_{T\in\mathcal{T}_h} |v|_{1,T}^2. \tag{5.19}$$

For simplicity, we assume that: the interface does not intersect the boundary, *i.e.*, $\Gamma \cap \partial\Omega = \emptyset$. Also, we make the following assumption on the regularity of the exact solution

**Assumpsion 5.3.1.** *Assume that the exact solution $u$ to the interface problem (5.1) is in $PH^2(\Omega)$ and the following estimate holds for some constant $C$:*

$$\|u\|_{2,\Omega} \leq C\left(\omega + \omega^{-1}\right)\left(\|f\|_{L^2(\Omega)} + \|g\|_{L^2(\partial\Omega)}\right). \tag{5.20}$$

Assumption 5.3.1 can be satisfied when the $\partial\Omega$ and $\Gamma$ are sufficiently smooth, see [50, 118] and [119] for more details. Next we recall a standard estimate for the trace of a $H^1$ function on $\partial\Omega$ in the following lemma.

**Lemma 5.1.** *Assume that $v \in H^1(\Omega)$, then there exists a constant $C$ such that*

$$\|v\|^2_{L^2(\partial\Omega)} \leq C \|v\|_{L^2(\Omega)} \left( \|v\|_{L^2(\Omega)} + |v|_{1,\Omega} \right). \tag{5.21}$$

*Proof.* This result is given in (4.37) in [96]. □

For each function $v \in PH^2(\Omega) \oplus S_h(\Omega)$, we let $J_h v$ be its interpolation in the standard continuous (i.e., $H^1$) linear or bilinear finite element space defined on the same mesh $\mathcal{T}_h$ such that

$$J_h v|_T = J_{h,T} v, \quad \text{with} \quad J_{h,T} v(X) = \sum_{i \in \mathcal{I}_T} v(A_i) \psi_{i,T}(X), \quad \forall X \in T, \quad \forall T \in \mathcal{T}_h, \tag{5.22}$$

where $\psi_{i,T}(X),\ i \in \mathcal{I}_T$ is the linear or bilinear shape functions on the element $T$. Upper bounds of $J_h v$ are given in the following lemma.

**Lemma 5.2.** *There exists a constant $C$ such that the following hold for all $v \in PH^2(\Omega) \oplus S_h(\Omega)$:*

$$\|J_h v\|_{L^2(\Omega)} \leq \|v\|_{L^2(\Omega)} + Ch|v|_{1,\Omega}, \tag{5.23}$$

$$|J_h v|_{1,\Omega} \leq C|v|_{1,\Omega}. \tag{5.24}$$

*Proof.* Let $v \in PH^2(\Omega) \oplus S_h(\Omega)$. Then $v|_T \in H^2(T)$ on $T \in \mathcal{T}_h^n$ and $v|_T \in PH^2(T) \oplus S_h(T)$ on $T \in \mathcal{T}_h^i$. Denote $Y_i(t, X) = tA_i + (1-t)X$, $t \in [0, 1]$. By the first order Taylor expansion, we have

$$v(A_i) = v(X) + \int_0^1 \nabla v \left( Y_i(t, X) \right) \cdot (A_i - X) \, dt. \tag{5.25}$$

Using (5.25) and the partition of unity of the linear and bilinear finite element shape functions on $T \in \mathcal{T}_h$, we have

$$J_h v(X) = J_{h,T} v(X) = v(X) + \sum_{i \in \mathcal{I}_T} \left( \int_0^1 \nabla v(Y_i(t,X)) \cdot (A_i - X) dt \right) \psi_i(X), \quad \forall X \in T. \tag{5.26}$$

Since there exists a constant $C$ such that $\|\psi_i\|_{L^\infty(T)} \leq C$ and $\|A_i - X\| \leq Ch$, from (5.26), we have

$$\begin{aligned}
\|J_h v\|_{L^2(T)} \leq & \|v\|_{L^2(T)} + C \left( \int_T \left( \sum_{i \in \mathcal{I}_T} \int_0^1 \nabla v(Y_i(t,X)) \cdot (A_i - X) dt \right)^2 dX \right)^{1/2} \\
\leq & \|v\|_{L^2(T)} + Ch \int_0^1 \left( \sum_{i \in \mathcal{I}_T} \int_T \|\nabla v(Y_i(t,X))\|^2 dX \right)^{\frac{1}{2}} dt \\
\leq & \|v\|_{L^2(T)} + Ch|v|_{1,T}.
\end{aligned} \tag{5.27}$$

Similarly, by $\|\nabla \psi_{i,T}\|_{L^\infty(T)} \leq Ch^{-1}$, we have

$$\begin{aligned}
\|\nabla J_h v\|_{L^2(T)} = & \left\| \sum_{i \in \mathcal{I}_T} v(A_i) \nabla \psi_{i,T}(X) \right\|_{L^2(T)} \\
= & \left( \int_T \left( \sum_{i \in \mathcal{I}_T} \int_0^1 \nabla v(Y_i(t,X))(A_i - X) dt \nabla \psi_{i,T}(X) \right)^2 dX \right)^{1/2} \\
\leq & Ch^{-1} Ch |v|_{1,T} \\
\leq & C|v|_{1,T}.
\end{aligned} \tag{5.28}$$

Then, summing (5.27) and (5.28) over all elements $T \in \mathcal{T}_h$ leads to estimates (5.23) and (5.24), respectively. □

Since the IFE space $S_h(\Omega)$ is not a subspace of $H^1(\Omega)$ in general [71, 100], the trace inequality cannot be applied to functions in $PH^2(\Omega) \oplus S_h(\Omega)$, for which, nevertheless, we can derive a similar trace inequality as follows.

**Theorem 5.1.** *There exists a constant $C$ such that for every $v \in PH^2(\Omega) \oplus S_h(\Omega)$ the following inequality holds:*

$$\|v\|^2_{L^2(\partial\Omega)} \leq C \left( \|v\|_{L^2(\Omega)} + h|v|_{1,\Omega} \right) \|v\|_{1,\Omega} \,. \tag{5.29}$$

*Proof.* Let $v$ be a function in $PH^2(\Omega) \oplus S_h(\Omega)$ and let $J_h v$ be its standard finite element interpolation described by (5.22), and we have

$$\|v\|^2_{L^2(\partial\Omega)} \leq 2 \left( \|v - J_h v\|^2_{L^2(\partial\Omega)} + \|J_h v\|^2_{L^2(\partial\Omega)} \right). \tag{5.30}$$

We estimate the second term on the right hand side of (5.30) first. Since $J_h v$ is in $H^1(\Omega)$, by Lemma 5.1 and Lemma 5.2, we have

$$\begin{aligned}
\|J_h v\|^2_{L^2(\partial\Omega)} \leq& C \, \|J_h v\|_{L^2(\Omega)} \left( \|J_h v\|_{L^2(\Omega)} + |J_h v|_{1,\Omega} \right) \\
\leq& C \left( \|v\|_{L^2(\Omega)} + Ch|v|_{1,\Omega} \right) \left( \|v\|_{L^2(\Omega)} + Ch|v|_{1,\Omega} + |v|_{1,\Omega} \right) \\
\leq& C \left( \|v\|_{L^2(\Omega)} + h|v|_{1,\Omega} \right) \|v\|_{1,\Omega}.
\end{aligned} \tag{5.31}$$

For the first term on the right hand side of (5.30), we note that $v \in H^2(T)$ on $T \in \mathcal{T}_h^b$ (where we recall that $\mathcal{T}_h^b$ is the set of boundary elements) because of the assumption that the interface $\Gamma$ does not touch boundary elements when $h$ is small enough. Then, using the standard trace inequality on $T \in \mathcal{T}_h^b$ and the approximation capability of finite element space, we have

$$
\begin{aligned}
\|v - J_h v\|^2_{L^2(\partial\Omega)} \leq & \sum_{T \in \mathcal{T}_h^b} \|v - J_h v\|^2_{L^2(\partial T)} \\
\leq & Ch^{-1} \sum_{T \in \mathcal{T}_h^b} \left( \|v - J_h v\|^2_{L^2(T)} + h^2 \|\nabla(v - J_h v)\|^2_{L^2(T)} \right) \\
\leq & Ch^{-1} \sum_{T \in \mathcal{T}_h^b} \left( Ch^2 |v|^2_{1,T} + h^2 \cdot C|v|_{1,T} \right)^2 \\
\leq & Ch \sum_{T \in \mathcal{T}_h^b} |v|^2_{1,T} \\
\leq & Ch|v|^2_{1,\Omega}.
\end{aligned}
\tag{5.32}
$$

Finally, the inequality (5.29) follows from applying (5.31) and (5.32) to (5.30). $\square$

For each function $u \in PH^2(\Omega)$, we recall that its interpolation in the IFE space $S_h(\Omega)$ is as [70, 71, 100]

$$
I_h u|_T = I_{h,T} u, \quad \text{with} \quad \begin{cases} I_{h,T} u(X) = \sum_{i \in \mathcal{I}_T} u(A_i)\phi_{i,T}(X), & \forall X \in T, \quad \forall T \in \mathcal{T}_h^i, \\ I_{h,T} u(X) = \sum_{i \in \mathcal{I}_T} u(A_i)\psi_{i,T}(X), & \forall X \in T, \quad \forall T \in \mathcal{T}_h^n. \end{cases}
\tag{5.33}
$$

The following theorem provides a description about the approximation capability of the IFE spaces in terms of the energy norm $|||\cdot|||_{\mathcal{H}}$.

**Theorem 5.2.** *There exists a constant $C$ such that the following estimate holds for every $u \in PH^2(\Omega)$:*

$$
|||I_h u - u|||_{\mathcal{H}} \leq Ch\|u\|_{2,\Omega}, \quad \forall u \in PH^2(\Omega),
\tag{5.34}
$$

*provided that $\omega h \leq C_0$ for some constant $C_0$.*

*Proof.* By Theorem 3.14 in [71], Theorem 3.7 in [100], and Theorem 4.3, it follows

$$\begin{aligned}\|\!|\!| I_h u - u \|\!|\!|_{\mathcal{H}}^2 &= \|\!|\!| I_h u - u \|\!|\!|_h^2 + \omega^2 \| I_h u - u\|_{L^2(\Omega)}, \\ &\leq Ch^2 \|u\|_{2,\Omega}^2 + C\omega^2 h^4 \|u\|_{2,\Omega}^2 \leq Ch^2 \|u\|_{2,\Omega}^2,\end{aligned}$$

which proves (5.34). □

We now proceed to the error estimation for the symmetric PPIFE methods described by (5.12), and we will follow Schatz's argument [131]. We start from the Gårding's inequality for $b_h^{PP}(.,.)$ in the following lemma.

**Lemma 5.3.** *There exist constants $C_1$ and $C_2$ such that the following inequality holds for $\sigma_e^0$ sufficiently large*

$$|b_h^{PP}(v,v)| \geq C_1 \|\!|\!| v \|\!|\!|_{\mathcal{H}}^2 - C_2 \omega^2 \|v\|_{L^2(\Omega)}, \quad \forall v \in S_h(\Omega). \tag{5.35}$$

*Proof.* First of all, we note that

$$\begin{aligned}|b_h^{PP}(v,v)| &\geq \frac{1}{\sqrt{2}} \left(\mathrm{Re}\left(b_h^{PP}(v,v)\right) + \mathrm{Im}\left(b_h^{PP}(v,v)\right)\right) \\ &= \frac{1}{\sqrt{2}} \left(\mathrm{Re}\left(a_h^{PP}(v,v)\right) + \mathrm{Im}\left(a_h^{PP}(v,v)\right) + \omega \|v\|_{L^2(\partial\Omega)}^2 - \omega^2 \|v\|_{L^2(\Omega)}^2\right).\end{aligned} \tag{5.36}$$

Next, we introduce the bilinear form $\tilde{a}_h(.,.) : V_h(\Omega) \times V_h(\Omega) \to \mathbb{C}$ such that

$$\tilde{a}_h(u,v) = a_h^{PP}(u,v) - i \sum_{e \in \mathring{\mathcal{E}}_h^i} \frac{\sigma_e^0}{|e|} \int_e [u]_e \, [\overline{v}]_e ds, \quad \forall v \in V_h(\Omega).$$

For each $v \in S_h(\Omega)$, we let $v = v_1 + iv_2$ with $v_1 = \mathrm{Re}(v) \in \tilde{S}_h(\Omega)$ and $v_2 = \mathrm{Im}(v) \in \tilde{S}_h(\Omega)$.

Since $a_h(.,.)$ and $\tilde{a}_h(.,.)$ are both bilinear and symmetric, we have

$$a_h^{PP}(v,v) = a_h^{PP}(v_1,v_1) + a_h^{PP}(v_2,v_2).$$

It follows that

$$\begin{aligned}\mathrm{Re}\big(a_h^{PP}(v,v)\big) + \mathrm{Im}\big(a_h^{PP}(v,v)\big) &= \tilde{a}_h(v_1,v_1) + \tilde{a}_h(v_2,v_2) + \sum_{e\in\mathring{\mathcal{E}}_h^i} \frac{\sigma_e^0}{|e|}\int_e [v_1]_e\,[\overline{v_1}]_e ds \\ &\quad + \sum_{e\in\mathring{\mathcal{E}}_h^i} \frac{\sigma_e^0}{|e|}\int_e [v_2]_e\,[\overline{v_2}]_e ds.\end{aligned} \tag{5.37}$$

Because $v_1, v_2 \in \tilde{S}_h(\Omega)$, we can apply Theorem 4.4 to (5.37) so that there exists a constant $\kappa > 0$ such that

$$\mathrm{Re}\left(a_h^{PP}(v,v)\right) + \mathrm{Im}\left(a_h^{PP}(v,v)\right) \geq \kappa(|||v_1|||_h^2 + |||v_2|||_h^2) = \kappa|||v|||_h^2. \tag{5.38}$$

Therefore, applying (5.38) to (5.36) we have

$$\begin{aligned}|b_h^{PP}(v,v)| &\geq \frac{1}{\sqrt{2}}\left(\kappa|||v|||_h^2 + \kappa\omega^2\|v\|_{L^2(\Omega)}^2 - \omega^2(1+\kappa)\|v\|_{L^2(\Omega)}^2\right), \\ &\geq \frac{1}{\sqrt{2}}\left(\kappa|||v|||_{\mathcal{H}}^2 - \omega^2(1+\kappa)\|v\|_{L^2(\Omega)}^2\right),\end{aligned}$$

which proves (5.35). □

The following lemma is about the continuity of the bilinear form $b_h^{PP}(\cdot,\cdot)$.

**Lemma 5.4.** *There exists a constant $C$ such that for every $y, v \in PH^2(\Omega) \oplus S_h(\Omega)$ the following inequality holds*

$$|b_h^{PP}(y,v)| \leq C|||y|||_{\mathcal{H}}|||v|||_{\mathcal{H}}, \tag{5.39}$$

*provided that $\omega h \leq C_0$ for some constant $C_0$.*

*Proof.* By the same arguments used for proving Theorem 4.5, we can show that there exists a constant $C$ such that

$$|a_h^{PP}(y, v)| \leq C|||y|||_h|||v|||_h.$$

Since $\|y\|_{\mathcal{H}} \geq k\|y\|_{L^2(\Omega)}$, then

$$\begin{aligned} |b_h^{PP}(y, v)| &\leq C|||y|||_h|||v|||_h + \omega^2\|y\|_{L^2(\Omega)}\|v\|_{L^2(\Omega)} + C\omega\|y\|_{L^2(\partial\Omega)}\|v\|_{L^2(\partial\Omega)} \\ &\leq C|||y|||_{\mathcal{H}}|||v|||_{\mathcal{H}} + |||y|||_{\mathcal{H}}|||v|||_{\mathcal{H}} + C\omega\|y\|_{L^2(\partial\Omega)}\|v\|_{L^2(\partial\Omega)}. \end{aligned} \tag{5.40}$$

For the third term on the right hand side of (5.40), applying Theorem 5.1, we have

$$\begin{aligned} \omega^2 \|y\|^2_{L^2(\partial\Omega)} \|v\|^2_{L^2(\partial\Omega)} \leq & C\omega^2 \left(\|y\|_{L^2(\Omega)} + h|y|_{1,\Omega}\right) \left(\|v\|_{L^2(\Omega)} + h|v|_{1,\Omega}\right) \|y\|_{1,\Omega} \|v\|_{1,\Omega} \\ = & C \left(\omega \|y\|_{L^2(\Omega)} + \omega h|y|_{1,\Omega}\right) \left(\omega \|v\|_{L^2(\Omega)} + \omega h|v|_{1,\Omega}\right) \|y\|_{1,\Omega} \|v\|_{1,\Omega} \\ \leq & C|||y|||^2_{\mathcal{H}}|||v|||^2_{\mathcal{H}}. \end{aligned} \tag{5.41}$$

Thus, applying (5.41) to (5.40) leads to (5.39). □

Following Schatz's argument [131], we now derive a posteriori error estimate for the symmetric PPIFE solution in the following lemma.

**Lemma 5.5.** *Let $u \in PH^2(\Omega)$ be the exact solution to the problem (5.1), and let $u_h$ be the solution produced by symmetric PPIFE method (5.12) with $\sigma_e^0$ large enough, then there exists a constant $C$ such that*

$$\|u - u_h\|_{L^2(\Omega)} \leq C\left(\omega + 1/\omega\right) h|||u - u_h|||_{\mathcal{H}}, \tag{5.42}$$

*provided that $\omega h \leq C_0$ for some constant $C_0$.*

*Proof.* We define an auxiliary function $z \in PH^2(\Omega)$ as the solution to the problem (5.1), with $f$ replaced by $e_h = u - u_h$ and $g$ replaced by the zero function. In the weak form (5.9) for $z$, choosing $v = e_h$ as the test function yields

$$\|e_h\|^2_{L^2(\Omega)} = b_h^{PP}(z, e_h).$$

Let $I_h z$ be the interpolant of $z$ in IFE space $S_h(\Omega)$ defined by (5.33). Then, it follows

$$\begin{aligned} b_h^{PP}(I_h z, e_h) &= b_h^{PP}(I_h z, u) - b_h^{PP}(I_h z, u_h) \\ &= (f, I_h z)_\Omega + (g, I_h z)_{\partial\Omega} - (f, I_h z)_\Omega - (g, I_h z)_{\partial\Omega} \\ &= 0. \end{aligned}$$

Thus $b_h^{PP}(z, e_h) = b_h^{PP}(z - I_h z, e_h)$. Therefore, by Lemma 5.4, Theorem 5.2 and Assumpsion 5.3.1, we have

$$\begin{aligned} \|e_h\|^2_{L^2(\Omega)} =& b_h^{PP}(z - I_h z, e_h) \\ &\leq C |||z - I_h z|||_{\mathcal{H}} |||e_h|||_{\mathcal{H}} \\ &\leq Ch\|z\|_{2,\Omega} |||e_h|||_{\mathcal{H}} \\ &\leq C\,(\omega + 1/\omega)\,h\|e_h\|_{L^2(\Omega)} |||e_h|||_{\mathcal{H}}, \end{aligned}$$

which proves (5.42). □

Now, we are ready to derive the optimal error bounds in both the energy norm and $L^2$ norm for the symmetric PPIFE methods described by (5.12).

**Theorem 5.3.** *Under the conditions of Lemma 5.5, there exists a constant $C$ such that*

$$|||u - u_h|||_{\mathcal{H}} \leq Ch\|u\|_{2,\Omega}, \tag{5.43}$$

*provided that $(\omega^2+1)h$ is sufficiently small.*

*Proof.* First, we assume that $(\omega^2+1)h$ is sufficiently small such that $kh \leq C_0$ for some constant $C_0$. Denote $e_h = u - u_h$, $\tilde{e}_h = u_h - I_h u$, then by Lemma 5.3 and Lemma 5.4, we have

$$C_1 |||\tilde{e}_h|||_{\mathcal{H}}^2 - C_2\omega^2 \|\tilde{e}_h\|_{L^2(\Omega)}^2 \leq b_h^{PP}(\tilde{e}_h, \tilde{e}_h) = b_h^{PP}(u - I_h u, \tilde{e}_h) \leq C|||u - I_h u|||_{\mathcal{H}} |||\tilde{e}_h|||_{\mathcal{H}}.$$

By the fact that $|||\tilde{e}_h|||_{\mathcal{H}} \geq \omega\|\tilde{e}_h\|_{L^2(\Omega)}$, we then have

$$\begin{aligned}|||\tilde{e}_h|||_{\mathcal{H}}^2 &\leq C|||u - I_h u|||_{\mathcal{H}} |||\tilde{e}_h|||_{\mathcal{H}} + C\omega^2\|\tilde{e}_h\|_{L^2(\Omega)}^2 \\ &\leq C|||u - I_h u|||_{\mathcal{H}} |||\tilde{e}_h|||_{\mathcal{H}} + C\omega|||\tilde{e}_h|||_{\mathcal{H}}\|\tilde{e}_h\|_{L^2(\Omega)}.\end{aligned}$$

Therefore, using Theorem 5.2, we have

$$\begin{aligned}|||\tilde{e}_h|||_{\mathcal{H}} &\leq C|||u - I_h u|||_{\mathcal{H}} + C\omega\|\tilde{e}_h\|_{L^2(\Omega)}, \\ &\leq Ch\|u\|_{2,\Omega} + C\omega\left(\|e_h\|_{L^2(\Omega)} + \|u - I_h u\|_{L^2(\Omega)}\right).\end{aligned}$$

Furthermore, by Lemma 5.5 and the approximation capability of IFE spaces [71, 100], we have

$$\begin{aligned}|||\tilde{e}_h|||_{\mathcal{H}} \leq& Ch\|u\|_{2,\Omega} + C\omega\left(C(\omega + 1/\omega)h|||e_h|||_{\mathcal{H}} + Ch^2\|u\|_{2,\Omega}\right) \\ \leq& Ch\|u\|_{2,\Omega} + C\omega(\omega + 1/\omega)h|||e_h|||_{\mathcal{H}} + C\omega h^2\|u\|_{2,\Omega}, \\ \leq& Ch\|u\|_{2,\Omega} + C(\omega^2+1)h|||e_h|||_{\mathcal{H}}.\end{aligned} \tag{5.44}$$

Hence, by (5.44), we have

$$\begin{aligned}\|e_h\|_{\mathcal{H}} &\leq \|u - I_h u\|_{\mathcal{H}} + \|\tilde{e}_h\|_{\mathcal{H}} \\ &\leq \|u - I_h u\|_{\mathcal{H}} + Ch\|u\|_{2,\Omega} + C(\omega^2+1)h\|e_h\|_{\mathcal{H}}.\end{aligned}$$

Then, by Theorem 5.2 again, the inequality above becomes

$$\left(1 - C(\omega^2+1)h\right)\|e_h\|_{\mathcal{H}} \leq Ch\|u\|_{2,\Omega},$$

which proves (5.43) provided that $(\omega^2+1)h$ is sufficiently small. □

**Remark 5.3.** *According to [131], if $u_h$ is a PPIFE solution corresponding to $u = 0$, then from Theorem 4.6 it follows that $u_h = 0$ provided that $h$ is sufficiently small guaranteeing $(\omega^2+1)h$ is sufficiently small. This implies that the linear system to solve $u_h$ induced from the symmetric PPIFE scheme (4.9) is nonsingular; therefore, the PPIFE solution $u_h$ defined by (5.12) exists and is unique.*

**Theorem 5.4.** *Under the conditions of Theorem 5.3, there exists a constant $C$, such that*

$$\|u - u_h\|_{L^2(\Omega)} \leq C\left(\omega + 1/\omega\right)h^2\|u\|_{2,\Omega}. \tag{5.45}$$

*Proof.* The estimate (5.45) follows directly from Lemma 5.5 and Theorem 5.3. □

## 5.4 Numerical Examples

We now present two numerical examples for the Helmholtz interface problems. The first example (to be precise, the first group of examples) aims to illustrate the feature of the IFE methods, especially the higher degree methods. While the second example aims to corroborate the theoretical results of error analysis in Section 5.3. In these numerical example, the solution domain is $\Omega = (-1,1) \times (-1,1)$ on which we form a rectangular mesh $\mathcal{T}_h$ by partitioning $\Omega$ into $N \times N$ congruent squares of size $h = 2/N$ or we construct a Cartesian triangular mesh $\mathcal{T}_h$ by further dividing each rectangular element in the previous rectangular mesh into two congruent triangles along its diagonal line. The Helmholtz interface problem to be considered is such that it has an interface $\Gamma : x^2 + y^2 - r_0^2 = 0$, $r_0 = \pi/6.28$ separating $\Omega$ into two subdomains

$$\Omega^- = \left\{(x,y) : x^2 + y^2 < r_0^2\right\}, \quad \Omega^+ = \Omega \backslash \overline{\Omega^-}.$$

**Example 5.4.1.** *Functions $f$ and $g$ in the Helmholtz interface problem (5.1) are chosen such that its exact solution is:*

$$u(x,y) = \begin{cases} \dfrac{1}{\beta^-} U(r), & (x,y) \in \Omega^-, \\ \dfrac{1}{\beta^+} U(r) + \left(\dfrac{1}{\beta^-} - \dfrac{1}{\beta^+}\right) U(r_0), & (x,y) \in \Omega^+, \end{cases} \tag{5.46}$$

*where $r = \sqrt{x^2+y^2}, U(r) = \frac{\cos(\omega r)}{\omega} - \frac{\cos(\omega) + i\sin(\omega)}{\omega(J_0(\omega) + iJ_1(\omega))} J_0(\omega r)$, and $J_\gamma(z), \gamma = 0, 1$ are the 0-th and 1-st order Bessel functions of the first kind.*

For the PPIFE and DGIFE scheme, we choose $\epsilon = -1$, so the PPIFE and DGIFE schemes are symmetric PPIFE (SPPIFE)/symmetric DGIFE (SDGIFE) schemes, respectively, and we choose the penalty parameter $\sigma_e^0 = 30\max\{\beta^-, \beta^+\}$. We apply these IFE methods to Helmholtz interface problems with $\beta^- = 1$, $\beta^+ = 5$ or 50 representing small and moderately large discontinuity in the coefficient $\beta$, and to Helmholtz interface problems with $\omega = 10$ or 50 for small and larger wave numbers.

Figures 5.1-5.4 compare the cubic DGIFE solutions to the exact solutions of two groups of Helmholtz interface problems. Figures 5.1 and 5.2 are for the interface problems whose coefficient $\beta$ is such that $\beta^- = 1, \beta^+ = 50$, but Figures 5.3 and 5.4 are for $\beta^- = 50, \beta^+ = 1$. These plots demonstrate that the proposed IFE methods can satisfactorily solve the Helmholtz interface problems with either a small wave number $\omega = 10$ or a moderately large wave number $\omega = 50$.

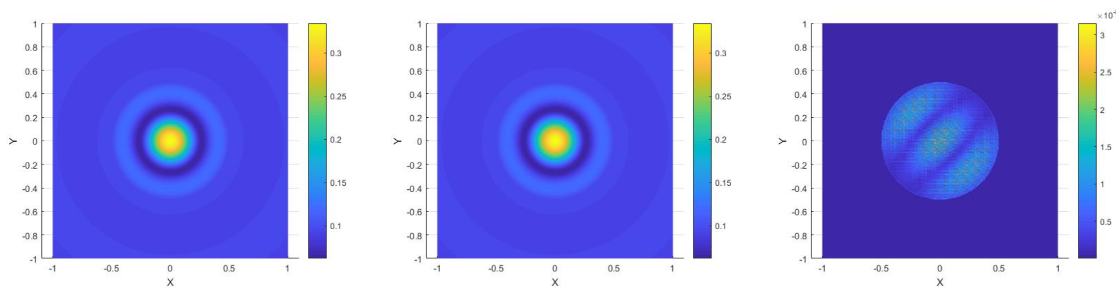

(a) cubic DGIFE solution (b) exact solution (c) error

Figure 5.1: magnitude of cubic DGIFE solution, exact solution and errors between them at finite element nodes when $\omega = 10$, $\beta^- = 1$, $\beta^+ = 50$, $N = 160$.

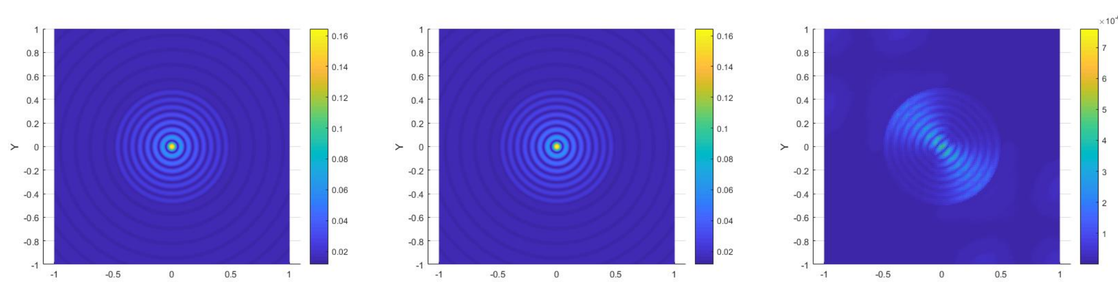

(a) cubic DGIFE solution (b) exact solution (c) error

Figure 5.2: magnitude of cubic DGIFE solution, exact solution and errors between them at finite element nodes when $\omega = 50$, $\beta^- = 1$, $\beta^+ = 50$, $N = 160$.

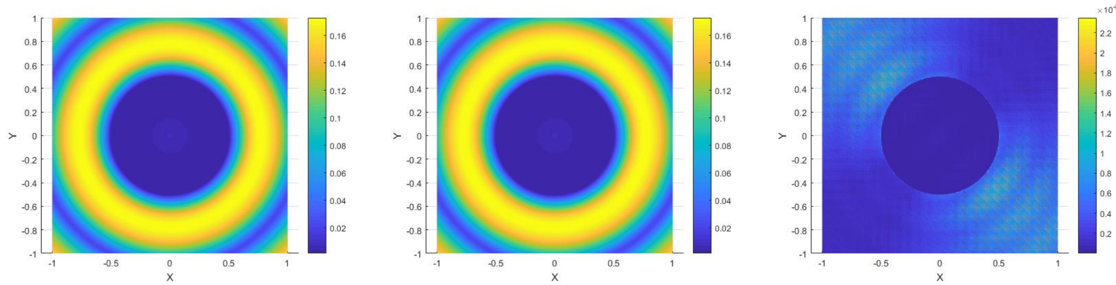

(a) cubic DGIFE solution (b) exact solution (c) error

Figure 5.3: magnitude of cubic DGIFE solution, exact solution and errors between them at finite element nodes when $\omega = 10$, $\beta^- = 50$, $\beta^+ = 1$, $N = 160$.

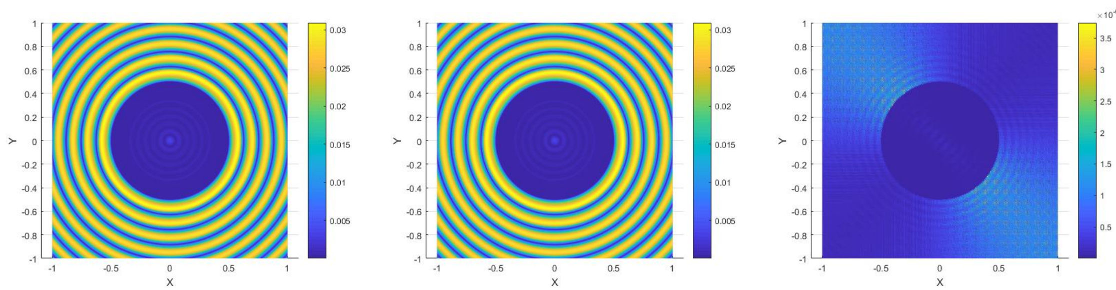

(a) cubic DGIFE solution (b) exact solution (c) error

Figure 5.4: magnitude of cubic DGIFE solution, exact solution and errors between them at finite element nodes when $\omega = 50$, $\beta^- = 50$, $\beta^+ = 1$, $N = 160$.

From Figures 5.1-5.4, we also observe that the solution $u$ oscillates more for the Helmholtz interface problem with a larger wave number, and $u$ has a smaller magnitude in the subdomain where $\beta$ has a larger value. It is well known that the oscillation in the exact solution $u$ to the Helmholtz equation dictates the mesh size for its numerical solution; otherwise, the accuracy or convergence of the numerical solution cannot be guaranteed if the mesh size is not sufficiently small to resolve the oscillation. For the convergence, we recall the *critical mesh size* discussed in [50] that indicates when the numerical solutions start to converge:

**Definition 5.1.** *(**critical mesh size**) For fixed $\omega$ and $f$, the critical mesh size is defined to be the maximum mesh size $H(\omega, f)$ such that*

**(C1)** *$e(h,\omega) < 1$ for $h < H(\omega, f)$,*

**(C2)** *$e(h,\omega) \to 0$ as $h \to 0$,*

*where $e(h,\omega) = |u - u_h|_{1,\Omega}/|u|_{1,\Omega}$ is the relative error in semi-$H^1$ norm.*

By the data in Table 5.1, we can see that the linear PPIFE solution converges from a coarse mesh with $h = 2/10$ when the wave number in the interface problem is small $\omega = 10$, and this suggests the critical mesh size $H(10, f) \lessapprox 2/10$. However, for the interface problem with a large wave number $\omega = 50$ but a small discontinuity in $\beta$, the critical mesh size for the PPIFE solution seems to be much smaller $H(50, f) \lessapprox 2/170$. When the discontinuity in $\beta$ is larger, the critical mesh size for the linear IFE solution $H(50, f) \lessapprox 2/230$ which is even smaller. Even though not presented here for the sake of controlling the page consumption, we have observed in our numerical experiments that, for either small or large discontinuity in $\beta$, the critical mesh size for the cubic PPIFE solution is about $2/10$ when the wave number is small $\omega = 10$, but for a large wave number $\omega = 50$ it becomes about $2/30$. Therefore, higher degree IFE methods can start to converge on rather coarse mesh even for higher wave numbers. Similar behaviors are also observed for the DGIFE solutions.

From the data in Table 5.1, we can see that IFE solutions do not converge optimally until the mesh is further reduced beyond the critical mesh size, and this motivates us to introduce the *optimal mesh size* to characterize this phenomenon:

**Definition 5.2.** *(**optimal mesh size**) For fixed $\omega$ and $f$, the optimal mesh size is defined to be the maximum mesh size $\tilde{H}(\omega, f)$ such that*

**(O1)** *$\|u - u_h\|_{0,\Omega} \approx Ch^{p+1}$ for $h < \tilde{H}(\omega, f)$,*

**(O2)** *$|u - u_h|_{1,\Omega} \approx Ch^{p}$ for $h < \tilde{H}(\omega, f)$,*

*where $p \geq 1$ is the degree of polynomials used in $S_h^p(\Omega)$ and $DS_h^p(\Omega)$.*

From the data presented in Table 5.1 and Table 5.2, we can see that when the wave number is small $\omega = 10$ and the discontinuity in $\beta$ is small, the optimal mesh size for the linear PPIFE solution seems to be $\tilde{H}(10, f) \lessapprox 2/360$. But when the discontinuity in $\beta$ is larger, the optimal mesh size for the linear PPIFE solution seems to be a little smaller $\tilde{H}(10, f) \lessapprox 2/420$. However, for a larger number $\omega = 50$, the data in Table 5.1 indicate that the optimal mesh size for the linear PPIFE solution seems to be drastically smaller such that $\tilde{H}(50, f) \lessapprox 2/1280$, and we note that $\tilde{H}(50, f) \ll H(50, f)$, i.e., the optimal mesh size for the linear PPIFE solution is much smaller than its critical mesh size. Similar characteristics is observed for bilinear PPIFE solution, linear DGIFE solution, and bilinear DGIFE solution, and this clearly demonstrates the inefficiency of using lower degree method to solve a Helmholtz interface problem with a large wave number.

On the other hand, for this Helmholtz interface problem with a small wave number $\omega = 10$, the data in Table 5.3 show that the optimal mesh size for cubic PPIFE solution seems to be such that $\tilde{H}(10, f) \lessapprox 2/40$ when $\beta$ has a small discontinuity, and $\tilde{H}(10, f) \lessapprox 2/80$ when $\beta$ has a larger discontinuity. For a large wave number $\omega = 50$, the data in Table 5.3 show that the optimal mesh size for cubic PPIFE solution seems to be such that $\tilde{H}(50, f) \lessapprox 2/260$ which is much larger than the optimal mesh size for the linear PPIFE solution. Therefore, the higher degree IFE methods are advantageous because they can converge optimally on much coarser mesh than lower degree PPIFE methods. Similar behavior has also been observed for DGIFE methods in our numerical experiments.

We can also see the advantage of higher degree IFE methods from the point of view of the global degrees of freedom and accuracy. According to the discussions above, for a small wave number $\omega = 10$ and a small discontinuity in $\beta$, the linear PPIFE solution starts to converge optimally once its mesh size is such that $h = \tilde{H}(10, f) \lessapprox 2/360$, and on such a mesh, the global degrees of freedom (GDOF) in this linear PPIFE solution is about $(361)^2 = 130321$.

In comparison, the cubic PPIFE solution starts to converge optimally once its mesh size is such that $h = \tilde{H}(10, f) \lessapprox 2/40$, and the GDOF in this cubic PPIFE solution is about $(3 \times 40 + 1))^2 = 14641$ which is about 9 times smaller than the GDOF of the linear PPIFE solution.

Far more importantly, by comparing data in Table 5.1, Table 5.2, and Table 5.3, we can see that, on meshes whose mesh sizes are smaller than the optimal mesh sizes, the cubic PPIFE solution is obviously far more accurate than the linear PPIFE solution even though the GDOF of the linear PPIFE solution is much larger. Similar advantages are also observed for higher degree DGIFE methods. Therefore, for wave propagation interface problems, the higher degree IFE methods should be preferred even though the development of higher degree IFE methods is still in its early stage, its research deserves more attention.

By design, the linear and bilinear IFE spaces are consistent with their corresponding FE spaces, i.e., the linear/bilinear IFE space becomes linear/bilinear FE space when $\beta^- = \beta^+$. Also, the formulations for the PPIFE method and the FE method are quite close to each other, they differ only on interface elements whose union forms a small band around the interface. Therefore, it is interesting to know how the PPIFE and FE solutions behave from the point of views of the critical mesh size and the optimal mesh size. From the data in Table 5.4, when the wave number is small $\omega = 10$, the critical mesh size for the linear FE solution is about $2/10$ which is not much different from the critical mesh size for the linear IFE solution according to the data in Table 5.1. For a larger wave number $\omega = 50$, the data in Table 5.4 indicate that the critical mesh size for the linear FE solution is about $2/140$ which is again not much different from the critical mesh size for the linear IFE solution which is about $2/170$ when the discontinuity in $\beta$ is small according to the data in Table 5.1, but the difference becomes a little more obvious when the discontinuity is larger. We also have observed that the critical mesh size of a cubic IFE method is just slightly smaller than that of its FE counterpart.

As for the optimal mesh size, by Table 5.4, when the wave number is small $\omega = 10$, the optimal mesh size for the linear FE solution seems to be about 2/100 which is obviously larger than the optimal mesh for the linear PPIFE solution which is about 2/360 when the discontinuity in $\beta$ is small. However, for a large wave number $\omega = 50$, the data in Table 5.5 suggest that the optimal mesh for the cubic FE solution is about 2/260 which is comparable to the optimal mesh size for the cubic PPIFE solution suggested by the data in Table 5.3. Similar behaviors are also observed for DGIFE and DG methods. In summary, for Helmholtz problems, higher degree IFE methods and FE method behave somewhat similarly, especially when the discontinuity in $\beta$ is small or from the point of view of the optimal mesh size.

**Example 5.4.2.** *In the second example, we let functions $f$ and $g$ in the interface problem* (5.1) *be generated with the following exact solution:*

$$u(x,y) = \begin{cases} \dfrac{2+i}{\beta^-} r^\alpha, & (x,y) \in \Omega^-, \\ \dfrac{2+i}{\beta^+} r^\alpha + \left( \dfrac{2+i}{\beta^-} - \dfrac{2+i}{\beta^+} \right) r_0^\alpha, & (x,y) \in \Omega^+, \end{cases} \tag{5.47}$$

where $\alpha = 1.5$, $r = \sqrt{x^2 + y^2}$. This numerical example is designed to validate the error estimates in Theorems 5.3 and 5.4. We note that the group of examples in Example 5.4.1 provides quite a few numerical examples to illustrate the features of the PPIFE methods developed there for solving the Helmholtz interface problems, showing optimal convergence rates.

However, the exact solutions in the examples presented in Example 5.4.1 have a regularity better than piecewise $H^r$ with $r > 2$. Hence, it is interesting to see how the PPIFE solution converges when the exact solution only has piecewise $H^2$ regularity. Actually, for the chosen $\alpha$ value in this example, it can be verified that, $u \in PH^2(\Omega)\backslash PH^3(\Omega)$. By choosing

$\sigma_e^0 = 30 \max\{\beta^-, \beta^+\}$ for the parameter required in (5.10), Table 5.6 presents errors of the symmetric linear PPIFE solutions $u_h$ generated on a sequence of uniform triangular meshes $\mathcal{T}_h$ of $\Omega$ in a certain configuration of $\omega$, $\beta^-$, $\beta^+$.

The results demonstrate that, for fixed $\omega$, the symmetric PPIFE solutions converge optimally in both the semi-$H^1$ and the $L^2$ norms to the exact solution $u \in PH^2(\Omega)\backslash PH^3(\Omega)$, and this validates the theoretical results established in Theorem 5.3 and Theorem 5.4 in Section 5.3.

## 5.5 Conclusion

In this chaper, we have considered two IFE methods: the PPIFE and DGIFE methods for solving the Helmholtz interface problem. For the Helmholtz interface problem with a small wave number, the proposed PPIFE and DGIFE methods can produce optimally convergent approximate solutions on interface-independent meshes whose mesh size is fine enough.

However, when the wave number is large, the lower degree (linear or bilinear) IFE methods do not seem to be good choices because they usually do not demonstrate the optimal convergence unless the mesh size is extremely small. Instead, our explorations strongly suggest to use higher degree IFE methods because they can quickly start to converge optimally and produce far more accurate numerical solutions when the mesh size is reduced. Numerical experiments demonstrate that a large discontinuity in the coefficient $\beta$ will challenge the PPIFE and DGIFE methods, but this kind of challenge seems to be at a level far lower than the challenge from a large wave number. We also have observed that higher degree IFE methods and higher FE methods behave somewhat similarly from the point of view of the *critical mesh size* and the *optimal mesh size*.

For the error analysis, we have conducted an error estimation for the symmetric linear/-

bilinear PPIFE methods. Under the assumption that the exact solution possesses a usual piecewise $H^2$ regularity, the optimal error estimates for the PPIFE solutions are derived in an energy norm and the usual $L^2$ norm provided that the mesh size is sufficiently small. The follow-up numerical example validates the theoretical results of error estimates.

| $\omega$ | $\beta^+$ | $N$ | $\|u-u_h\|_{0,\Omega}$ | rate | $\|u-u_h\|_{1,\Omega}$ | rate | $e(h,w)$ |
|---|---|---|---|---|---|---|---|
| 10 | 5 | 10 | 8.2104e-02 | NA | 7.4639e-01 | NA | 7.2748e-01 |
| | | 20 | 4.9816e-02 | 0.7208 | 4.7736e-01 | 0.6448 | 4.6526e-01 |
| | | 40 | 1.6991e-02 | 1.5519 | 2.0544e-01 | 1.2164 | 2.0023e-01 |
| | | 80 | 4.5312e-03 | 1.9068 | 8.7699e-02 | 1.2281 | 8.5477e-02 |
| | | 160 | 1.1495e-03 | 1.9789 | 4.1293e-02 | 1.0867 | 4.0247e-02 |
| | | 320 | 2.8953e-04 | 1.9892 | 2.0298e-02 | 1.0245 | 1.9784e-02 |
| | | 640 | 7.2356e-05 | 2.0005 | 1.0106e-02 | 1.0062 | 9.8499e-03 |
| | | 1280 | 1.8062e-05 | 2.0021 | 5.0476e-03 | 1.0015 | 4.9197e-03 |
| 10 | 50 | 10 | 6.4644e-02 | NA | 7.5030e-01 | NA | 7.5659e-01 |
| | | 20 | 3.3762e-02 | 0.9371 | 4.0855e-01 | 0.8769 | 4.1197e-01 |
| | | 40 | 2.0716e-02 | 0.7047 | 2.4551e-01 | 0.7347 | 2.4756e-01 |
| | | 80 | 1.0567e-02 | 0.9712 | 1.2749e-01 | 0.9454 | 1.2856e-01 |
| | | 160 | 3.4762e-03 | 1.6039 | 5.1411e-02 | 1.3102 | 5.1841e-02 |
| | | 320 | 9.1923e-04 | 1.9190 | 2.1448e-02 | 1.2612 | 2.1627e-02 |
| | | 640 | 2.3301e-04 | 1.9800 | 1.0022e-02 | 1.0976 | 1.0106e-02 |
| | | 1280 | 5.8619e-05 | 1.9910 | 4.9165e-03 | 1.0275 | 4.9576e-03 |
| 50 | 5 | 80 | 3.9451e-02 | -0.3967 | 1.6817e+00 | -0.3401 | 1.4876e+00 |
| | | 160 | 2.8478e-02 | 0.4702 | 1.1843e+00 | 0.5059 | 1.0357e+00 |
| | | 170 | 2.5688e-02 | 1.7007 | 1.0693e+00 | 1.6846 | 9.4531e-01 |
| | | 180 | 2.2661e-02 | 2.1937 | 9.4548e-01 | 2.1536 | 8.3582e-01 |
| | | 190 | 1.9804e-02 | 2.4923 | 8.2939e-01 | 2.4231 | 7.3319e-01 |
| | | 200 | 1.7282e-02 | 2.6557 | 7.2717e-01 | 2.5642 | 6.4283e-01 |
| | | 320 | 5.1669e-03 | 2.5689 | 2.3826e-01 | 2.3740 | 2.1095e-01 |
| | | 640 | 1.2047e-03 | 2.1006 | 7.5049e-02 | 1.6666 | 6.6484e-02 |
| | | 1280 | 2.7773e-04 | 2.1170 | 3.0119e-02 | 1.3171 | 2.6673e-02 |
| | | 2560 | 6.8813e-05 | 2.0129 | 1.4235e-02 | 1.0813 | 1.2664e-02 |
| 50 | 50 | 160 | 4.0513e-02 | 0.0049 | 1.8752e+00 | 0.0178 | 1.7055e+00 |
| | | 210 | 3.3354e-02 | 0.7150 | 1.5637e+00 | 0.6680 | 1.4222e+00 |
| | | 220 | 2.7486e-02 | 4.1599 | 1.2931e+00 | 4.0842 | 1.1761e+00 |
| | | 230 | 2.2856e-02 | 4.1500 | 1.0792e+00 | 4.0680 | 9.8156e-01 |
| | | 240 | 1.9322e-02 | 3.9462 | 9.1595e-01 | 3.8543 | 8.3306e-01 |
| | | 250 | 1.6556e-02 | 3.7845 | 7.8804e-01 | 3.6846 | 7.1673e-01 |
| | | 320 | 7.5321e-03 | 3.1904 | 3.7059e-01 | 3.0562 | 3.3705e-01 |
| | | 640 | 1.4355e-03 | 2.3915 | 8.6787e-02 | 2.0943 | 7.8931e-02 |
| | | 1280 | 3.3874e-04 | 2.0833 | 3.1457e-02 | 1.4641 | 2.8610e-02 |
| | | 2560 | 8.3515e-05 | 2.0201 | 1.4101e-02 | 1.1576 | 1.2825e-02 |

Table 5.1: Errors in linear SPPIFE solution and convergence rates for $\beta^- = 1$, different $\beta^+$ and $\omega$

| $\omega$ | $\beta^+$ | $N$ | $\|u-u_h\|_{0,\Omega}$ | rate | $\|u-u_h\|_{1,\Omega}$ | rate | $e(h,w)$ |
|---|---|---|---|---|---|---|---|
| | | 320 | 2.8953e-04 | NA | 2.0298e-02 | NA | 1.9784e-02 |
| | | 330 | 2.7060e-04 | 2.1969 | 1.9676e-02 | 1.0115 | 1.9178e-02 |
| 10 | 5 | 340 | 2.5617e-04 | 1.8364 | 1.9092e-02 | 1.0099 | 1.8608e-02 |
| | | 350 | 2.4053e-04 | 2.1725 | 1.8540e-02 | 1.0115 | 1.8070e-02 |
| | | 360 | 2.2829e-04 | 1.8539 | 1.8022e-02 | 1.0064 | 1.7565e-02 |
| | | 370 | 2.1555e-04 | 2.0964 | 1.7529e-02 | 1.0129 | 1.7084e-02 |
| | | 380 | 2.0469e-04 | 1.9384 | 1.7066e-02 | 1.0037 | 1.6633e-02 |
| | | 390 | 1.9430e-04 | 2.0050 | 1.6622e-02 | 1.0129 | 1.6201e-02 |
| | | 400 | 2.0469e-04 | 2.0265 | 1.6206e-02 | 1.0029 | 1.5795e-02 |
| | | 410 | 1.9430e-04 | 1.9657 | 1.5806e-02 | 1.0114 | 1.5405e-02 |
| | | 400 | 5.9551e-04 | NA | 1.5353e-02 | NA | 1.6780e-02 |
| | | 420 | 5.4036e-04 | 1.9919 | 1.5761e-02 | 1.1128 | 1.5893e-02 |
| 10 | 50 | 440 | 4.9144e-04 | 2.0400 | 1.4969e-02 | 1.1085 | 1.5094e-02 |
| | | 460 | 4.5041e-04 | 1.9613 | 1.4260e-02 | 1.0924 | 1.4379e-02 |
| | | 480 | 4.1440e-04 | 1.9577 | 1.4260e-02 | 1.0840 | 1.3731e-02 |
| | | 500 | 3.8156e-04 | 2.0225 | 1.3617e-02 | 1.0848 | 1.3136e-02 |
| | | 520 | 3.5217e-04 | 2.0434 | 1.3027e-02 | 1.0795 | 1.2591e-02 |
| | | 540 | 3.2554e-04 | 2.0840 | 1.1996e-02 | 1.0773 | 1.2090e-02 |
| | | 560 | 2.8306e-04 | 1.9568 | 1.1538e-02 | 1.0611 | 1.1207e-02 |
| | | 580 | 2.6451e-04 | 1.9994 | 1.1118e-02 | 1.0574 | 1.0812e-02 |

Table 5.2: Errors in linear SPPIFE solution and convergence rates for $\beta_1 = 1$, different $\beta_2$ and $\omega$

| $\omega$ | $\beta^+$ | $N$ | $\|u-u_h\|_{0,\Omega}$ | rate | $\|u-u_h\|_{1,\Omega}$ | rate | $e(h,w)$ |
|---|---|---|---|---|---|---|---|
| 10 | 5 | 40 | 1.7107e-06 | NA | 4.1486e-04 | NA | 4.1486e-04 |
| | | 50 | 6.9536e-07 | 4.0343 | 2.1274e-04 | 2.9930 | 2.1274e-04 |
| | | 60 | 3.3424e-07 | 4.0180 | 1.2326e-04 | 2.9937 | 1.2326e-04 |
| | | 70 | 1.7995e-07 | 4.0168 | 7.7668e-05 | 2.9960 | 7.7668e-05 |
| | | 80 | 1.0543e-07 | 4.0033 | 5.2073e-05 | 2.9941 | 5.2073e-05 |
| 10 | 50 | 80 | 1.0522e-07 | NA | 5.1511e-05 | NA | 5.1942e-05 |
| | | 90 | 6.5444e-08 | 4.0319 | 3.6176e-05 | 3.0005 | 3.6478e-05 |
| | | 100 | 4.2864e-08 | 4.0164 | 2.6386e-05 | 2.9950 | 2.6607e-05 |
| | | 110 | 2.9224e-08 | 4.0187 | 1.9829e-05 | 2.9973 | 1.9995e-05 |
| | | 120 | 2.0628e-08 | 4.0033 | 1.5276e-05 | 2.9982 | 1.5404e-05 |
| | | 130 | 1.4951e-08 | 4.0218 | 1.2009e-05 | 3.0060 | 1.2110e-05 |
| 50 | 5 | 160 | 1.0869e-06 | 4.3450 | 9.8166e-04 | 2.9970 | 8.6781e-04 |
| | | 180 | 6.5893e-07 | 4.2427 | 6.8980e-04 | 2.9983 | 6.0979e-04 |
| | | 200 | 4.2458e-07 | 4.1736 | 5.0307e-04 | 2.9978 | 4.4472e-04 |
| | | 220 | 2.8662e-07 | 4.1252 | 3.7808e-04 | 2.9972 | 3.3423e-04 |
| | | 240 | 2.0079e-07 | 4.0882 | 2.9128e-04 | 2.9976 | 2.5750e-04 |
| | | 260 | 1.4498e-07 | 4.0646 | 2.2913e-04 | 2.9993 | 2.0256e-04 |
| | | 280 | 1.0736e-07 | 4.0497 | 1.8349e-04 | 3.0001 | 1.6220e-04 |
| | | 300 | 8.1240e-08 | 4.0363 | 1.4921e-04 | 2.9984 | 1.3190e-04 |
| | | 320 | 6.2625e-08 | 4.0245 | 1.2296e-04 | 2.9963 | 1.0870e-04 |
| 50 | 50 | 160 | 1.0830e-06 | 4.4365 | 9.4940e-04 | 2.9972 | 8.6348e-04 |
| | | 180 | 6.5049e-07 | 4.3017 | 6.6717e-04 | 2.9970 | 6.0680e-04 |
| | | 200 | 4.1663e-07 | 4.2111 | 4.8660e-04 | 2.9963 | 4.4257e-04 |
| | | 220 | 2.8016e-07 | 4.1513 | 3.6573e-04 | 2.9960 | 3.3263e-04 |
| | | 240 | 1.9577e-07 | 4.1099 | 2.8179e-04 | 2.9962 | 2.5629e-04 |
| | | 260 | 1.4112e-07 | 4.0807 | 2.2170e-04 | 2.9956 | 2.0164e-04 |
| | | 280 | 1.0438e-07 | 4.0646 | 1.7754e-04 | 2.9965 | 1.6147e-04 |
| | | 300 | 7.8916e-08 | 4.0491 | 1.4437e-04 | 2.9958 | 1.3131e-04 |
| | | 320 | 6.0794e-08 | 4.0364 | 1.1898e-04 | 2.9948 | 1.0821e-04 |

Table 5.3: Errors in cubic SPPIFE solution and convergence rates for $\beta_1 = 1$, different $\beta_2$ and $\omega$

| $\omega$ | $\beta^+$ | $N$ | $\|u-u_h\|_{0,\Omega}$ | rate | $\|u-u_h\|_{1,\Omega}$ | rate | $e(h,w)$ |
|---|---|---|---|---|---|---|---|
| 10 | 1 | 10 | 1.4494e-01 | NA | 1.5230e+00 | NA | 9.2162e-01 |
| | | 20 | 6.4454e-02 | 1.1692 | 7.9105e-01 | 0.9450 | 4.7870e-01 |
| | | 40 | 1.8912e-02 | 1.8572 | 3.1627e-01 | 1.3221 | 1.9139e-01 |
| | | 80 | 4.9128e-03 | 1.9713 | 1.3738e-01 | 1.1335 | 8.3135e-02 |
| | | 90 | 3.8919e-03 | 1.9778 | 1.2056e-01 | 1.1089 | 7.2956e-02 |
| | | 100 | 3.1583e-03 | 1.9823 | 1.0748e-01 | 1.0901 | 6.5040e-02 |
| | | 110 | 2.6138e-03 | 1.9856 | 9.7007e-02 | 1.0755 | 5.8703e-02 |
| 50 | 1 | 80 | 4.2659e-02 | NA | 2.1287e+00 | NA | 1.2300e+00 |
| | | 90 | 4.1340e-02 | 0.2668 | 2.0649e+00 | 0.2584 | 1.1931e+00 |
| | | 100 | 4.0504e-02 | 0.1937 | 2.0246e+00 | 0.1874 | 1.1698e+00 |
| | | 110 | 3.9731e-02 | 0.2023 | 1.9877e+00 | 0.1929 | 1.1485e+00 |
| | | 120 | 3.8340e-02 | 0.4094 | 1.9218e+00 | 0.3876 | 1.1104e+00 |
| | | 130 | 3.6248e-02 | 0.7011 | 1.8218e+00 | 0.6671 | 1.0527e+00 |
| | | 140 | 3.3800e-02 | 0.9438 | 1.7040e+00 | 0.9021 | 9.8458e-01 |
| | | 150 | 3.1281e-02 | 1.1224 | 1.5821e+00 | 1.0758 | 9.1415e-01 |
| | | 160 | 2.8836e-02 | 1.2611 | 1.4632e+00 | 1.2106 | 8.4544e-01 |

Table 5.4: Errors in linear FE solution for $\beta_1 = \beta_2 = 1$

| $\omega$ | $\beta^+$ | $N$ | $\|u-u_h\|_{0,\Omega}$ | rate | $\|u-u_h\|_{1,\Omega}$ | rate | $e(h,w)$ |
|---|---|---|---|---|---|---|---|
| 50 | 1 | 240 | 3.1879e-07 | 4.1290 | 4.6238e-04 | 2.9985 | 2.6717e-04 |
| | | 250 | 2.6955e-07 | 4.1100 | 4.0911e-04 | 2.9986 | 2.3638e-04 |
| | | 260 | 2.2952e-07 | 4.0982 | 3.6372e-04 | 2.9987 | 2.1016e-04 |
| | | 270 | 1.9674e-07 | 4.0840 | 3.2480e-04 | 2.9987 | 1.8767e-04 |
| | | 280 | 1.6963e-0 | 4.0763 | 2.9124e-04 | 2.9989 | 1.6828e-04 |
| | | 290 | 1.4708e-07 | 4.0655 | 2.6215e-04 | 2.9989 | 1.5147e-04 |
| | | 300 | 1.2816e-07 | 4.0607 | 2.3680e-04 | 2.9990 | 1.3683e-04 |
| | | 310 | 1.1222e-07 | 4.0518 | 2.1463e-04 | 2.9990 | 1.2401e-04 |
| | | 320 | 9.8681e-08 | 4.0491 | 1.9513e-04 | 2.9991 | 1.1275e-04 |

Table 5.5: Errors in cubic FE solution for $\beta_1 = \beta_2 = 1$.

| $N$ | $\|u - u_h\|_{0,\Omega}$ | rate | $\|u - u_h\|_{1,\Omega}$ | rate |
|---|---|---|---|---|
| 10 | 3.6019e-02 | NA | 5.2313e-01 | NA |
| 20 | 1.6412e-02 | 1.1340 | 2.5292e-01 | 1.0485 |
| 40 | 6.6539e-03 | 1.3025 | 1.1802e-01 | 1.0997 |
| 80 | 1.3425e-03 | 2.3092 | 5.1500e-02 | 1.1964 |
| 160 | 2.7744e-04 | 2.2747 | 2.4983e-02 | 1.0436 |
| 320 | 7.7328e-05 | 1.8431 | 1.2427e-02 | 1.0075 |
| 640 | 1.9455e-05 | 1.9909 | 6.1961e-03 | 1.0040 |
| 1280 | 4.7698e-06 | 2.0281 | 3.0947e-03 | 1.0015 |

Table 5.6: Errors of the linear PPIFE solution, $\omega = 10$, $\beta^- = 1$, $\beta^+ = 10$.

# Chapter 6

# IFE methods for hyperbolic interface problems

## 6.1 Introduction

In this chapter, we investigate the error estimation for a fully discrete PPIFE method presented in [143] under piecewise $H^2$ regularity assumption in space for the second order hyperbolic interface problems described by:

$$u_{tt} - \nabla \cdot (c^2 \nabla u) = f, \quad \text{in } \Omega^- \cup \Omega^+, \ t \in [0, T], \tag{6.1a}$$

$$u|_{\partial\Omega} = g(X, t), \quad t \in [0, T], \tag{6.1b}$$

$$u(X, 0) = w_0(X), \ u_t(X, 0) = w_1(X) \quad X \in \Omega, \tag{6.1c}$$

together with the following jump conditions across the interface:

$$[u]_\Gamma \ := \ u^+|_\Gamma - u^-|_\Gamma = 0, \tag{6.1d}$$

$$\left[c^2 \nabla u \cdot \mathbf{n}\right]_\Gamma \ := \ (c^+)^2 \nabla u^+ \cdot \mathbf{n}|_\Gamma - (c^-)^2 \nabla u^- \cdot \mathbf{n}|_\Gamma = 0. \tag{6.1e}$$

Here the domain $\Omega \subseteq \mathbb{R}^2$ is divided by an interface curve $\Gamma$ into two subdomains $\Omega^-$ and $\Omega^+$ with $\overline{\Omega} = \overline{\Omega^- \cup \Omega^+ \cup \Gamma}$, and the coefficient $c$ is a piecewise positive constant function such that

$$c(X) = \begin{cases} c^- & \text{for } X \in \Omega^-, \\ c^+ & \text{for } X \in \Omega^+. \end{cases}$$

We will prove that this PPIFE method is unconditionally stable and establish optimal *a priori* error estimates in both an energy norm and the $L^2$ norm under the standard regularity assumption for the exact solution [9], *i.e.*, $u$ is piecewise $H^2$ in space. To validate the theoretical error analysis, numerical results are presented for standing waves as well as realistic traveling wave propagations with incident, reflected and transmitted waves around a material interface.

This chapter is organized as follows: In Section 6.2, we recall the fully discrete PPIFE scheme from [143] for the hyperbolic interface problem and discuss its stability. In Section 6.3, we conduct an error analysis of this PPIFE method and derive optimal error bounds for this method in an energy norm and the $L^2$ norm. In Section 6.4 we present several numerical examples to validate the theoretical results. We discuss our results and conclude with a few remarks in Section 6.5.

## 6.2 A Fully discrete PPIFE method

*In the rest of this thesis, we will use $K$ instead of $T$ to denote an element in $\mathcal{T}_h$ since we use $T$ to represent the endpoint of the time interval.*

For functions of both the spatial variable $X$ in a domain $\tilde{\Omega}$ and temporal variable $t \in [0, T]$, we will use the standard function spaces $L^2(0, T; L^2(\tilde{\Omega}))$ and $L^2(0, T; PH^2(\tilde{\Omega}))$ whose norms are defined by:

$$
\begin{aligned}
\|v\|_{L^2(0,T;L^2(\tilde{\Omega}))} &= \left(\int_0^T \|v(X,t)\|^2_{L^2(\tilde{\Omega})} dt\right)^{1/2}, \quad \forall v(X,t) \in L^2(0,T;L^2(\tilde{\Omega})), \\
\|v\|_{L^2(0,T;PH^2(\tilde{\Omega}))} &= \left(\int_0^T \|v(X,t)\|^2_{2,\tilde{\Omega}} dt\right)^{1/2}, \quad \forall v(X,t) \in L^2(0,T;PH^2(\tilde{\Omega})).
\end{aligned}
$$

Besides, we also consider the space $L^\infty(0,T;PH^2(\tilde{\Omega}))$, equipped with the norms

$$
\|v\|_{L^\infty(0,T;PH^2(\tilde{\Omega}))} = \operatorname*{ess\,sup}_{t\in[0,T]} \|v(X,t)\|_{2,\tilde{\Omega}}, \quad \forall\, v(X,t) \in L^\infty(0,T;PH^2(\tilde{\Omega})).
$$

We recall some set notations about the edges in Chapter 2: the set of interior interface edges is $\mathring{\mathcal{E}}_h^i$, the set of boundary edges is $\mathcal{E}_h^b$, and the set of boundary interface edges is $\mathcal{E}_h^{bi}$.

Then we recall the PPIFE method which has been discussed in [143] for solving the hyperbolic interface problem (6.1). Assume that the initial and boundary data and the source term $f$ in (6.1a) have enough smoothness such that the exact solution $u(.,t)$ of (6.1) is in $PH^2(\Omega)$ for all $t \geq 0$. Then, a weak formulation of (6.1) can be derived similarly as the elliptic interface problem in Section 4.2, which is slightly more general than that in [143], allowing the interface to intersect with the boundary of the domain (i.e. $\Gamma \cap \partial\Omega \neq \emptyset$). Specifically, the weak form is to find $u$: $[0,T] \to PH^2(\Omega)$ that satisfies (6.1d), (6.1e), and

$$
\begin{aligned}
&(u_{tt}, v) + a_h(u,v) = L_f(v), && \forall v \in V_{h,0}(\Omega),\ t > 0, \\
&u(X,0) = w_0(X), \quad u_t(X,0) = w_1(X), && \forall X \in \Omega,
\end{aligned}
\tag{6.2a}
$$

where the bilinear form $a_h : V_h(\Omega) \times V_h(\Omega) \to \mathbb{R}$ is defined as

$$\begin{aligned} a_h(u,v) = &\sum_{K\in\mathcal{T}_h}\int_K c^2\nabla u\cdot\nabla v dX - \sum_{e\in\mathring{\mathcal{E}}_h^i}\int_e\{c^2\nabla u\cdot\mathbf{n}_e\}_e[v]_e ds \\ &+\epsilon\sum_{e\in\mathring{\mathcal{E}}_h^i}\int_e\{c^2\nabla v\cdot\mathbf{n}_e\}_e[u]_e ds + \sum_{e\in\mathring{\mathcal{E}}_h^i}\frac{\sigma_e^0}{|e|}\int_e[u]_e\,[v]_e ds - \sum_{e\in\mathcal{E}_h^{bi}}\int_e c^2\nabla u\cdot\mathbf{n}_e v ds \\ &+\epsilon\sum_{e\in\mathcal{E}_h^{bi}}\int_e c^2\nabla v\cdot\mathbf{n}_e u ds + \sum_{e\in\mathcal{E}_h^{bi}}\frac{\sigma_e^0}{|e|}\int_e u\,v ds, \qquad \forall u,v\in V_h(\Omega), \end{aligned} \tag{6.2b}$$

and the linear form $L_f : V_h(\Omega) \to \mathbb{R}$ is defined by

$$L_f(v) = \int_\Omega f v dX + \epsilon\sum_{e\in\mathcal{E}_h^{bi}}\int_e c^2\nabla v\cdot\mathbf{n}_e\; g ds + \sum_{e\in\mathcal{E}_h^{bi}}\frac{\sigma_e^0}{|e|}\int_e v g ds, \qquad \forall v\in V_h(\Omega), \tag{6.2c}$$

where $\epsilon$ is the penalty parameter, the constant $\sigma_e^0 \geq 0$, and the spaces $V_h(\Omega)$ and $V_{h,0}(\Omega)$ are defined by (2.4) and (2.5).

To discretize the temporal variable $t$, we introduce a uniform partition of $[0,T]$:

$$\Pi_\tau = \{0 = t^0 < t^1 < \cdots < t^M = T\}, \quad \tau = t^n - t^{n-1},\; n = 1,2,\ldots,M.$$

For a function $v(X,t)$, we let $v^n = v(X,t^n)$ and introduce the following notations

$$\begin{aligned} v^{n,1/4} &= \frac{v^{n+1}+2v^n+v^{n-1}}{4}, \quad v^{n+1/2} = \frac{v^{n+1}+v^n}{2}, \\ \partial_t v^n &= \frac{v^{n+1}-v^{n-1}}{2\tau}, \quad \partial_t v^{n+1/2} = \frac{v^{n+1}-v^n}{\tau}, \quad \partial_{tt}v^n = \frac{v^{n+1}-2v^n+v^{n-1}}{\tau^2}. \end{aligned} \tag{6.3}$$

Since the IFE space $S_h(\Omega)$ ($S_{h,0}(\Omega)$) defined by (4.8) is a subset of $V_h(\Omega)$ ($V_{h,0}(\Omega)$), the above weak formulation suggests the following fully-discrete PPIFE method discussed in [143] for the interface problem (6.1): find a sequence $\{u_h^n\}_{n=1}^M \subset S_h(\Omega)$ such that

$$
\begin{aligned}
&(\partial_{tt} u_h^n, v_h) + a_h\left(u_h^{n,1/4}, v_h\right) = L_{f^{n,\frac{1}{4}}}(v_h), \qquad \forall v_h \in S_{h,0}(\Omega), \\
&u_h^0 = \tilde{w}_{h0}, \quad u_h^1 = \tilde{u}_h^*, \qquad\qquad\qquad\qquad \forall X \in \Omega,
\end{aligned}
\tag{6.4}
$$

where $\tilde{w}_{h0}$ and $\tilde{u}_h^*$ are the elliptic projections (to be defined in Definition 6.1) of $w_0$ and $u^*$, respectively, with $u^* = w_0 + \tau w_1(X) + \frac{\tau^2}{2} u_{tt}(X, 0)$ in which $u_{tt}(X, 0)$ is provided by (6.1a). Following the convention of interior penalty discontinuous Galerkin methods [127], we consider three typical choices for the parameter $\epsilon$ in $a_h(\cdot, \cdot)$: $\epsilon = -1, 0, 1$, which leads (6.4) to the symmetric PPIFE method, incomplete PPIFE method, and non-symmetric PPIFE method (SPPIFE, IPPIFE,NPPIFE), respectively.

We now discuss the stability of this PPIFE method. Following the standard convention in the stability/error analysis, we assume that the interface problem has a homogeneous boundary condition such that $g = 0$ in (6.1b). Also, we let $\mathring{\mathcal{N}}_h$ be the set of interior nodes of the mesh $\mathcal{T}_h$, and we assume that all the nodes of $\mathcal{T}_h$ are indexed such that the first $\left|\mathring{\mathcal{N}}_h\right|$ of them are interior nodes. Using the basis functions $\{\phi_i\}_{i=1}^{|\mathcal{N}_h|}$ of the IFE space $S_h(\Omega)$ described by (4.8), we can write this PPIFE method in the matrix form as follows. First, we express the IFE solution $u_h^n$ defined by (6.4) as $u_h^n = \sum\limits_{i=1}^{|\mathring{\mathcal{N}}_h|} c_i^n \phi_i$, let $\mathbf{M}$ be the mass matrix such that $(\mathbf{M})_{i,j} = (\phi_i, \phi_j)$, let $\mathbf{K}$ be the stiffness matrix such that $(\mathbf{K})_{i,j} = a_h(\phi_i, \phi_j)$, and let $\mathbf{F}$ be the vector such that $(\mathbf{F})_i = L_{f^{n,\frac{1}{4}}}(\phi_i)$, with $1 \le i, j \le \left|\mathring{\mathcal{N}}_h\right|$. Then, the coefficients $\mathbf{c}^{(n)} = (c_1^n, c_2^n, \ldots, c_{|\mathring{\mathcal{N}}_h|}^n)^T$ of the IFE solution $u_h^n$ are determined by the fully discrete PPIFE scheme in the matrix form as follows:

$$
\left(\mathbf{M} + \frac{\tau^2}{4}\mathbf{K}\right)\mathbf{c}^{(n+1)} = \left(2\mathbf{M} - \frac{\tau^2}{2}\mathbf{K}\right)\mathbf{c}^{(n)} - \left(\mathbf{M} + \frac{\tau^2}{4}\mathbf{K}\right)\mathbf{c}^{(n-1)} + \tau^2\mathbf{F}. \tag{6.5}
$$

We will still use the energy norms in (4.36) and (4.37) (with $\beta$ replaced by $c^2$) to discuss the

PPIFE method. We recall the coercivity [111] and the continuity [63] of the bilinear form $a_h(\cdot,\cdot)$: for $\sigma_e^0$ in (6.2b) large enough, there exists some constants $\kappa > 0$ and $C > 0$ such that

$$a_h(v,v) \geq \kappa \|v\|_h^2, \qquad \forall v \in S_{h,0}(\Omega), \tag{6.6a}$$

$$|a_h(u,v)| \leq C |\!|\!| u |\!|\!|_h \, |\!|\!| v |\!|\!|_h, \qquad \forall u,v \in V_{h,0}(\Omega). \tag{6.6b}$$

The coercivity given in (6.6a) guarantees that the PPIFE method described by (6.4) or by its matrix form (6.5) is well defined. Also, we note that the PPIFE method (6.4) is similar to the well known Dupont's finite element method [48]; hence, this PPIFE method has properties similar to those of its finite element counterpart. For example, following the standard stability analysis [31], we can show that the SPPIFE method is unconditionally stable.

**Theorem 6.1.** *The fully discrete symmetric PPIFE method (6.4) is unconditionally stable.*

*Proof.* By the symmetry and the coercivity of the bilinear form, we know that the generalized eigenvalue problem $\mathbf{K}\mathbf{v} = \lambda\mathbf{M}\mathbf{v}$ has a set of $\left|\mathring{\mathcal{N}}_h\right|$ eigen-pairs $(\lambda_1,\mathbf{v}_1), (\lambda_2,\mathbf{v}_2), \ldots, (\lambda_{\left|\mathring{\mathcal{N}}_h\right|}, \mathbf{v}_{\left|\mathring{\mathcal{N}}_h\right|})$ such that $\lambda_i > 0$ and $\mathbf{v}_i^T\mathbf{M}\mathbf{v}_j = \delta_{ij},\ 1 \leq i,j \leq \left|\mathring{\mathcal{N}}_h\right|$. From (6.5), assume the source term $f = 0$ and use $\mathbf{c}^{(n)} = \sum_{i=1}^{|\mathring{\mathcal{N}}_h|} \alpha_i^{(n)}\mathbf{v}_i$ to obtain

$$\sum_{i=1}^{|\mathring{\mathcal{N}}_h|} \left( \left(\mathbf{M} + \frac{\tau^2}{4}\mathbf{K}\right)\alpha_i^{(n+1)} - \left(2\mathbf{M} - \frac{\tau^2}{2}\mathbf{K}\right)\alpha_i^{(n)} + \left(\mathbf{M} + \frac{\tau^2}{4}\mathbf{K}\right)\alpha_i^{(n-1)} \right)\mathbf{v}_i = 0,$$

which yields

$$\left( \left(1 + \frac{\tau^2\lambda_i}{4}\right)\alpha_i^{(n+1)} - \left(2 - \frac{\tau^2\lambda_i}{2}\right)\alpha_i^{(n)} + \left(1 + \frac{\tau^2\lambda_i}{4}\right)\alpha_i^{(n-1)} \right)\mathbf{M}\mathbf{v}_i = 0, \quad i = 1,2,\ldots,|\mathring{\mathcal{N}}_h|.$$

Assuming $\alpha_i^{(n)} = \chi^n$, we obtain the principal equation

$$(1+\rho)\chi^2 - 2(1-\rho)\chi + (1+\rho) = 0, \qquad \rho = \frac{\tau^2\lambda_i}{4},$$

with roots

$$\chi^{\pm} = \frac{(1-\rho) \pm 2\sqrt{\rho}\, i}{1+\rho}.$$

A direct computation shows that $|\chi^{\pm}| = 1$, which implies the absolute stability of the PPIFE method. □

Then we will proceed to derive error estimates for the PPIFE methods.

## 6.3 Error estimates for the PPIFE method

In this section, we will conduct an error analysis for the PPIFE method discussed in Section 6.2. Without loss of generality and following usual convention in error analysis of finite element methods, we still make the following assumption: (i) the interface problem has a homogeneous Dirichlet boundary condition, *i.e.*, $g = 0$ in (6.1b); (ii) the interface does not intersect the boundary, *i.e.*, $\Gamma \cap \partial\Omega = \emptyset$. To proceed, we herein introduce the definition of elliptic projection:

**Definition 6.1.** *(elliptic projection) For a function $u \in PH^2(\Omega)$, its elliptic projection is the IFE function $\tilde{u}_h \in S_{h,0}(\Omega)$ determined by:*

$$a_h(\tilde{u}_h, v_h) = a_h(u, v_h), \quad \forall v_h \in S_{h,0}(\Omega). \tag{6.7}$$

The elliptic projection $\tilde{u}_h$ for every $u \in PH^2(\Omega)$ exists and is unique because of the coercivity of $a_h(\cdot,\cdot)$. Assuming that the exact solution $u$ to the interface problem (6.1) is such that $u(\cdot,t) \in PH^2(\Omega)$, we can then use the elliptic projection $\tilde{u}_h(\cdot,t)$ of the exact solution $u$ at the time level $t \in [0,T]$ to split the error in the IFE solution $u_h$ determined by (6.4) as: $u(X,t) - u_h(X,t) = \eta(X,t) - \xi(X,t)$, with

$$\eta(X,t) = u(X,t) - \tilde{u}_h(X,t), \quad \xi(X,t) = u_h(X,t) - \tilde{u}_h(X,t). \tag{6.8}$$

We derive the bound for $\eta$ which is the error in the elliptic projection. We first consider the estimation in the energy norm $\|\cdot\|_h$.

**Lemma 6.1.** *Assume that $\sigma_e^0$ in $a_h(.,.)$ defined by (6.2b) is large enough and the mesh is fine enough. Then there exists a constant $C$ such that for every $t \in [0,T]$, the following estimates hold*

$$\left\| \frac{\partial^k \eta(\cdot,t)}{\partial t^k} \right\|_h \le Ch \left\| \frac{\partial^k u(\cdot,t)}{\partial t^k} \right\|_{2,\Omega}, \quad \textit{if } \frac{\partial^k u(\cdot,t)}{\partial t^k} \in PH^2(\Omega), \quad k = 0,1,\dots 4,. \tag{6.9}$$

*Proof.* By definition of elliptic projection, we note that

$$a_h(u,v_h) = a_h(\tilde{u}_h,v_h), \quad \forall v_h \in S_{h,0}(\Omega).$$

Then, following the same arguments for proving Theorem 4.6, we have

$$\|\eta\|_h \le \|\!|\eta|\!\|_h \le Ch\, \|u\|_{2,\Omega}\,, \tag{6.10}$$

which leads to the estimate in (6.9) for $k = 0$. The other estimates in (6.9) can be proved similarly by using the fact that the time differentiation and elliptic projection commute [113].

□

The estimation of the elliptic projection in the $L^2$ norm follows the usual duality argument. Specifically, we consider the following auxiliary elliptic interface problem for fixed $t \in [0, T]$: find $w$ such that

$$-\nabla \cdot (c^2 \nabla w) = \tilde{f}, \qquad \text{in } \Omega^- \cup \Omega^+, \tag{6.11a}$$

$$w|_{\partial\Omega} = 0, \tag{6.11b}$$

$$[w]_\Gamma = 0, \quad \left[c^2 \nabla w \cdot \mathbf{n}\right]_\Gamma = 0. \tag{6.11c}$$

According to [45] and assuming that $\Gamma$ has piecewise $C^2$ smoothness, we know that this auxiliary elliptic interface problem has a solution $w \in PH^2(\Omega)$ such that

$$\|w\|_{2,\Omega} \leq C \left\| \tilde{f} \right\|_{L^2(\Omega)}, \quad \forall \tilde{f} \in L^2(\Omega). \tag{6.12}$$

Then we have the following lemma about the elliptic projection error in $L^2$ norm

**Lemma 6.2.** *Under the conditions of Lemma 6.1, there exists a constant $C$ such that for every $t \in [0, T]$, the following estimates hold*

$$\left\| \frac{\partial^k \eta(.,t)}{\partial t^k} \right\|_{L^2(\Omega)} \leq Ch^2 \left\| \frac{\partial^k u(.,t)}{\partial t^k} \right\|_{2,\Omega}, \quad \textit{if } \frac{\partial^k u(\cdot,t)}{\partial t^k} \in PH^2(\Omega), \quad k = 0, 1, \ldots, 4. \tag{6.13}$$

*Proof.* For fixed $t \in [0, T]$, consider the auxiliary elliptic problem (6.11) and let

$$\tilde{f} = \eta, \tag{6.14}$$

then it can be derived that $w$ is the solution of the following weak problem

$$a_h(w, v) = (\eta, v)_\Omega, \quad \forall v \in V_{h,0}(\Omega).$$

Choosing $v = \eta$, it follows $a_h(w, \eta) = \|\eta\|^2_{L^2(\Omega)}$. Then, following the same arguments in proving Theorem 4.7 and utilizing (6.12), together with (6.9), we have

$$\|\eta\|_{L^2(\Omega)} \le Ch\|\eta\|_h \le Ch^2 \|u\|_{2,\Omega},$$

which yields the estimate in (6.13) for $k = 0$. By letting $\tilde{f} = \frac{\partial^k \eta}{\partial t^k}$ ($k = 1, 2, 3, 4$), respectively, in (6.14), we can prove the other estimates in (6.13) in a similar way. □

We now present the estimation for the finite difference approximations of time derivatives of $\eta(X, t)$.

**Lemma 6.3.** *Under the conditions of Lemma 6.1 and $u_{tt} \in L^\infty(0, T; PH^2(\Omega))$, then there exists a constant $C > 0$ independent of the interface location such that the following estimates hold*

$$\|\partial_{tt}\eta^n\|_{L^2(\Omega)} \le Ch^2 \|u_{tt}\|_{L^\infty(0,T;PH^2(\Omega))}, \quad n = 1, 2, \ldots, M-1, \tag{6.15}$$

$$\tau \sum_{n=1}^{N-1} \left\|\partial_{tt}(\partial_t \eta^{n+1/2})\right\|^2_{L^2(\Omega)} \le Ch^4 \|u_{ttt}\|^2_{L^2(0,T;PH^2(\Omega))}, \quad N = 2, 3, \ldots, M-1. \tag{6.16}$$

*Proof.* From the estimate (3.37) in [113], the following holds

$$\|\partial_{tt}\eta^n\|^2_{L^2(\Omega)} \le \frac{1}{3\tau} \int_{t^{n-1}}^{t^{n+1}} \|\eta_{tt}\|^2_{L^2(\Omega)}\, dt,$$

from which (6.15) follows easily by using (6.13). For the estimate in (6.16), by the Taylor expansion at $t = t^n$ with integral remainder, we have

$$\eta^{n+2} = \eta^n + 2\tau\eta^n_t + 2\tau^2\eta^n_{tt} + \int_{t^n}^{t^{n+2}} \eta_{ttt}\frac{(t^{n+2} - t)^2}{2} dt,$$

$$\eta^{n+1} = \eta^n + \tau\eta^n_t + \frac{\tau^2}{2}\eta^n_{tt} + \int_{t^n}^{t^{n+1}} \eta_{ttt}\frac{(t^{n+1} - t)^2}{2} dt,$$

$$\eta^{n-1} = \eta^n - \tau\eta_t^n + \frac{\tau^2}{2}\eta_{tt}^n + \int_{t^{n-1}}^{t^n} \eta_{ttt}\frac{(t-t^{n-1})^2}{2}dt,$$

which in turn yields

$$\begin{aligned}
&(\eta^{n+2}-\eta^{n+1}) - 2(\eta^{n+1}-\eta^n) + (\eta^n - \eta^{n-1}) \\
=& \int_{t^n}^{t^{n+2}} \eta_{ttt}\frac{(t^{n+2}-t)^2}{2}dt + 3\int_{t^n}^{t^{n+1}} \eta_{ttt}\frac{(t-t^{n+1})^2}{2}dt + \int_{t^{n-1}}^{t^n} \eta_{ttt}\frac{(t-t^{n-1})^2}{2}dt.
\end{aligned}$$

Therefore

$$\begin{aligned}
\tau \left\| \partial_{tt}(\partial_t \eta^{n+\frac{1}{2}}) \right\|_{L^2(\Omega)}^2 &= \frac{1}{\tau^5}\left\| (\eta^{n+2}-\eta^{n+1}) - 2(\eta^{n+1}-\eta^n) + (\eta^n - \eta^{n-1}) \right\|_{L^2(\Omega)}^2 \\
&\le C\left\|\eta_{ttt}\right\|_{L^2(t^{n-1},t^{n+2},L^2(\Omega))}^2,
\end{aligned}$$

where we have used the Cauchy-Schwarz inequality. Then, summing the estimate from $n = 1$ to $n = N-1$ and applying Lemma 6.2 leads to (6.16). $\square$

We now discuss estimates about $\xi$. We note that $\xi$ is an IFE function. For a preparation, we recall the patch of each element $K \in \mathcal{T}_h$ defined in (4.10)

$$\omega_K = \left\{ \cup\tilde{K} \mid \tilde{K} \in \mathcal{T}_h \text{ such that } \tilde{K}\cap K \neq \emptyset \right\}.$$

We assume that the mesh $\mathcal{T}_h$ satisfies the *Patch Assumption* defined in Section 4.3, i.e., there exists a constant $C$ such that for each interface edge $e \in \mathring{\mathcal{E}}_h^i$ associated with an interface element $K$ with $e^s = e\cap\Omega^s$, $s = \pm$, there exist auxiliary triangles $K_e^s \subset \omega_K$, possessing $e^s$ as one of its edges, such that $K_e^s \subset \Omega^s$ and $|e^s|/|K_e^s| \le Ch^{-1}$, for $s = \pm$, respectively. Then, on each interface edge $e \in \mathring{\mathcal{E}}_h^i$ associated with an interface element $K$, by applying the standard trace inequality on $e^s = e \cap \Omega^s$, $s = \pm$, we have the following estimate for $v \in PH^2(\Omega)$:

$$\begin{aligned} &\left\| c^2 \nabla v \cdot \mathbf{n}_e \right\|_{L^2(e)} \leq c_{\max}^2 \left( \| v_x \mathbf{n}_{e,x} + v_y \mathbf{n}_{e,y} \|_{L^2(e)} \right) \leq \sqrt{2} c_{\max}^2 \left( \| \nabla v \|_{L^2(e^-)} + \| \nabla v \|_{L^2(e^+)} \right) \\ &\leq C \sum_{s=-,+} (|e^s| / |K_e^s|)^{1/2} \left( \| \nabla v \|_{L^2(K_e^s)} + h \left\| \nabla^2 v \right\|_{L^2(K_e^s)} \right) \leq C h^{-1/2} \| v \|_{2,\omega_K}, \end{aligned} \tag{6.18}$$

where $c_{\max} = \max\{c^-, c^+\}$. Summing (6.18) over all interior interface edges we obtain

$$\sum_{e \in \mathring{\mathcal{E}}_h^i} \left\| \{ |e|^{1/2} c^2 \nabla v \cdot \mathbf{n}_e \} \right\|_{L^2(e)} \leq C \| v \|_{2,\Omega}, \quad \forall\, v \in PH^2(\Omega). \tag{6.19}$$

**Lemma 6.4.** *Let $u$ be the solution of (6.1) such that*

$$u(.,t) \in PH^2(\Omega), \quad t \geq 0, \quad \text{and} \quad u_{ttt} \in L^\infty(0,T; PH^2(\Omega)).$$

*and $\sigma_e^0$ in (6.2b) large enough. Then there exists a constant $C$ independent of interface location such that*

$$\left\| \xi^1 \right\|_{L^2(\Omega)} \leq C \tau^3 \| u_{ttt} \|_{L^\infty(0,T;PH^2(\Omega))}, \tag{6.20}$$

$$\left\| \xi^{1/2} \right\|_{L^2(\Omega)} \leq C \tau^3 \| u_{ttt} \|_{L^\infty(0,T;PH^2(\Omega))}, \tag{6.21}$$

$$\left\| \xi^{1/2} \right\|_h \leq C \tau^3 \| u_{ttt} \|_{L^\infty(0,T;PH^2(\Omega))}, \tag{6.22}$$

$$\left\| \partial_t \xi^{1/2} \right\|_{L^2(\Omega)} \leq C \tau^2 \| u_{ttt} \|_{L^\infty(0,T;PH^2(\Omega))}. \tag{6.23}$$

*Proof.* By the coercivity of the bilinear form $a_h(\cdot,\cdot)$ in (6.6a) and the elliptic projection in (6.7) we obtain

$$\left\| \xi^1 \right\|_h^2 \leq C a_h \left( \xi^1, \xi^1 \right) = C a_h \left( u_h^1 - \tilde{u}_h^1, \xi^1 \right) = C a_h \left( \tilde{u}_h^* - \tilde{u}_h^1, \xi^1 \right) = C a_h \left( u^* - u^1, \xi^1 \right).$$

Then, by the boundedness of $a_h(\cdot,\cdot)$ given in (6.6b), it follows

$$\|\xi^1\|_h^2 \le C|||u^* - u^1|||_h |||\xi^1|||_h. \tag{6.24}$$

Since $u^* - u^1 \in PH^2(\Omega)$, the jump $[u^* - u^1]|_e = 0$ for $e \in \mathring{\mathcal{E}}_h^i$ and

$$|||u^* - u^1|||_h^2 = \sum_{K\in\mathcal{T}_h} \int_K c^2 \left\|\nabla(u^* - u^1)\right\|^2 dX + \sum_{e\in\mathring{\mathcal{E}}_h^i} (\sigma_e^0)^{-1} \int_e \left\||e|^{1/2}\{c^2\nabla(u^* - u^1)\cdot \mathbf{n_e}\}\right\|^2 ds$$
$$\le C\left\|u^* - u^1\right\|_{2,\Omega}^2,$$

where we have used (6.19). Substituting this bound into (6.24) and using the equivalence of the norms $|||\xi^1|||_h$ and $\|\xi^1\|_h$ for $\xi^1 \in S_h(\Omega)$ (see Lemma 4.1), lead to

$$\|\xi^1\|_h \le C|||u^* - u^1|||_h \le C\left\|u^* - u^1\right\|_{2,\Omega}.$$

Next, by the Taylor expansion with integral remainder, we have

$$\left\|\xi^1\right\|_h \le C\left\|u^* - u^1\right\|_{2,\Omega} = C\left\|\int_0^\tau \frac{(\tau - t)^2}{2} u_{ttt}(.,t)dt\right\|_{2,\Omega} \le C\tau^3 \left\|u_{ttt}\right\|_{L^\infty(0,T;PH^2(\Omega))}. \tag{6.25}$$

On the other hand, applying piecewise Poincaré-Friedrichs inequality [12, 24], we have

$$\|\xi\|_{L^2(\Omega)} \le C\|\xi\|_h, \quad \forall \xi \in S_h(\Omega). \tag{6.26}$$

By definition, $\xi^0 = 0$; hence, $\xi^{1/2} = \frac{1}{2}\xi^1$ and the estimates in (6.20), (6.21) and (6.22) follow directly from (6.25). Furthermore, estimate in (6.23) also follows from (6.25) by the fact that $\partial_t \xi^{\frac{1}{2}} = \frac{\xi^1}{2\tau} = \frac{\xi^{\frac{1}{2}}}{\tau}$. □

In the next lemma we state and prove estimates for time discretizations of $u$ and $u_{tt}$

**Lemma 6.5.** *Let $u$ be the exact solution of (6.1) satisfying the conditions specified in Lemma 6.3. Then there exists a constant $C$ independent of the interface location such that*

$$\begin{aligned} \left\| u^{n,\frac{1}{4}} - u^n \right\|_{L^2(\Omega)} &\le C\tau^2 \left\| u_{tt} \right\|_{L^\infty(0,T;PH^2(\Omega))}, \quad n = 1,2,\ldots,M-1, \quad (6.27) \\ \tau \sum_{n=1}^{N} \left\| \partial_{tt} u^n - u_{tt}^n \right\|_{L^2(\Omega)}^2 &\le C\tau^4 \left\| u_{tttt} \right\|_{L^2(0,T;PH^2(\Omega))}^2, \quad n = 1,2,\ldots,M-1. \quad (6.28) \end{aligned}$$

*Proof.* To prove (6.27), we apply Taylor's theorem with integral remainder to write

$$u^{n+1} = u^n + \tau u_t^n + \int_{t^n}^{t^{n+1}} \left( t^{n+1} - t \right) u_{tt} dt, \quad u^{n-1} = u^n - \tau u_t^n + \int_{t^{n-1}}^{t^n} \left( t - t_{n-1} \right) u_{tt} dt,$$

then

$$\begin{aligned} \left\| u^{n,\frac{1}{4}} - u^n \right\|_{L^2(\Omega)} &= \frac{1}{4} \left\| \int_{t^n}^{t^{n+1}} (t^{n+1} - t) u_{tt} dt - \int_{t^{n-1}}^{t^n} (t - t^{n-1}) u_{tt} dt \right\|_{L^2(\Omega)} \\ &\le C\tau^2 \left\| u_{tt} \right\|_{L^\infty(0,T,PH^2(\Omega))}. \end{aligned}$$

Similarly, for (6.28), we can use the following Taylor expansions:

$$u^{n+1} = u^n + \tau u_t^n + \frac{\tau^2}{2} u_{tt}^n + \frac{\tau^3}{6} u_{ttt}^n + \int_{t^n}^{t^{n+1}} \frac{(t^{n+1} - t)^3}{6} u_{tttt} dt,$$

$$u^{n-1} = u^n - \tau u_t^n + \frac{\tau^2}{2} u_{tt}^n - \frac{\tau^3}{6} u_{ttt}^n + \int_{t^{n-1}}^{t^n} \frac{(t - t^{n-1})^3}{6} u_{tttt} dt,$$

so that

$$\begin{aligned} \left\| \partial_{tt} u^n - u_{tt}^n \right\|_{L^2(\Omega)}^2 &= \frac{1}{\tau^4} \left\| \int_{t^n}^{t^{n+1}} \frac{(t^{n+1} - t)^3}{6} u_{tttt} dt + \int_{t^{n-1}}^{t^n} \frac{(t - t^{n-1})^3}{6} u_{tttt} dt \right\|_{L^2(\Omega)}^2 \quad (6.29) \\ &\le C\tau^3 \left\| u_{tttt} \right\|_{L^2(t^{n-1},t^{n+1},PH^2(\Omega))}^2, \end{aligned}$$

where we have used Cauchy-Schwarz inequality. □

The following lemmas establish estimates for three inner products to appear in the error estimation for the PPIFE methods. The first one involves $\eta$ and $\xi$ and the second one involves $u$ and $\xi$.

**Lemma 6.6.** *Let $u$ be the exact solution of (6.1) satisfying the conditions specified in Lemmas 6.1, 6.3 and 6.4, then the following estimates hold for all $\delta > 0$ and $N = 1, 2, \ldots, M-1$:*

$$\begin{aligned} \tau \sum_{n=1}^{N} |(\partial_{tt}\eta^n, \partial_t \xi^n)_\Omega| \leq C \Big( & h^4 \|u_{ttt}\|^2_{L^2(0,T;PH^2(\Omega))} + h^4 \|u_{tt}\|^2_{L^\infty(0,T;PH^2(\Omega))} \\ & + \tau^6 \|u_{ttt}\|^2_{L^\infty(0,T;PH^2(\Omega))} \Big) + \delta \left\|\xi^{N+1/2}\right\|^2_{L^2(\Omega)} + \frac{\tau}{2}\sum_{n=0}^{N-1} \left\|\xi^{n+\frac{1}{2}}\right\|^2_{L^2(\Omega)}, \end{aligned} \tag{6.30}$$

*where $C$ is a constant such that $C = \max\{C_1, C_2/\delta\}$, with generic constants $C_1$ and $C_2$ independent of $\delta$.*

*Proof.* When $N = 1$, we use (6.3) to write

$$\partial_t \xi^1 = \frac{\xi^2 - \xi^0}{2\tau} = \frac{(\xi^2 + \xi^1) - (\xi^0 + \xi^1)}{2\tau} = \frac{\xi^{1+\frac{1}{2}} - \xi^{\frac{1}{2}}}{\tau},$$

therefore,

$$\begin{aligned} \tau \left|(\partial_{tt}\eta^1, \partial_t \xi^1)_\Omega\right| &= \left|\left(\partial_{tt}\eta^1, \xi^{1+\frac{1}{2}} - \xi^{\frac{1}{2}}\right)_\Omega\right| \leq \left|\left(\partial_{tt}\eta^1, \xi^{1+\frac{1}{2}}\right)_\Omega\right| + \left|(\partial_{tt}\eta^1, \xi^{1/2})_\Omega\right| \\ &\leq \left(\frac{1}{4\delta}\left\|\partial_{tt}\eta^1\right\|^2_{L^2(\Omega)} + \delta\left\|\xi^{1+1/2}\right\|^2_{L^2(\Omega)}\right) + \left(\frac{1}{2}\left\|\partial_{tt}\eta^1\right\|^2_{L^2(\Omega)} + \frac{1}{2}\left\|\xi^{1/2}\right\|^2_{L^2(\Omega)}\right), \end{aligned} \tag{6.31}$$

where we used Young's inequality

$$|(u, v)| \leq \delta \|u\|^2_{L^2(\Omega)} + \frac{1}{4\delta}\|v\|^2_{L^2(\Omega)}, \text{ for } \delta > 0.$$

Applying (6.15) and (6.21) to (6.31), we establish (6.30) for $N = 1$. For case $N > 1$, by

(6.3), we have

$$\partial_t \xi^n = \frac{\xi^{n+1} - \xi^{n-1}}{2\tau} = \frac{(\xi^{n+1} + \xi^n) - (\xi^n + \xi^{n-1})}{2\tau} = \frac{\xi^{n+\frac{1}{2}} - \xi^{n-\frac{1}{2}}}{\tau}.$$

Therefore

$$\begin{aligned}
\tau \left| \sum_{n=1}^{N} (\partial_{tt}\eta^n, \partial_t \xi^n)_\Omega \right| &= \left| \sum_{n=1}^{N} \left(\partial_{tt}\eta^n, \xi^{n+1/2} - \xi^{n-1/2}\right)_\Omega \right| \\
&= \left| \sum_{n=1}^{N} \left(\partial_{tt}\eta^n, \xi^{n+1/2}\right)_\Omega - \sum_{n=0}^{N-1} \left(\partial_{tt}\eta^{n+1}, \xi^{n+1/2}\right)_\Omega \right| \\
&= \left| \sum_{n=1}^{N-1} \left(\partial_{tt}\eta^n - \partial_{tt}\eta^{n+1}, \xi^{n+1/2}\right)_\Omega + \left(\partial_{tt}\eta^N, \xi^{N+1/2}\right)_\Omega - \left(\partial_{tt}\eta^1, \xi^{1/2}\right)_\Omega \right|.
\end{aligned}$$

By the definition of the finite difference operator $\partial_t$ given in (6.3), we then have

$$\begin{aligned}
\tau \left| \sum_{n=1}^{N} (\partial_{tt}\eta^n, \partial_t \xi^n)_\Omega \right| = &\left| \tau \sum_{n=1}^{N-1} \left(\partial_{tt}\left(-\partial_t \eta^{n+1/2}\right), \xi^{n+1/2}\right)_\Omega + \left(\partial_{tt}\eta^N, \xi^{N+1/2}\right)_\Omega - \left(\partial_{tt}\eta^1, \xi^{1/2}\right)_\Omega \right| \\
\le &\ \frac{\tau}{2} \sum_{n=1}^{N-1} \left\| \partial_{tt}(\partial_t \eta^{n+1/2}) \right\|_{L^2(\Omega)}^2 + \frac{\tau}{2} \sum_{n=1}^{N-1} \left\| \xi^{n+1/2} \right\|_{L^2(\Omega)}^2 \\
&+ \left( \frac{1}{4\delta} \left\| \partial_{tt}\eta^N \right\|_{L^2(\Omega)}^2 + \delta \left\| \xi^{N+\frac{1}{2}} \right\|_{L^2(\Omega)}^2 \right) + \left( \frac{1}{2} \left\| \partial_{tt}\eta^1 \right\|_{L^2(\Omega)}^2 + \frac{1}{2} \left\| \xi^{1/2} \right\|_{L^2(\Omega)}^2 \right).
\end{aligned}$$

Again, we have used Cauchy-Schwarz and Young's inequalities. We complete the proof by using (6.15), (6.16) and (6.21) to the right hand side of the above inequality to establish (6.30) for $N > 1$. □

**Lemma 6.7.** *Let $u$ be the exact solution to (6.1) satisfying the conditions specified in Lemma*

*6.1 and $u_{tttt} \in L^\infty(0,T;PH^2(\Omega))$. Then the following estimates hold for $\delta \le 1$,*

$$\begin{aligned}\left|\tau\sum_{n=1}^{N}(\partial_{tt}u^n - u_{tt}^n, \partial_t\xi^n)_\Omega\right| \le C\tau^4\left\|u_{tttt}\right\|^2_{L^2(0,T;PH^2(\Omega))} + \frac{\tau}{2}\sum_{n=0}^{N-1}\left\|\partial_t\xi^{n+\frac{1}{2}}\right\|^2_{L^2(\Omega)} \\ +\frac{\tau\delta}{4}\left\|\partial_t\xi^{N+1/2}\right\|^2_{L^2(\Omega)}, N = 1,2,\ldots,M-1,\end{aligned} \tag{6.32}$$

$$\begin{aligned}\left|\tau\sum_{n=1}^{N}(u_{tt}^{n,1/4} - \partial_{tt}u^n, \partial_t\xi^n)_\Omega\right| &\le C\tau^4\left\|u_{tttt}\right\|^2_{L^2(0,T;PH^2(\Omega))} \\ &+\frac{\tau}{2}\sum_{n=0}^{N-1}\left\|\partial_t\xi^{n+\frac{1}{2}}\right\|^2_{L^2(\Omega)} + \frac{\tau\delta}{4}\left\|\partial_t\xi^{N+1/2}\right\|^2_{L^2(\Omega)},\ N = 1,2,\ldots,M-1,\end{aligned} \tag{6.33}$$

*where $C$ is a constant such that $C = \max\{C_1, C_2/\delta\}$, with generic constants $C_1$ and $C_2$ independent of $\delta$.*

*Proof.* To prove (6.32), we use (6.3) for $n \ge 1$ and Young's inequality to obtain

$$\begin{aligned}\left\|\partial_t\xi^n\right\|^2_{L^2(\Omega)} &= \left\|\frac{\xi^{n+1}-\xi^{n-1}}{2\tau}\right\|^2_{L^2(\Omega)} = \left\|\frac{\xi^{n+1}-\xi^n+\xi^n-\xi^{n-1}}{2\tau}\right\|^2_{L^2(\Omega)} \\ &= \frac{1}{4}\left\|\partial_t\xi^{n+1/2}+\partial_t\xi^{n-1/2}\right\|^2_{L^2(\Omega)} \le \frac{1}{2}\left(\left\|\partial_t\xi^{n+1/2}\right\|^2_{L^2(\Omega)} + \left\|\partial_t\xi^{n-1/2}\right\|^2_{L^2(\Omega)}\right).\end{aligned} \tag{6.34}$$

When $N = 1$, by Young's inequality, we have

$$\begin{aligned}\left|\tau\sum_{n=1}^{N}\left(\partial_{tt}u^n - u_{tt}^n, \partial_t\xi^n\right)_\Omega\right| &= \left|\tau\left(\partial_{tt}u^1 - u_{tt}^1, \partial_t\xi^1\right)_\Omega\right| \\ &\le \frac{\tau}{2\delta}\left\|\partial_{tt}u^1 - u_{tt}^1\right\|^2_{L^2(\Omega)} + \frac{\tau\delta}{2}\left\|\partial_t\xi^1\right\|^2_{L^2(\Omega)}.\end{aligned}$$

Next, using (6.28) and (6.34) to the previous inequality we obtain

$$\left|\tau\sum_{n=1}^{N}\left(\partial_{tt}u^n - u_{tt}^n, \partial_t\xi^n\right)_\Omega\right| \le C\tau^4\left\|u_{tttt}\right\|^2_{L^2(0,T;PH^2(\Omega))} + \frac{\tau\delta}{4}\left(\left\|\partial_t\xi^{1+\frac{1}{2}}\right\|^2_{L^2(\Omega)} + \left\|\partial_t\xi^{1/2}\right\|^2_{L^2(\Omega)}\right),$$

which leads to the estimate in (6.32) for $N = 1$ if $\delta \le 2$. When $N > 1$, by Young's inequality again, we have

$$\left|\tau\sum_{n=1}^{N}\left(\partial_{tt}u^n-u_{tt}^n,\partial_t\xi^n\right)_\Omega\right|\le\frac{\tau}{2}\sum_{n=1}^{N-1}\|\partial_{tt}u^n-u_{tt}^n\|_{L^2(\Omega)}^2+\frac{\tau}{2}\sum_{n=1}^{N-1}\|\partial_t\xi^n\|_{L^2(\Omega)}^2$$
$$+\frac{\tau}{2\delta}\left\|\partial_{tt}u^N-u_{tt}^N\right\|_{L^2(\Omega)}^2+\frac{\tau\delta}{2}\left\|\partial_t\xi^N\right\|_{L^2(\Omega)}^2. \tag{6.35}$$

Next we apply (6.28) to the first and third terms and apply (6.34) to the second and fourth terms of the right hand side of (6.35) to yield

$$\left|\tau\sum_{n=1}^{N}\left(\partial_{tt}u^n-u_{tt}^n,\partial_t\xi^n\right)_\Omega\right|\le C\tau^4\left\|u_{tttt}\right\|_{L^2(0,T;PH^2(\Omega))}^2$$
$$+\frac{\tau}{4}\sum_{n=1}^{N-1}\left(\left\|\partial_t\xi^{n+1/2}\right\|_{L^2(\Omega)}^2+\left\|\partial_t\xi^{n-1/2}\right\|_{L^2(\Omega)}^2\right)+\frac{\tau\delta}{4}\left(\left\|\partial_t\xi^{N+1/2}\right\|_{L^2(\Omega)}^2+\left\|\partial_t\xi^{N-1/2}\right\|_{L^2(\Omega)}^2\right)$$
$$\le C\tau^4\|u_{tttt}\|_{L^2(0,T;PH^2(\Omega))}^2+\frac{\tau}{4}\sum_{n=0}^{N-1}\left\|\partial_t\xi^{n+1/2}\right\|_{L^2(\Omega)}^2$$
$$+\frac{\tau}{4}\sum_{n=0}^{N-2}\left\|\partial_t\xi^{n+1/2}\right\|_{L^2(\Omega)}^2+\frac{\tau\delta}{4}\left(\left\|\partial_t\xi^{N+1/2}\right\|_{L^2(\Omega)}^2+\left\|\partial_t\xi^{N-1/2}\right\|_{L^2(\Omega)}^2\right).$$

Taking $\delta\le 1$ in the estimate above leads to

$$\left|\tau\sum_{n=1}^{N}\left(\partial_{tt}u^n-u_{tt}^n,\partial_t\xi^n\right)_\Omega\right|\le C\tau^4\left\|u_{tttt}\right\|_{L^2(0,T;PH^2(\Omega))}^2+\frac{\tau}{2}\sum_{n=0}^{N-1}\left\|\partial_t\xi^{n+1/2}\right\|_{L^2(\Omega)}^2$$
$$+\frac{\tau\delta}{4}\left\|\partial_t\xi^{N+1/2}\right\|_{L^2(\Omega)}^2,$$

which proves (6.32) for $N>1$. To prove (6.33), we first note that $u_{tt}^{n,1/4}-\partial_{tt}u^n=\left(u_{tt}^{n,\frac14}-u_{tt}^n\right)+\left(u_{tt}^n-\partial_{tt}u^n\right)$. Thus, for $n=1,2,\dots,M-1$, we have

$$\left|\tau\sum_{n=1}^{N}\left(u_{tt}^{n,1/4}-\partial_{tt}u^n,\partial_t\xi^n\right)_\Omega\right|\le\left|\tau\sum_{n=1}^{N}\left(u_{tt}^{n,\frac14}-u_{tt}^n,\partial_t\xi^n\right)_\Omega\right|$$
$$+\left|\tau\sum_{n=1}^{N}\left(u_{tt}^n-\partial_{tt}u^n,\partial_t\xi^n\right)_\Omega\right|. \tag{6.36}$$

By (6.27), we obtain

$$\left\| u_{tt}^{n,\frac{1}{4}} - u_{tt}^{n} \right\|_{L^2(\Omega)} \leq C_0 \tau^2 \|u_{tttt}\|_{L^\infty(0,T;PH^2(\Omega))}, \quad n = 1, 2, \ldots, M-1, \tag{6.37}$$

where $C_0$ is a constant independent of $\delta$. Finally, the estimate in (6.33) follows from applying (6.37) together with the Cauchy-Schwarz and (6.32) to (6.36). □

With all the preparations above, we can now derive an error estimate for $\xi^{n+1/2}$.

**Theorem 6.2.** *Let $u$ be the exact solution of (6.1) and $\frac{\partial^k u}{\partial t^k} \in L^\infty(0,T;PH^2(\Omega))$, $k = 0, 1, \ldots, 4$ . Then, for $\sigma_e^0$ in (6.2b) large enough, there exists a constant $C$ such that the following estimate holds:*

$$\left\| \partial_t \xi^{n+\frac{1}{2}} \right\|_{L^2(\Omega)} + \left\| \xi^{n+\frac{1}{2}} \right\|_h \leq C \left(h^2 + \tau^2\right), \quad n = 1, 2, \ldots, M-1, \tag{6.38}$$

*where $C$ is a constant such that $C = \max\{C_1, C_2/\delta\}$, with generic constants $C_1$ and $C_2$ independent of $\delta$.*

*Proof.* When $n = 0$, (6.38) is an immediate consequence of Lemma 6.4. When $n \geq 1$, we note that $a_h(\eta^n, v_h) = 0, \forall\, v_h \in S_h(\Omega)$, and we write

$$\begin{aligned}
& (\partial_{tt}\xi^n, v_h)_\Omega + a_h\left(\xi^{n,1/4}, v_h\right) - (\partial_{tt}\eta^n, v_h)_\Omega \\
= \quad & (\partial_{tt}\left(\xi^n - \eta^n\right), v_h)_\Omega + a_h\left(\xi^{n,1/4}, v_h\right) - a_h\left(\eta^{n,1/4}, v_h\right) \\
= \quad & (\partial_{tt}\left(u_h^n - u^n\right), v_h)_\Omega + a_h\left(u_h^{n,1/4}, v_h\right) - a_h\left(u^{n,1/4}, v_h\right) \\
= \quad & (\partial_{tt} u_h^n, v_h)_\Omega + a_h(u_h^{n,1/4}, v_h) - \left(a_h(u^{n,1/4}, v_h) + \left(u_{tt}^{n,1/4}, v_h\right)_\Omega\right) \\
& + \left(u_{tt}^{n,1/4} - \partial_{tt} u^n, v_h\right)_\Omega, \quad \forall v_h \in S_{h,0}(\Omega).
\end{aligned} \tag{6.39}$$

By (6.2) and (6.4), the first three terms on the right hand side of (6.39) vanish and we have

$$(\partial_{tt}\xi^n, v_h)_\Omega + a_h\left(\xi^{n,1/4}, v_h\right) - (\partial_{tt}\eta^n, v_h)_\Omega = \left(u_{tt}^{n,1/4} - \partial_{tt}u^n, v_h\right)_\Omega, \quad \forall v_h \in S_{h,0}(\Omega). \quad (6.40)$$

It is easy to check the following identities

$$\begin{aligned}(\partial_{tt}\xi^n, \partial_t\xi^n)_\Omega = & \left(\frac{\xi^{n+1} - 2\xi^n + \xi^{n-1}}{\tau^2}, \partial_t\xi^n\right)_\Omega = \left(\frac{\partial_t\xi^{n+1/2} - \partial_t\xi^{n-1/2}}{\tau}, \frac{\partial_t\xi^{n+1/2} + \partial_t\xi^{n-1/2}}{2}\right)_\Omega \\ = & \frac{1}{2\tau}\left(\left\|\partial_t\xi^{n+1/2}\right\|_{L^2(\Omega)}^2 - \left\|\partial_t\xi^{n-1/2}\right\|_{L^2(\Omega)}^2\right),\end{aligned} \quad (6.41)$$

and

$$\begin{aligned}& a_h(\xi^{n,1/4}, \partial_t\xi^n) = \frac{1}{2\tau}\left(a_h\left(\frac{\xi^{n+1}+\xi^n}{2}, \frac{\xi^{n+1}+\xi^n}{2}\right) - a_h\left(\frac{\xi^n+\xi^{n-1}}{2}, \frac{\xi^n+\xi^{n-1}}{2}\right)\right) \\ & = \frac{1}{2\tau}\left(a_h\left(\xi^{n+\frac{1}{2}}, \xi^{n+\frac{1}{2}}\right) - a_h\left(\xi^{n-\frac{1}{2}}, \xi^{n-\frac{1}{2}}\right)\right).\end{aligned} \quad (6.42)$$

Letting $v_h = \partial_t\xi^n$ in (6.40) and then using (6.41) and (6.42), we have

$$\begin{aligned}& \frac{1}{2\tau}\left(\left\|\partial_t\xi^{n+\frac{1}{2}}\right\|_{L^2(\Omega)}^2 - \left\|\partial_t\xi^{n-\frac{1}{2}}\right\|_{L^2(\Omega)}^2\right) + \frac{1}{2\tau}\left(a_h(\xi^{n+\frac{1}{2}}, \xi^{n+\frac{1}{2}}) - a_h(\xi^{n-\frac{1}{2}}, \xi^{n-\frac{1}{2}})\right) \\ = & (\partial_{tt}\eta^n, \partial_t\xi^n)_\Omega + (u_{tt}^{n,1/4} - \partial_{tt}u^n, \partial_t\xi^n)_\Omega.\end{aligned} \quad (6.43)$$

Summing (6.43) over $n$, by the telescoping property, we obtain

$$\begin{aligned}& \left\|\partial_t\xi^{N+\frac{1}{2}}\right\|_{L^2(\Omega)}^2 + a_h\left(\xi^{N+\frac{1}{2}}, \xi^{N+\frac{1}{2}}\right) \\ = & \left\|\partial_t\xi^{1/2}\right\|_{L^2(\Omega)}^2 + a_h\left(\xi^{\frac{1}{2}}, \xi^{\frac{1}{2}}\right) + 2\tau\sum_{n=1}^N\left((\partial_{tt}\eta^n, \partial_t\xi^n)_\Omega + \left(u_{tt}^{n,1/4} - \partial_{tt}u^n, \partial_t\xi^n\right)_\Omega\right).\end{aligned}$$

By the coercivity and continuity of $a_h(\cdot,\cdot)$ described in (4.49) and (4.55), we obtain

$$\begin{aligned}
&\left\|\partial_t \xi^{N+\frac{1}{2}}\right\|_{L^2(\Omega)}^2 + \kappa \left\|\xi^{N+\frac{1}{2}}\right\|_h^2 \\
\le\ & \left\|\partial_t \xi^{1/2}\right\|_{L^2(\Omega)}^2 + C\left|\!\left|\!\left|\xi^{\frac{1}{2}}\right|\!\right|\!\right|_h^2 + 2\tau \sum_{n=1}^{N} \left( (\partial_{tt}\eta^n, \partial_t \xi^n)_\Omega + \left(u_{tt}^{n,1/4} - \partial_{tt} u^n, \partial_t \xi^n\right)_\Omega \right) \\
\le\ & \left\|\partial_t \xi^{1/2}\right\|_{L^2(\Omega)}^2 + C\left\|\xi^{\frac{1}{2}}\right\|_h^2 + 2\tau \sum_{n=1}^{N} \left( |(\partial_{tt}\eta^n, \partial_t \xi^n)_\Omega| + \left|\left(u_{tt}^{n,1/4} - \partial_{tt} u^n, \partial_t \xi^n\right)_\Omega\right| \right),
\end{aligned} \tag{6.44}$$

where we used the equivalence of $\|\xi\|_h$ and $|\!|\!|\xi|\!|\!|_h$ for $\xi \in S_h(\Omega)$. Applying (6.22),(6.23),(6.30) and(6.33) to the right hand side of (6.44) with $\delta \le 1$ we obtain

$$\begin{aligned}
\left\|\partial_t \xi^{N+\frac{1}{2}}\right\|_{L^2(\Omega)}^2 + \kappa \left\|\xi^{N+\frac{1}{2}}\right\|_h^2 \le C(\tau^4 + h^4) + \frac{\tau\delta}{2} \left\|\partial_t \xi^{N+\frac{1}{2}}\right\|_{L^2(\Omega)}^2 + 2\delta \left\|\xi^{N+\frac{1}{2}}\right\|_{L^2(\Omega)}^2 \\
+ \tau \sum_{n=0}^{N-1} \left( \left\|\partial_t \xi^{n+1/2}\right\|_{L^2(\Omega)}^2 + \left\|\xi^{n+1/2}\right\|_{L^2(\Omega)}^2 \right).
\end{aligned} \tag{6.45}$$

Applying the piecewise Poincaré-Friedrichs inequality (6.26) to $\left\|\xi^{n+1/2}\right\|_{L^2(\Omega)}$ on the right hand side of (6.45), then the following holds for $\delta$ small enough:

$$\begin{aligned}
&\left\|\partial_t \xi^{N+\frac{1}{2}}\right\|_{L^2(\Omega)}^2 + \left\|\xi^{N+\frac{1}{2}}\right\|_h^2 \le C(\tau^4 + h^4) + C\tau \sum_{n=0}^{N-1} \left( \left\|\partial_t \xi^{n+1/2}\right\|_{L^2(\Omega)}^2 + \left\|\xi^{n+1/2}\right\|_h^2 \right) \\
\le & C(\tau^4 + h^4) + C\tau \sum_{n=0}^{N-1} \left( \left\|\partial_t \xi^{n+1/2}\right\|_{L^2(\Omega)}^2 + \kappa \left\|\xi^{n+1/2}\right\|_h^2 \right).
\end{aligned}$$

By the standard discrete Gronwall-Bellmann inequality and Lemma 6.4, we have

$$\begin{aligned}
&\left\|\partial_t \xi^{N+\frac{1}{2}}\right\|_{L^2(\Omega)}^2 + \left\|\xi^{N+\frac{1}{2}}\right\|_h^2 \le C(\tau^4 + h^4) + CN\tau \left( \left\|\partial_t \xi^{1/2}\right\|_{L^2(\Omega)}^2 + \kappa \left\|\xi^{1/2}\right\|_h^2 \right) \\
\le & C(\tau^4 + h^4) + CT \left( \left\|\partial_t \xi^{1/2}\right\|_{L^2(\Omega)}^2 + \kappa \left\|\xi^{1/2}\right\|_h^2 \right) \le C(h^4 + \tau^4), \quad N = 1, 2, \ldots, M-1,
\end{aligned}$$

which proves the estimate in (6.38). $\square$

We are now ready to state and prove our main theorems which provide the optimal *a priori* error estimates for the PPIFE solution to the hyperbolic interface problem (6.1) in the energy norm $\|\cdot\|_h$ and the $L^2$ norm, respectively.

**Theorem 6.3.** *Let $u$ be the exact solution of (6.1) satisfying the conditions of Theorem 6.2, then we have the following estimate*

$$\left\|u_h^{n+1/2} - u^{n+1/2}\right\|_h \leq C\left(h+\tau^2\right), \quad n = 0, 1, \ldots, M-1, \tag{6.46}$$

*where $C$ is a constant such that $C = \max\{C_1, C_2/\delta\}$, with generic constants $C_1$ and $C_2$ independent of $\delta$.*

*Proof.* From Theorem 6.2, we have

$$\left\|\xi^{n+1/2}\right\|_h \leq C\left(h^2+\tau^2\right), \quad n = 0, 1, \ldots, M-1.$$

Then, applying the triangle inequality and (6.9), we have

$$\left\|u_h^{n+1/2} - u^{n+1/2}\right\|_h \leq \left\|\xi^{n+1/2}\right\|_h + \left\|\eta^{n+1/2}\right\|_h \leq C(h+\tau^2), \quad n = 0, 1, \ldots, M.$$

□

**Theorem 6.4.** *Let $u$ be the exact solution of (6.1) satisfying the conditions of Theorem 6.2, then we have the following estimate*

$$\|u_h^n - u^n\|_{L^2(\Omega)} \leq C(h^2+\tau^2), \quad n = 0, 1, \ldots, M, \tag{6.47}$$

*where $C$ is a constant such that $C = \max\{C_1, C_2/\delta\}$, with generic constants $C_1$ and $C_2$ independent of $\delta$.*

*Proof.* From Theorem 6.2, we have

$$\left\|\partial_t \xi^{n+1/2}\right\|_{L^2(\Omega)} = \left\|\frac{\xi^{n+1} - \xi^n}{\tau}\right\|_{L^2(\Omega)} \leq C(h^2 + \tau^2), \quad n = 0, 1, \ldots, M-1,$$

which for $\tau < 1$ yields

$$\left\|\xi^{n+1} - \xi^n\right\|_{L^2(\Omega)} \leq C(h^2 + \tau^2). \tag{6.48}$$

On the other hand, by Theorem 6.2 and Inequality (6.26), we also have

$$\left\|\xi^{n+1/2}\right\|_{L^2(\Omega)} \leq C \left\|\xi^{n+1/2}\right\|_h \leq C(h^2 + \tau^2),$$

which can be written as

$$\left\|\xi^{n+1} + \xi^n\right\|_{L^2(\Omega)} \leq C(h^2 + \tau^2). \tag{6.49}$$

Combining (6.48) and (6.49) we have

$$\|\xi^n\|_{L^2(\Omega)} \leq C(h^2 + \tau^2), \quad n = 0, 1, 2, \ldots, M. \tag{6.50}$$

Applying the triangle inequality we have

$$\|u_h^n - u^n\|_{L^2(\Omega)} \leq \|\xi^n\|_{L^2(\Omega)} + \|\eta^n\|_{L^2(\Omega)}, \quad n = 0, 1, \ldots, M.$$

Finally, applying (6.50) and Lemma 6.2 to the above inequality yields the estimate in (6.47).

$\square$

## 6.4 Numerical Examples

Numerical examples demonstrating the optimal convergence feature of the PPIFE method were already reported in [143]. We present a few numerical examples in this section to demonstrate other features of this PPIFE method. Without loss of generality, all the examples are posed on rectangular domains which are partitioned by Cartesian triangular meshes. Such a mesh $\mathcal{T}_h$ is obtained by dividing a rectangular domain into $Ns \times Ns$ rectangles and each rectangle is further divided into 2 right-angle triangles by the line connecting the lower right vertex to the upper left vertex.

**Example 6.4.1.**

We note the exact solutions in those examples reported [143] all have a piecewise $H^3$ regularity in the space variable. The main purpose of this example is to show, as predicted by the error analysis in the previous section, that the PPIFE method actually converges optimally if the exact solution has a piecewise $H^2$ regularity in the space variable. Specifically, let us consider the hyperbolic interface problem (6.1) posed on the domain $\Omega = (-1,1) \times (-1,1)$ which is divided by the circular interface $\Gamma = \{(x,y) | x^2 + y^2 - r_0^2 = 0\}$ with $r_0 = \pi/6.28$ into two sub-domains:

$$\Omega^- = \left\{(x,y) : x^2 + y^2 < r_0^2\right\}, \quad \text{and} \quad \Omega^+ = \Omega \backslash \overline{\Omega^-}.$$

We select $c^- = 1,\ c^+ = \sqrt{10}$, $T = 1$, and let $f$, $g$, $w_0(X)$, $w_1(X)$ in the interface problem (6.1) be generated such that the following $u(X,t)$ is the exact solution of the interface problem:

$$u(X,t) = \begin{cases} \dfrac{1}{\beta^-} r^\alpha \cos(2t), & (X,t) \in \Omega^- \times [0,1], \\ \left(\dfrac{1}{\beta^+} r^\alpha + (\dfrac{1}{\beta^-} - \dfrac{1}{\beta^+}) r_0^\alpha\right) \cos(2t), & (X,t) \in \Omega^+ \times [0,1]. \end{cases} \tag{6.51}$$

where $\alpha = 1.5, r = \sqrt{x^2 + y^2}$. We note that $u(X,t)$ represents a standing wave, and it can be verified that $u(X,t) \in PH^2(\Omega)\backslash PH^3(\Omega)$ for each fixed $t$. Therefore, $u(X,t)$ does not possess the regularity required by the error analysis in [143], but it satisfies the regularity requirement in Section 6.3.

We apply the SPPIFE with $\sigma_e^0 = 30\max\{(c^-)^2, (c^+)^2\} = 300$ to solve the interface problem configured above on the Cartesian triangular meshes $\mathcal{T}_h$ for $t \in [0,1]$, uniformly divided as $0 = t_0 < t_1 < t_2 < \cdots < t_M = 1$, with $M = Ns$, *i.e.*, $h = 2/Ns$ and $\tau = 1/Ns$. We present the PPIFE errors $\|(u - u_h)(\cdot,t)\|_{0,\Omega}$ and $|(u - u_h)(\cdot,t)|_{1,\Omega}$ at $t = 1$ and their rates of convergence in Table 6.1. The data presented in Table 6.1 clearly demonstrate the optimal convergence, in both semi-$H^1$ and $L^2$ norms, of the PPIFE method for the second-order hyperbolic interface problem whose exact solution is just in $PH^2(\Omega)\backslash PH^3(\Omega)$, and this example corroborates the error analysis of the PPIFE method presented in Section 6.3.

Numerical results presented in Table 6.2 are generated on a mesh for the domain $\Omega$ with $N_s = 640$ but with a variety of time steps. On this fixed spatial mesh, the IFE method produces numerical solutions whose errors are within the bounds given in Theorem 6.3 and Theorem 6.4 for time step sizes chosen from $\tau = 0.25$ to $\tau = 0.0015625$, and of course, the numerical result with a smaller time step size is more accurate. These results suggest that the stability of the IFE method is not influenced by the ratio of the time step size and the mesh size for the space variable, and this corroborates the unconditional stability of the IFE method given in Theorem 6.1

| $Ns$ | $\|u - u_h\|_{0,\Omega}$ | rate | $\|u - u_h\|_{1,\Omega}$ | rate |
|---|---|---|---|---|
| 10 | 2.0414e-03 | NA | 3.4810e-02 | NA |
| 20 | 2.9650e-04 | 2.7835 | 7.3560e-03 | 2.2425 |
| 40 | 8.1983e-05 | 1.8546 | 4.3716e-03 | 0.7508 |
| 80 | 1.9021e-05 | 2.1077 | 1.8753e-03 | 1.2210 |
| 160 | 4.6367e-06 | 2.0364 | 8.9223e-04 | 1.0716 |
| 320 | 1.1541e-06 | 2.0063 | 4.2540e-04 | 1.0686 |
| 640 | 2.9069e-07 | 1.9893 | 2.0765e-04 | 1.0347 |
| 1280 | 7.4786e-08 | 1.9586 | 1.0297e-04 | 1.0120 |

Table 6.1: SPPIFE Errors and convergence rates at $t = 1$ for Example 6.4.1 when $M = N_s$.

| $\tau/h$ | $\|u - u_h\|_{0,\Omega}$ | $\|u - u_h\|_{1,\Omega}$ |
|---|---|---|
| 80 | 2.1499e-03 | 1.1510e-02 |
| 40 | 1.8691e-04 | 1.2218e-03 |
| 20 | 1.0086e-05 | 8.2378e-04 |
| 10 | 4.8491e-06 | 1.0108e-03 |
| 5 | 1.4629e-06 | 3.8330e-04 |
| 2.5 | 3.7134e-07 | 2.7363e-04 |
| 0.5 | 2.9069e-07 | 2.0765e-04 |

Table 6.2: SPPIFE Errors for different time step sizes at $t = 1$ for Example 6.4.1 when $N_s = 640$.

**Example 6.4.2.**

The second example is a hyperbolic interface problem simulating travelling waves with a linear interface across which the jump conditions are determined by the well known Snell's law. Specifically, we consider the interface problem (6.1) on the domain $\Omega = (-10, 10) \times (-10, 10)$ split by the interface $\Gamma = \{(x, y) \in \Omega \mid x = 0.37\}$ into

$$\Omega^- = \{(x, y) \in \Omega \mid x - 0.37 < 0\}, \quad \text{and} \quad \Omega^+ = \Omega \backslash \overline{\Omega^-}.$$

The exact solution $u$ consists of an incident wave $u^I$ starting in $\Omega^-$ and travels at speed $c^-$ in the direction of $\boldsymbol{v} = (2, 1)$ until it hits the interface $\Gamma$ which causes it to split into a reflected wave $u^R$ and transmitted wave $u^T$ [120, 147]:

$$\begin{aligned} u^I(X,t) &= \frac{1}{(c^-)^2}\zeta\left(t - \frac{xcos(\theta_I) + ysin(\theta_I)}{c^-}\right), \\ u^R(X,t) &= \frac{R}{(c^-)^2}\zeta\left(t - \frac{-xcos(\theta_I) + ysin(\theta_I)}{c^-}\right), \\ u^T(X,t) &= \frac{Tr}{(c^+)^2}\zeta\left(t - \frac{xcos(\theta_T) + ysin(\theta_T)}{c^+}\right), \end{aligned} \tag{6.52}$$

with $R = \frac{\rho^+ c^+ cos(\theta_I) - \rho^- c^- cos(\theta_T)}{\rho^+ c^+ cos(\theta_I) + \rho^- c^- cos(\theta_T)}$, $Tr = \frac{2\rho^- c^+ cos(\theta_I)}{\rho^+ c^+ cos(\theta_I) + \rho^- c^- cos(\theta_T)}$, $\zeta(\xi) = sin(\xi)\exp(-4\xi^2)$, where $\rho^- = 1/(c^-)^2$, $\rho^+ = 1/(c^+)^2$, $\theta_I = arctan(1/2)$, and $\theta_T$ determined by $\frac{sin\theta_T}{c^+} = \frac{sin\theta_I}{c^-}$. The functions $f$, $g$, $w_0$ and $w_1$ in the interface problem (6.1) are generated such that the following function $u(X, t)$ is the exact solution:

$$u(X,t) = \begin{cases} u^I(X,t) + u^R(x,y,t), & (X,t) \in \Omega^- \times [0, 0.6], \\ u^T(X,t), & (X,t) \in \Omega^+ \times [0, 0.6]. \end{cases} \tag{6.53}$$

Also we choose $c^- = 1.5$ and $c^+ = 0.34$ in (6.1) for simulating an acoustic wave propagation in the domain $\Omega$ formed with air-water-like materials. We apply the SPPIFE method to solve this interface problem on Cartesian triangular meshes and present the related numerical results at time $t = 0.6$ in Table 6.3 which clearly indicate the optimal convergence of the PPIFE method when the mesh is fine enough. We also plot the PPIFE solution with $Ns =$

160 and $\tau = 0.00375$ and the corresponding pointwise errors $t = 0.6$ in Figure 6.1. Both the data and the plots presented here suggest that the PPIFE method can handle traveling waves in interface problems.

| $Ns$ | $\|u - u_h\|_{0,\Omega}$ | rate | $\|u - u_h\|_{1,\Omega}$ | rate |
|---|---|---|---|---|
| 40 | 4.5917e-01 | NA | 2.9764e+00 | NA |
| 80 | 1.9732e-01 | 1.2185 | 2.3571e+00 | 0.3366 |
| 160 | 6.6826e-02 | 1.5621 | 1.3879e+00 | 0.7641 |
| 320 | 2.0061e-02 | 1.7360 | 6.7514e-01 | 1.0397 |
| 640 | 5.1868e-03 | 1.9515 | 3.2171e-01 | 1.0694 |
| 1280 | 1.3067e-03 | 1.9890 | 1.5845e-01 | 1.0217 |

Table 6.3: Errors of SPPIFE solutions, $c^- = 1.5$, $c^+ = 0.34$ at $t = 0.6$.

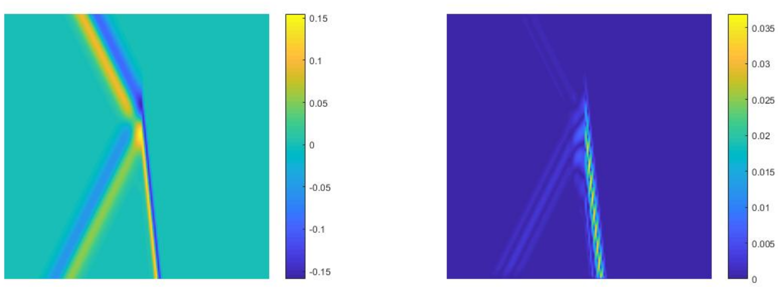


Figure 6.1: SPPIFE solution $u_h$ (left) and the error $u - u_h$ (right) at $t = 0.6$ for Example 6.4.2 with $c^- = 1.5$, $c^+ = 0.34$, $Ns = 160$.

**Example 6.4.3.**

In this example, we consider an application of the PPIFE method to a hyperbolic interface problem with a more sophisticated material interface. Specifically, we consider a non-square domain $\Omega = (-2, 2)\times(-2, 3)$ split by an elliptic interface $\Gamma = \left\{(x, y)| \frac{(x-x_0)^2}{r_x^2} + \frac{(y-y_0)^2}{r_y^2} - 1 = 0\right\}$

into:

$$\Omega^- = \left\{(x,y) \,|\frac{(x-x_0)^2}{r_x^2} + \frac{(y-y_0)^2}{r_y^2} < 1\right\}, \quad \text{and} \quad \Omega^+ = \Omega\backslash\overline{\Omega^-},$$

where $(x_0, y_0) = (1.15, 0)$, $r_x = \pi/4.84, r_y = \pi/1.97$. Let $c^- = 1$, $c^+ = 2$, and let $f = 0, g = 0, w_1 = 0, T = 0.6$ in the interface problem (6.1) and $u_{tt}(X, 0) = 0$ in (6.4), but the initial pulse $w_0 = u(X, 0)$ is selected to be

$$u(X,0) = \begin{cases} 0, & X \notin S, \\ a \cdot \exp\left(\frac{-r^2}{|(x-x_c)^2+(y-y_c)^2-r^2|}\right), & X \in S, \end{cases}$$

where $S = \{(x, y)|(x-x_c)^2 + (y-y_c)^2 - r^2 < 0\}$, with $r = 0.2, a = 20, (x_c, y_c) = (0, 0.8)$. We note that the exact solution to this interface problem is not easy to derive, if not impossible. Hence, instead of using actual numerical errors to demonstrate the performance of the PPIFE method, in Figure 6.2, we compare the numerical results generated by the PPIFE method against the corresponding numerical results produced by the standard linear finite element method with a fitted mesh for this interface problem which are theoretically supposed to be accurate. The meshes, both the Cartesian meshes and body-fitting meshes, used to generate numerical results in this example are illustrated in Figure 6.3.

For the numerical results presented in Figure 6.2, the PPIFE method uses $\sigma_e^0 = 120$ on the Cartesian mesh with $Ns = 641$ with $\tau = 0.6/N_s$ and this mesh has 821762 elements. On the other hand, the fitted mesh used by the finite element solution has 1343488 elements. The plots in Figure 6.2 compare numerical results before and after the wave hits the interface, we can see that the PPIFE solution simulates the wave propagation as well as the standard finite element solution even though the PPIFE solution uses a much simpler Cartesian mesh with significantly less degrees of freedom than the finite element solution.

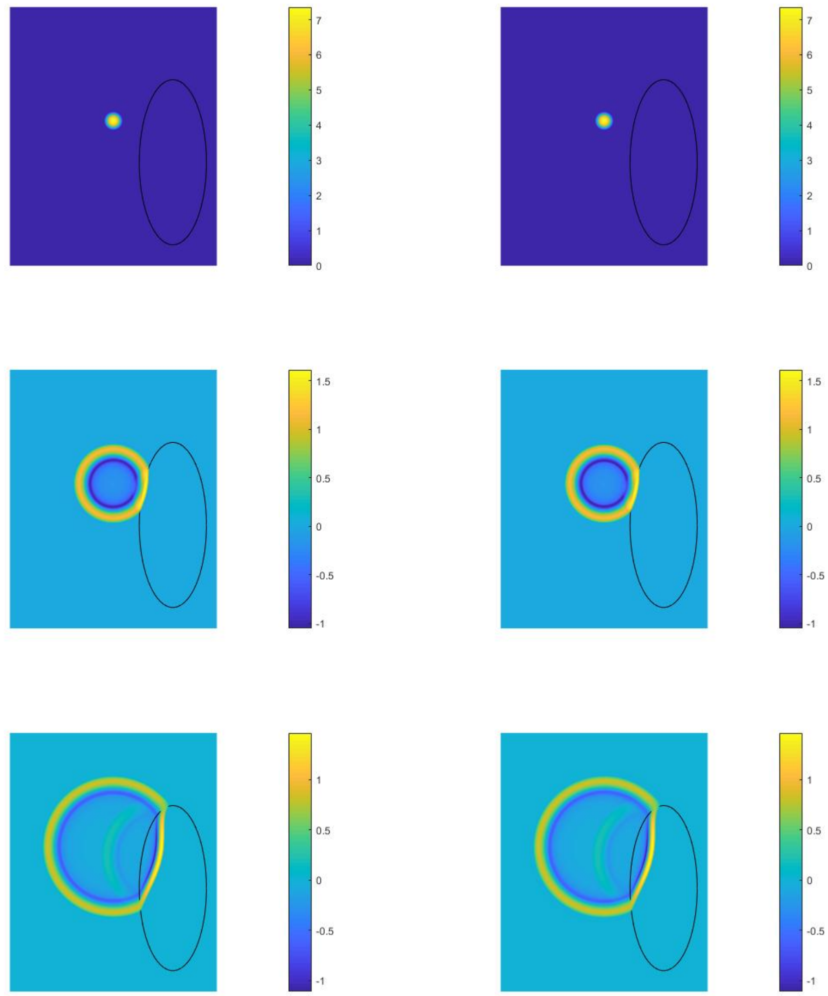

Figure 6.2: SPPIFE solution $u_h$ on Cartesian mesh with $Ns = 641$ (left) and FE solution $u$ (right) at $t = 0, 0.305, 0.6$ (top to bottom) for Example 6.4.3 with $c^- = 1$, $c^+ = 2$.

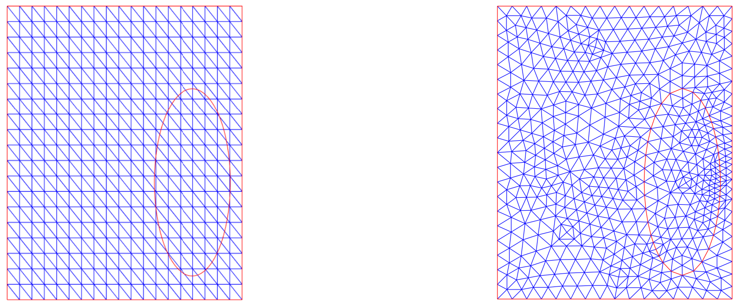

Figure 6.3: Cartesian mesh for PPIFE methods (left) and the body-fitting mesh for standard FE method (right)

## 6.5 Conclusion

We have investigated a fully discrete PPIFE methods for solving second-order hyperbolic interface problems in inhomogeneous media. This method is able to solve the interface problems on Cartesian meshes which do not align with the interface in general. We have performed an *a priori* error analysis for this method under a piecewise $H^2$ regularity assumption in space, proving that it converges optimally in an energy norm and the $L^2$ norm. Numerical examples with both simple linear and more sophisticated interfaces as well as both standing and traveling wave solutions are presented, and these numerical results corroborate the theoretical error analysis.

# Chapter 7

# IFE methods for parabolic interface problems

## 7.1 Introduction

We now study the error estimation of the PPIFE methods for parabolic interface problems under piecewise $H^2$ regularity assumption in space. We recall the interface problem herein:

$$\frac{\partial u}{\partial t} - \nabla \cdot (\beta \nabla u) = f, \quad \text{in } \Omega^- \cup \Omega^+, t \in [0, T], \tag{7.1a}$$

$$u|_{\partial\Omega} = g(X, t), \quad t \in [0, T], \tag{7.1b}$$

$$u|_{t=0} = u_0(X), \quad X \in \partial\Omega, \tag{7.1c}$$

together with the following jump conditions:

$$[u]_\Gamma \ := \ u^+|_\Gamma - u^-|_\Gamma = 0, \tag{7.1d}$$

$$\big[\beta \nabla u \cdot \mathbf{n}\big]_\Gamma \ := \ \beta^+ \nabla u^+ \cdot \mathbf{n}|_\Gamma - \beta^- \nabla u^- \cdot \mathbf{n}|_\Gamma = 0, \tag{7.1e}$$

where the domain $\Omega \subseteq \mathbb{R}^2$ is divided by an interface curve $\Gamma$ into two subdomains $\Omega^-$ and $\Omega^+$, with $\overline{\Omega} = \overline{\Omega^- \cup \Omega^+ \cup \Gamma}$ and the coefficient $\beta$ is a piecewise positive constant function such that

$$\beta(X) = \begin{cases} \beta^- & \text{for } X \in \Omega^-, \\ \beta^+ & \text{for } X \in \Omega^+. \end{cases}$$

By adopting a patch technique for the essential error analysis on each element [63], we present a new error analysis for PPIFE methods considered in [111] and we are able to show that these methods can converge optimally in a suitably designed energy norm and the standard $L^2$ norm under the usual piecewise $H^2$ regularity assumption. To be specific, we will show that a standard semi-discrete PPIFE method and two typical fully discrete PPIFE methods converge optimally in both the energy norm and the $L^2$ norm under the usual piecewise $H^2$ regularity assumption in the space variable for the exact solution.

The layout of this chapter is as follows. In Section 7.2, we recall a group of PPIFE schemes from [113] for parabolic interface problems, including a semi-discrete scheme and two typical fully discrete schemes: the Backward Euler scheme and Crank-Nicolson scheme. Error estimates for these PPIFE methods are derived in Section 7.3. In Section 7.4, a numerical example is presented to validate the theoretical results established in Section 7.3.

## 7.2 PPIFE methods to be analyzed

In this section, we recall PPIFE methods for parabolic interface problems developed in [113]. Throughout this chapter, as we stated in Chapter 6, since we will use $T$ to represent the endpoint of the time domain, we use $K$ instead of $T$ to denote element in the mesh $\mathcal{T}_h$ of $\Omega$. We also recall some set notations about the edges from Chapter 2: the set of interior interface edges is $\mathring{\mathcal{E}}_h^i$, the set of boundary edges is $\mathcal{E}_h^b$, the set of boundary interface edges is $\mathcal{E}_h^{bi}$.

Similar to the elliptic interface problem in Section 4.2, we can derive a weak form of the parabolic interface problem described in (7.1), which is essentially the same as that in [113], with a slightly more general configuration that allows the interface to intersect with the boundary of the domain, i.e., $\Gamma \cap \partial\Omega \neq \emptyset$. These considerations lead to the following weak formulation of the parabolic interface problems (7.1): find $u$: $[0,T] \to PH^2(\Omega)$ that satisfies (7.1d), (7.1e) and

$$\begin{aligned} (u_t, v) + a_h(u, v) &= L_f(v), \quad \forall v \in V_{h,0}(\Omega), \\ u(X,0) &= u_0(X), \quad \forall X \in \Omega, \end{aligned} \tag{7.2}$$

in which the bilinear form $a_h(\cdot,\cdot) : V_h(\Omega) \times V_h(\Omega) \to \mathbb{R}$ is defined by

$$\begin{aligned} a_h(u,v) = &\sum_{K\in\mathcal{T}_h} \int_K \beta \nabla u \cdot \nabla v dX - \sum_{e\in\mathring{\mathcal{E}}_h^i} \int_e \{\beta\nabla u \cdot \mathbf{n}_e\}_e [v]_e ds \\ &+ \epsilon \sum_{e\in\mathring{\mathcal{E}}_h^i} \int_e \{\beta\nabla v \cdot \mathbf{n}_e\}_e [u]_e ds + \sum_{e\in\mathring{\mathcal{E}}_h^i} \frac{\sigma_e^0}{|e|} \int_e [u]_e\, [v]_e ds - \sum_{e\in\mathcal{E}_h^{bi}} \int_e \beta\nabla u \cdot \mathbf{n}_e v ds \\ &+ \epsilon \sum_{e\in\mathcal{E}_h^{bi}} \int_e \beta \nabla v \cdot \mathbf{n}_e u ds + \sum_{e\in\mathcal{E}_h^{bi}} \frac{\sigma_e^0}{|e|} \int_e u\, v ds, \qquad \forall u, v \in V_h(\Omega), \end{aligned} \tag{7.3}$$

with $V_h(\Omega)$ and $V_{h,0}(\Omega)$ defined in (2.4) and (2.5), and the linear form $L_f : V_h(\Omega) \to \mathbb{R}$ is defined by

$$L_f(v) = \int_\Omega f v dX + \epsilon \sum_{e\in\mathcal{E}_h^{bi}} \int_e \beta\nabla v \cdot \mathbf{n}_e\ g ds + \sum_{e\in\mathcal{E}_h^{bi}} \frac{\sigma_e^0}{|e|} \int_e v g ds, \qquad \forall v \in V_h(\Omega). \tag{7.4}$$

Since the linear/bilinear global IFE space $S_h(\Omega)$ defined in (4.8) is a subspace of $V_h(\Omega)$, the above weak form of the interface problem naturally suggests the following PPIFE methods [113] to be analyzed in the next section.

**Semi-discrete PPIFE methods**: find $u_h : [0, T] \to S_h(\Omega)$ such that

$$
\begin{aligned}
(u_{h,t}, v_h) + a_h(u_h, v_h) &= L_f(v_h), \quad \forall v_h \in S_{h,0}(\Omega), \\
u_h(X, 0) &= \tilde{u}_{h0}(X), \quad \forall X \in \Omega,
\end{aligned}
\tag{7.5}
$$

where $\tilde{u}_{h0} \in S_h(\Omega)$ is either an IFE function defined as the elliptic projection as defined in (6.7) or the interpolation of $u_0$ in the IFE space $S_h(\Omega)$.

**Fully discrete PPIFE methods**: we will use a uniform partition in time such that

$$
\begin{aligned}
\Pi_\tau &= \{0 = t^0 < t^1 < ... < t^M = T\}, \\
\tau &= t^n - t^{n-1}, \quad n = 1, 2, ..., M,
\end{aligned}
\tag{7.6}
$$

with $M$ a positive integer. For a function $\phi(X, t)$, as usual, we let $\phi^n(X) = \phi(X, t^n)$, and let

$$
\partial_t \phi^n(X) = \frac{\phi^n(X) - \phi^{n-1}(X)}{\tau}. \tag{7.7}
$$

A group of fully-discrete PPIFE methods can be described as: find a sequence $\{u_h^n\}_{n=1}^M \subset S_h(\Omega)$ such that

$$
\begin{aligned}
&(\partial_t u_h^n, v_h) + a_h\left(\theta u_h^n + (1-\theta) u_h^{n-1}, v_h\right) = \theta L_{f^n}(v_h) \\
&\qquad\qquad\qquad\qquad + (1-\theta) L_{f^{n-1}}(v_h), \quad \forall v_h \in S_{h,0}(\Omega), \\
&u_h^0(X) = \tilde{u}_{h0}(X), \quad \forall X \in \Omega,
\end{aligned}
\tag{7.8}
$$

where $\theta \in [0, 1]$. Two cases are of special interests when $\theta = 1$ and $\theta = 1/2$, and the above reduces to the backward Euler PPIFE method and Crank-Nicolson PPIFE method, respectively.

We note that the bilinear form $a_h(\cdot, \cdot)$ in (7.3) is almost the same as that used in the interior penalty DG finite element methods for the standard elliptic boundary value problem [36, 78, 127] except that the penalties are applied only over interface edges instead of all the edges. Following the convention in DG finite element methods, we usually consider three choices for the parameter $\epsilon$ in this bilinear form: $\epsilon = -1$, 0, or 1, which leads to a symmetric bilinear form $a_h(\cdot, \cdot)$ when $\epsilon = -1$, and a nonsymmetric bilinear form, otherwise. The related PPIFE methods described either by (7.5) or (7.8) will be called SPPIFE methods or NPPIFE methods, respectively.

The PPIFE methods in this paper can be extended to the parabolic interface problem with a non-homogeneous flux jump condition by constructing an additional IFE function according to the technique presented in [74]. In addition, these PPIFE methods can be extended to the parabolic interface problem where $\beta(X)$ in (7.1a) is a variable matrix. Indeed, we may employ the averaging idea presented in [79, 81] by which $\beta^{\pm}$ can be specified as the average of $\beta(X)$ on $K^{\pm}$ respectively, for constructing the needed IFE functions on each interface element $K$. However, the remaining issue is the related error analysis.

## 7.3 Error analysis of parabolic PPIFE methods

In this section, we will derive *a priori* error estimates for the PPIFE methods recalled in the previous section. Without loss of generality and following usual convention in error analysis of finite element methods, we assume that: (i) the interface problem has a homogeneous Dirichlet boundary condition, *i.e.*, $g = 0$ in (7.1b); (ii) the interface does not intersect the boundary, *i.e.*, $\Gamma \cap \partial\Omega = \emptyset$. We note that assumption (ii) here is just a technicality for a clear presentation of main ideas in the error estimations and the analysis can be extended to the case without assumption (ii). This is because the error estimations for the related elliptic interface problems given in the previous chapter have such an extension under a suitable assumption about how the interface intersects with the boundary of $\Omega$.

We will still use the energy norms $\|v\|_h$ and $|||v|||_h$ defined in (4.36) and (4.37) for $v \in V_h(\Omega)$ in the error analysis. Recall that $\|\cdot\|_h$ and $|||\cdot|||_h$ are norms on $V_h(\Omega)$ [63] such that

$$\|v\|_h \leq |||v|||_h, \quad \forall v \in V_h(\Omega) \;\text{ and }\; |||v|||_h \leq C\|v\|_h, \quad \forall v \in S_{h,0}(\Omega), \tag{7.9}$$

for a certain constant $C$, where $S_{h,0}(\Omega)$ is defined in (4.8). The following lemma recalls coercivity of the bilinear linear form $a_h(\cdot,\cdot)$ defined in (7.3) with respect to either of these two energy type norms.

**Lemma 7.1.** *If $\sigma_e^0$ is sufficiently large, then there exists a positive constant $\kappa$ such that*

$$a_h(v,v) \geq \kappa\|v\|_h^2 \;\; \textit{and} \;\; a_h(v,v) \geq \kappa|||v|||_h^2, \quad \forall v \in S_{h,0}(\Omega). \tag{7.10}$$

*Proof.* These results follow directly from Lemma 4.1 in [111] and Theorem 4.4. □

From (6.7), we can see that the elliptic projection $\tilde{u}_h$ of a function $u$ also satisfies

$$a_h\left((\tilde{u}_h)_t, v_h\right) = a_h(u_t, v_h), \quad a_h((\tilde{u}_h)_{tt}, v_h) = a_h(u_{tt}, v_h), \quad \forall v_h \in S_{h,0}(\Omega), \tag{7.11}$$

provided that $u_t(\cdot,t) \in PH^2(\Omega)$ and $u_{tt}(\cdot,t) \in PH^2(\Omega)$ are suitably defined. Note that here we also have the error estimates for the elliptic projection as it is stated in Lemma 6.1 and Lemma 6.2, except for that the bilinear form $a_h(.,.)$ is defined by (7.3), where the coefficient $\beta$ is used, rather than $c^2$.

**Error estimate for the semi-discrete PPIFE method**:

In the following discussions, we will use the standard splitting $u-u_h = \eta-\xi$ with $\eta = u-\tilde{u}_h$,

$\xi = u_h - \tilde{u}_h$ and $\tilde{u}_h$ is the elliptic projection of $u$ defined by (6.7). We first estimate the error in the $\|\cdot\|_h$ norm for the PPIFE solutions.

**Theorem 7.1.** *Assume that the exact solution $u$ to the parabolic interface problem (7.1) is in $H^1(0,T;PH^2(\Omega))$ for $\epsilon=-1$ but in $H^2(0,T;PH^2(\Omega))$ for $\epsilon=0,1$, and $u_0\in PH^2(\Omega)$. Let $u_h$ be the PPIFE solution defined by the semi-discrete method (7.5) and $u_h(\cdot,0)=\tilde{u}_{h,0}$ being the elliptic projection of $u_0$. Then there exists a constant $C$ such that, for $\epsilon=-1$, we have*

$$\|u(\cdot,t)-u_h(\cdot,t)\|_h \le Ch\left(\|u_0\|_{2,\Omega}+\|u_t\|_{L^2(0,T;PH^2(\Omega))}\right), \quad \forall t\ge 0, \tag{7.12}$$

*and for $\epsilon=0$ or $1$, we have*

$$\begin{aligned}&\|u(\cdot,t)-u_h(\cdot,t)\|_h\\ \le& Ch\left(\|u_0\|_{2,\Omega}+\|u_t(\cdot,0)\|_{2,\Omega}+\|u_t\|_{L^2(0,T;PH^2(\Omega))}+\|u_{tt}\|_{L^2(0,T;PH^2(\Omega))}\right), \forall t\ge 0.\end{aligned} \tag{7.13}$$

*Proof.* For $\epsilon=-1$, by arguments similar to those for (3.16) in [113], we have

$$\frac{1}{2}\int_0^t \|\xi_t\|^2_{L^2(\Omega)}dt+\frac{1}{2}a_h(\xi,\xi)\le C\int_0^t \|\eta_t\|^2_{L^2(\Omega)}dt. \tag{7.14}$$

By the piecewise Poincaré-Friedrichs inequality [12, 24], there holds

$$\|\eta_t\|_{L^2(\Omega)}\le C\|\eta_t\|_h. \tag{7.15}$$

Then, applying (7.15), Lemma 4.1, and the coercivity of $a_h(\cdot,\cdot)$ to (7.14), we have

$$\|\xi_t\|_{L^2(0,t;L^2(\Omega))}+\|\xi\|_h\le Ch\|u_t\|_{L^2(0,T;PH^2(\Omega))}. \tag{7.16}$$

Because $u - u_h = \eta - \xi$, by the triangle inequality, (6.9) with $k = 0$, and (7.16), we have

$$\|u(\cdot,t) - u_h(\cdot,t)\|_h \le Ch\left(\|u\|_{2,\Omega} + \|u_t\|_{L^2(0,T;PH^2(\Omega))}\right), \quad \forall t \ge 0. \tag{7.17}$$

By $u \in H^1(0,T,PH^2(\Omega))$, we have

$$\begin{aligned} \|u(\cdot,t)\|_{2,\Omega} &\le \|u_0\|_{2,\Omega} + \int_0^t \|u_\tau\|_{2,\Omega} d\tau \\ &\le \|u_0\|_{2,\Omega} + C\|u_t\|_{L^2(0,T,PH^2(\Omega))}. \end{aligned} \tag{7.18}$$

Then, estimate in (7.12) follows from applying (7.18) to (7.17).

For $\epsilon = 0$ or 1, by arguments similar to those for the second last inequality in the proof for Theorem 3.1 in [113], we have

$$\int_0^t \|\xi_t\|^2_{L^2(\Omega)} d\tau + \|\xi\|_h^2 \le C\int_0^t \left(\|\eta_t\|_h^2 + \|\eta_{tt}\|_h^2\right) d\tau + C\|\eta_t(\cdot,0)\|_h^2, \tag{7.19}$$

where we have used the estimate in (7.15). Applying (6.9) with $k = 1$ and $k = 2$ to (7.19) leads to

$$\|\xi\|_h \le Ch\left(\|u_t(\cdot,0)\|_{2,\Omega} + \|u_t\|_{L^2(0,T;PH^2(\Omega))} + \|u_{tt}\|_{L^2(0,T;PH^2(\Omega))}\right). \tag{7.20}$$

From $u - u_h = \eta - \xi$ again, applying the triangle inequality and estimates in (6.9) with $k = 0$ and (7.20), we have

$$\|u - u_h\|_h \le Ch\left(\|u\|_{2,\Omega} + \|u_t(\cdot,0)\|_{2,\Omega} + \|u_t\|_{L^2(0,T;PH^2(\Omega))} + \|u_{tt}\|_{L^2(0,T;PH^2(\Omega))}\right). \tag{7.21}$$

Finally, the estimate in (7.13) follows by applying (7.18) to (7.21). $\square$

We now estimate the error in the usual $L^2$ norm.

**Theorem 7.2.** *Assume that the exact solution $u$ to the parabolic interface problem (7.1) is in $H^1(0,T;PH^2(\Omega))$. Let $u_h$ be the PPIFE solution defined by the semi-discrete method (7.5) and $u_h(\cdot,0)=\tilde{u}_{h,0}$ being the elliptic projection of $u_0$. Then, there exists a constant $C$ such that*

$$\|u(\cdot,t)-u_h(\cdot,t)\|_{L^2(\Omega)} \le Ch^2\left(\|u_0\|_{2,\Omega}+\|u_t\|_{L^2(0,T;PH^2(\Omega))}\right). \tag{7.22}$$

*Proof.* By (7.2) and (7.5), we have

$$(u_t-u_{h,t},v)+a_h(u-u_h,v)=0, \quad \forall v\in S_{h,0}(\Omega),$$

which leads to

$$(\xi_t-\eta_t,v)+a_h(\xi-\eta,v)=0, \quad \forall v\in S_{h,0}(\Omega). \tag{7.23}$$

Because $\eta=u-\tilde{u}_h$, by (6.7), we have $a_h(\eta,v)=0$ for $v\in S_h(\Omega)$. Thus, by (7.23), we have

$$(\xi_t,v)+a_h(\xi,v)=(\eta_t,v), \quad \forall v\in S_{h,0}(\Omega). \tag{7.24}$$

Using $v=\xi$ in (7.24) and applying the coercivity of $a_h(\cdot,\cdot)$ given in (7.10), we have

$$\frac{1}{2}\frac{d}{dt}\|\xi\|^2_{L^2(\Omega)} \le \|\eta_t\|_{L^2(\Omega)}\|\xi\|_{L^2(\Omega)}. \tag{7.25}$$

Then, integrating (7.25) leads to

$$\|\xi(t)\|_{L^2(\Omega)} \le \|\xi(0)\|_{L^2(\Omega)}+\int_0^t \|\eta_t\|_{L^2(\Omega)}dt, \tag{7.26}$$

in which $\|\xi(0)\|_{L^2(\Omega)}=0$ since $\tilde{u}_{h,0}$ is assumed to be the elliptic projection of $u_0$. Therefore, applying (6.13) with $k = 1$ to (7.26) we have

$$\|\xi(t)\|_{L^2(\Omega)} \leq \int_0^t \|\eta_t\|_{L^2(\Omega)} d\tau \leq Ch^2 \|u_t\|_{L^2(0,T;PH^2(\Omega))}. \tag{7.27}$$

Then, by the triangle inequality, (7.27), and (6.13) with $k = 0$, we have

$$\|u - u_h\|_{L^2(\Omega)} \leq \|\xi(t)\|_{L^2(\Omega)} + \|\eta(t)\|_{L^2(\Omega)} \leq Ch^2 \left(\|u_t\|_{L^2(0,T;PH^2(\Omega))} + \|u(.,t)\|_{2,\Omega}\right). \tag{7.28}$$

Finally, the estimate in (7.22) follows from applying (7.18) to (7.28). □

We now proceed to conduct the error analysis for the fully discrete PPIFE methods.

**Error estimates for fully discrete PPIFE methods**:

We provide error estimates for two types of fully discrete PPIFE methods: backward Euler methods and Crank-Nicolson methods.

***Backward Euler methods***: The backward Euler methods correspond to the scheme in (7.8) when $\theta = 1$. First we have the following error estimate on backward Euler PPIFE solutions in the energy norm $\|\cdot\|_h$.

**Theorem 7.3.** *Assume that the exact solution $u$ to the parabolic interface problem (7.1) is in $H^2(0,T;PH^2(\Omega)) \cap H^3(0,T;L^2(\Omega))$ and $u_0 \in PH^2(\Omega)$. Let the sequence $\{u_h^n\}_{n=0}^M$ be the solution to the backward Euler PPIFE method described by (7.8) with $\theta = 1$. Then for $\sigma_e^0$ in $a_h(\cdot,\cdot)$ large enough, there exists a positive constant $C$ independent of $h$ and $\tau$ such that, for $\epsilon = -1$, we have, for $n = 1, 2, ..., M$,*

$$\begin{aligned} &\|u_h^n - u^n\|_h \leq \\ &\quad C\left(h\left(\|u_0\|_{2,\Omega} + \|u_t\|_{L^2(0,T;PH^2(\Omega))}\right) + \tau \|u_{tt}\|_{L^2(0,T;L^2(\Omega))}\right), \end{aligned} \tag{7.29}$$

*and for $\epsilon = 0$ or $1$, we have*

$$
\begin{aligned}
&\|u_h^n - u^n\|_h \leq \\
&Ch\left(\|u_0\|_{2,\Omega} + \|u_t\|_{L^2(0,T;PH^2(\Omega))} + \|u_{tt}\|_{L^2(0,T;PH^2(\Omega))} + \left(\frac{1}{\tau}\|u_t\|_{L^2(0,\tau;PH^2(\Omega))}\right)^{\frac{1}{2}}\right) \\
&+ C\tau\left(\|u_{tt}\|_{L^2(0,T;L^2(\Omega))} + \|u_{ttt}\|_{L^2(0,T;L^2(\Omega))} + \left(\frac{1}{\tau}\|u_{tt}\|_{L^2(0,\tau;L^2(\Omega))}\right)^{\frac{1}{2}}\right).
\end{aligned}
\tag{7.30}
$$

*Proof.* The proof follows the same arguments as those used in the proof of Theorem 3.2 in [113] except for using Lemma 6.1 for all the estimates about $\|\eta_t\|_h$ and $\|\eta_{tt}\|_h$. □

Then, we consider the error estimates in $L^2$ norm for the backward Euler PPIFE solutions.

**Theorem 7.4.** *Assume that the exact solution $u$ to the parabolic interface problem (7.1) is in $H^1(0,T;PH^2(\Omega)) \cap H^2(0,T;L^2(\Omega))$ and $u_0 \in PH^2(\Omega)$. Let the sequence $\{u_h^n\}_{n=0}^M$ be the solution to the PPIFE backward Euler methods described by (7.8) with $\theta = 1$ and $u_h^0 = \tilde{u}_{h,0}$ being the elliptic projection of $u_0$. Then for $\sigma_e^0$ in $a_h(\cdot,\cdot)$ large enough, there exists a positive constant $C$ independent of $h$ and $\tau$ such that for $n = 1, 2, ..., M$,*

$$
\begin{aligned}
&\|u_h^n - u^n\|_{L^2(\Omega)} \leq \\
&\qquad C\left(h^2\left(\|u_0\|_{2,\Omega} + \|u_t\|_{L^2(0,T;PH^2(\Omega))}\right) + \tau\,\|u_{tt}\|_{L^2(0,T;L^2(\Omega))}\right).
\end{aligned}
\tag{7.31}
$$

*Proof.* Recall the following identity from [113] ((3.24) in that article):

$$
(\partial_t\xi^n, v_h) + a_h(\xi^n, v_h) = (\partial_t\eta^n, v_h) + (r^n, v_h), \quad \forall v_h \in S_{h,0}(\Omega), \tag{7.32}
$$

where $r^n = -(u_t^n - \partial_t u^n)$. Letting $v_h = \xi^n$ in (7.32) yields

$$
\left(\frac{\xi^n - \xi^{n-1}}{\tau}, \xi^n\right) + a_h(\xi^n, \xi^n) = (\partial_t\eta^n, \xi^n) + (r^n, \xi^n).
$$

Using the coercivity of $a_h(\cdot,\cdot)$ in Lemma 7.1, and applying Hölder inequality to the right hand side of the above equation, we have

$$\frac{(\xi^n,\xi^n)-(\xi^{n-1},\xi^n)}{\tau}+\kappa\left\|\xi^n\right\|_h^2\le C\left(\left\|\partial_t\eta^n\right\|_{L^2(\Omega)}\left\|\xi^n\right\|_{L^2(\Omega)}+\left\|r^n\right\|_{L^2(\Omega)}\left\|\xi^n\right\|_{L^2(\Omega)}\right).$$

By Hölder inequality again, we have

$$\left\|\xi^n\right\|_{L^2(\Omega)}^2-\left\|\xi^{n-1}\right\|_{L^2(\Omega)}\left\|\xi^n\right\|_{L^2(\Omega)}\le C\tau\left(\left\|\partial_t\eta^n\right\|_{L^2(\Omega)}\left\|\xi^n\right\|_{L^2(\Omega)}+\left\|r^n\right\|_{L^2(\Omega)}\left\|\xi^n\right\|_{L^2(\Omega)}\right),$$

which leads to

$$\left\|\xi^n\right\|_{L^2(\Omega)}-\left\|\xi^{n-1}\right\|_{L^2(\Omega)}\le C\tau\left(\left\|\partial_t\eta^n\right\|_{L^2(\Omega)}+\left\|r^n\right\|_{L^2(\Omega)}\right).$$

Summing the inequality above from $n=1$ to $k$, we have

$$\left\|\xi^k\right\|_{L^2(\Omega)}-\left\|\xi^0\right\|_{L^2(\Omega)}\le C\tau\sum_{n=1}^{k}\left(\left\|\partial_t\eta^n\right\|_{L^2(\Omega)}+\left\|r^n\right\|_{L^2(\Omega)}\right). \tag{7.33}$$

According to (3.28) in [113], and using the estimate in (6.13) with $k=1$, we have

$$\left\|\partial_t\eta^n\right\|_{L^2(\Omega)}^2\le\frac{1}{\tau}\int_{t^{n-1}}^{t^n}\left\|\eta_t\right\|_{L^2(\Omega)}^2dt\le\frac{Ch^4}{\tau}\int_{t^{n-1}}^{t^n}\left\|u_t\right\|_{2,\Omega}^2dt. \tag{7.34}$$

From (3.29) in [113], it follows

$$\left\|r^n\right\|_{L^2(\Omega)}^2\le\frac{\tau}{3}\int_{t^{n-1}}^{t^n}\left\|u_{tt}\right\|_{L^2(\Omega)}^2dt. \tag{7.35}$$

Applying (7.34) and (7.35) to (7.33), and noting the fact that $\|\xi^0\|_{L^2(\Omega)}=0$ since $\tilde{u}_{h0}$ is chosen to be the elliptic projection of $u_0$ in (7.8), it follows

$$\|\xi^k\|^2_{L^2(\Omega)} \leq Ch^4\|u_t\|^2_{L^2(0,T;PH^2(\Omega))} + C\tau^2\|u_{tt}\|^2_{L^2(0,T;L^2(\Omega))} \tag{7.36}$$

Then the estimate in (7.31) follows from applying the triangle inequality, (6.13) with $k = 0$, together with (7.18), and (7.36) to the standard splitting $u - u_h = \eta - \xi$. □

***Crank Nicolson methods***: We now consider the error in the IFE solutions produced by the Crank-Nicolson schemes described by (7.8) with $\theta = 1/2$. First, we have the following error estimate in the energy norm for the SPPIFE Crank-Nicolson scheme.

**Theorem 7.5.** *Assume that the exact solution $u$ to the parabolic interface problem (7.1) is in $H^1(0,T;PH^2(\Omega)) \cap H^3(0,T;L^2(\Omega))$ and $u_0 \in PH^2(\Omega)$. Let the sequence $\{u_h^n\}_{n=0}^M$ be the solution to the PPIFE Crank-Nicolson methods described by (7.8) with $\theta = 1/2$ and $\epsilon = -1$ . Then for $\sigma_e^0$ in $a_h(\cdot,\cdot)$ large enough, there exists a positive constant $C$ independent of $h$ and $\tau$ such that for $n = 1, 2, ..., M$,*

$$\begin{aligned} &\|u_h^n - u^n\|_h \leq \\ &\qquad C\left(h\left(\|u_0\|_{2,\Omega} + \|u_t\|_{L^2(0,T;PH^2(\Omega))}\right) + \tau^2\left\|u_{ttt}\right\|_{L^2(0,T;L^2(\Omega))}\right). \end{aligned} \tag{7.37}$$

*Proof.* The proof follows the same arguments as those used in the proof of Theorem 3.3 in [113] except for using Lemma 4.1 for all the estimates about $\|\eta_t\|_h$ and $\|\eta_{tt}\|_h$. □

We then consider the $L^2$ error estimate of the Crank-Nicolson PPIFE solutions.

**Theorem 7.6.** *Assume that the exact solution $u$ to the parabolic interface problem (7.1) is in $H^1(0,T;PH^2(\Omega)) \cap H^3(0,T;L^2(\Omega))$ and $u_0 \in PH^2(\Omega)$. Let the sequence $\{u_h^n\}_{n=0}^M$ be the solution to the PPIFE Crank-Nicolson methods described by (7.8) with $\theta = 1/2$ and $u_h^0 = \tilde{u}_{h,0}$ being the elliptic projection of $u_0$. Then for $\sigma_e^0$ large enough, there exists a positive constant*

*$C$ independent of $h$ and $\tau$ such that for $n = 1, 2, ..., M$,*

$$\begin{aligned} &\|u_h^n - u^n\|_{L^2(\Omega)} \leq \\ &\qquad C\left(h^2\left(\|u_0\|_{2,\Omega} + \|u_t\|_{L^2(0,T;PH^2(\Omega))}\right) + \tau^2\|u_{ttt}\|_{L^2(0,T;L^2(\Omega))}\right). \end{aligned} \tag{7.38}$$

*Proof.* By (7.5) and (7.8), and the definition in (6.7), we have

$$(\partial_t\xi^n, v_h) + \frac{1}{2}a_h\left(\xi^n + \xi^{n-1}, v_h\right) = (\partial_t\eta^n, v_h) + (r_1^n, v_h) + (r_2^n, v_h), \quad \forall v_h \in S_{h,0}(\Omega), \tag{7.39}$$

where $r_1^n = -u_t^{n-1/2} + \frac{1}{2}(u_t^n + u_t^{n-1})$, $r_2^n = \partial_t u^n - u_t^{n-1/2}$.

Letting $v_h = \xi^n + \xi^{n-1}$ in (7.39) yields

$$\begin{aligned} &\partial_t\|\xi^n\|^2_{L^2(\Omega)} + \frac{1}{2}a_h\left(\xi^n + \xi^{n-1}, \xi^n + \xi^{n-1}\right) \\ = &\left(\partial_t\eta^n, \xi^n + \xi^{n-1}\right) + \left(r_1^n, \xi^n + \xi^{n-1}\right) + \left(r_2^n, \xi^n + \xi^{n-1}\right). \end{aligned} \tag{7.40}$$

By the coercivity of $a_h(\cdot,\cdot)$ given in Lemma 7.1 and applying Hölder inequality to the right hand side of (7.40), we have

$$\begin{aligned} &\partial_t\|\xi^n\|^2_{L^2(\Omega)} + \frac{1}{2}\kappa\|\xi^n + \xi^{n-1}\|_h^2 \\ \leq\ &\|\partial_t\eta^n\|_{L^2(\Omega)}\|\xi^n + \xi^{n-1}\|_{L^2(\Omega)} + \|r_1^n\|_{L^2(\Omega)}\|\xi^n + \xi^{n-1}\|_{L^2(\Omega)} \\ &+ \|r_2^n\|_{L^2(\Omega)}\|\xi^n + \xi^{n-1}\|_{L^2(\Omega)}. \end{aligned} \tag{7.41}$$

By the piecewise Poincaré-Friedrichs inequality [12, 24] we have

$$\|\xi^n + \xi^{n-1}\|_{L^2(\Omega)} \leq C\|\xi^n + \xi^{n-1}\|_h.$$

Therefore, from (7.41), we have

$$
\begin{aligned}
&\partial_t \|\xi^n\|^2_{L^2(\Omega)} + \frac{1}{2}\kappa \left\|\xi^n + \xi^{n-1}\right\|^2_h \\
\leq\ & C\left(\|\partial_t \eta^n\|_{L^2(\Omega)} + \|r_1^n\|_{L^2(\Omega)} + \|r_2^n\|_{L^2(\Omega)}\right)\left\|\xi^n + \xi^{n-1}\right\|_h, \\
\leq\ & C\left(\|\partial_t \eta^n\|_{L^2(\Omega)} + \|r_1^n\|_{L^2(\Omega)} + \|r_2^n\|_{L^2(\Omega)}\right)^2 + \frac{1}{4}\kappa\left\|\xi^n + \xi^{n-1}\right\|^2_h,
\end{aligned}
\tag{7.42}
$$

which yields

$$
\partial_t \|\xi^n\|^2_{L^2(\Omega)} \leq C\left(\|\partial_t \eta^n\|^2_{L^2(\Omega)} + \|r_1^n\|^2_{L^2(\Omega)} + \|r_2^n\|^2_{L^2(\Omega)}\right). \tag{7.43}
$$

According to (3.48) and (3.49) in [113], we have

$$
\|r_i^n\|^2_{L^2(\Omega)} \leq C\tau^3 \int_{t^{n-1}}^{t^n} \|u_{ttt}(.,t)\|^2_{L^2(\Omega)} dt, \quad i = 1, 2. \tag{7.44}
$$

Then, applying (7.34) and (7.44) to the right hand side of (7.43), we have

$$
\frac{\|\xi^n\|^2_{L^2(\Omega)} - \|\xi^{n-1}\|^2_{L^2(\Omega)}}{\tau} \leq C\left(\frac{h^4}{\tau}\int_{t^{n-1}}^{t^n} \|u_t\|^2_{2,\Omega} dt + \tau^3 \int_{t^{n-1}}^{t^n} \|u_{ttt}(.,t)\|^2_{L^2(\Omega)} dt\right). \tag{7.45}
$$

Summing (7.45) from $n = 1$ to $k$ and using the fact that $\xi^0 = 0$, we have

$$
\|\xi^k\|^2_{L^2(\Omega)} \leq C\left(h^4 \int_0^T \|u_t\|^2_{2,\Omega} dt + \tau^4 \int_0^T \|u_{ttt}(.,t)\|^2_{L^2(\Omega)} dt\right). \tag{7.46}
$$

Finally, the estimate in (7.38) follows from utilizing the triangle inequality, (6.13) with $k = 0$, together with (7.18), and the estimate in (7.46) to the standard splitting $u - u_h = \eta - \xi$. □

**Remark 7.1.** *We note that Theorem 7.5 gives an error estimate in an energy norm that is comparable to the usual semi-$H^1$ norm for the SPPIFE Crank-Nicolson scheme. With the error estimate in the $L^2$ norm given in Theorem 7.6, we can derive the error estimate in semi-$H^1$ norm for the NPPIFE Crank-Nicolson schemes subject to a CFL condition.*

*Specifically, we start from the fact that* $\xi^n \in S_{h,0}(\Omega), n = 0, 1, ..., M$. *Then, by the inverse inequality of IFE function [72, 111],*

$$|\xi^n|_{1,T} \leq Ch^{-1}\|\xi^n\|_{L^2(T)}, \quad \forall T \in \mathcal{T}_h^i,$$

*together with the standard inverse inequality on the non-interface elements, we have*

$$|\xi^n|_{1,\Omega} \leq Ch^{-1}\|\xi^n\|_{L^2(\Omega)}.$$

*Thus, by (7.46), we have*

$$|\xi^n|_{1,\Omega}^2 \leq Ch^2 \left( \int_0^T \|u_t\|_{2,\Omega}^2 dt + \frac{\tau^4}{h^4} \int_0^T \|u_{ttt}(.,t)\|_{L^2(\Omega)}^2 dt \right).$$

*By definition, we have* $|v|_{1,\Omega} \leq \|v\|_h$ *for* $v \in S_h(\Omega)$. *Hence, by (6.9) with* $k = 0$ *and the inequality above, we have*

$$|u - u_h^n|_{1,\Omega}^2 \leq |\xi^n|_{1,\Omega}^2 + |\eta^n|_{1,\Omega}^2 \leq Ch^2 \left( \|u_t\|_{L^2(0,T;PH^2(\Omega))}^2 + \frac{\tau^4}{h^4}\|u_{ttt}\|_{L^2(0,T;L^2(\Omega))}^2 + \|u\|_{2,\Omega}^2 \right).$$

*Finally, applying (7.18) to the inequality above, we obtain the following error estimate under the conditions of Theorem 7.6: for* $n = 1, 2, ..., M$,

$$\begin{aligned} &|u_h^n - u^n|_{1,\Omega} \leq \\ &\qquad Ch \left( \|u_0\|_{2,\Omega} + \|u_t\|_{L^2(0,T;PH^2(\Omega))} + \frac{\tau^2}{h^2} \|u_{ttt}\|_{L^2(0,T;L^2(\Omega))} \right). \end{aligned} \tag{7.47}$$

*The result in (7.47) guarantees the optimal order of convergence in semi-*$H^1$ *norm for the NPPIFE Crank-Nicolson method provided that the time step* $\tau$ *satisfies the CFL condition* $\tau \leq Ch$.

## 7.4 Numerical Example

In this section, we will numerically demonstrate the optimal convergence of the PPIFE methods proved in Section 7.3. We note that several numerical examples were reported in [113] that showed the optimal convergence of these PPIFE methods for the parabolic interface problems, but the exact solutions in those numerical examples are piecewise $H^3$ functions. In contrast, the numerical examples to be presented in this section are for an exact solution in the function space $PH^2(\Omega)\backslash PH^3(\Omega)$. In preparing numerical results, we approximately compute the $L^2$ and $H^1$ semi-norm of the errors in IFE solutions element by element using Gaussian quadrature with a sufficient accuracy, and we compute the $L^\infty$ norm of the errors approximately as the maximal absolute value of the errors at all the Gaussian quadrature points in all elements.

Consider the domain $\Omega = (-1,1)\times(-1,1)$ separated by an elliptical interface $\Gamma$ defined by $x^2/r_x^2 + y^2/r_y^2 - 1 = 0$ into two subdomains

$$\Omega^- = \left\{(x,y) : x^2/r_x^2 + y^2/r_y^2 < 1\right\}, \quad \Omega^+ = \Omega\backslash\overline{\Omega^-},$$

where $r_x = \pi/4.28, r_y = \pi/6.28$. Each Cartesian triangular mesh $\mathcal{T}_h$ in our numerical examples is obtained by first partitioning $\Omega$ into $N\times N$ congruent squares and then cutting each square into two triangles by its diagonal line. And the time domain is $t\in[0,1]$, which is uniformly partitioned by $0 = t_0 < t_1 < t_2 < ... < t_M = 1$, with $M = N$. Functions $f$, $g$, and $u_0$ in the interface problem (7.1) are generated with the following exact solution:

$$u(t,x,y) = \begin{cases} \dfrac{1}{\beta^-} r^\alpha e^t, & (x,y)\in\Omega^-, \\ \left(\dfrac{1}{\beta^+} r^\alpha + \left(\dfrac{1}{\beta^-} - \dfrac{1}{\beta^+}\right)\right) e^t, & (x,y)\in\Omega^+, \end{cases} \tag{7.48}$$

where $\alpha = 1.5, r = \sqrt{x^2/r_x^2 + y^2/r_y^2}$. It can be verified that, for fixed $t$, $u \in PH^2(\Omega)\backslash PH^3(\Omega)$; hence, this function $u(t,x,y)$ does not have the regularity required by the error analysis in [113], but it has a sufficient regularity for the error estimates derived in the previous section.

Table 7.1 presents errors of the SPPIFE ($\epsilon = -1$ in (7.3)) solution $u_h(1,x,y)$ generated on a sequence of uniform triangular meshes of $\Omega$ for two typical configurations of $\beta^-$ and $\beta^+$, where $\beta^- : \beta^+ = 1 : 20$ represents a moderate discontinuity in the diffusion coefficient $\beta$, while $\beta^- : \beta^+ = 1 : 1000$ represents a larger discontinuity. The data in this table clearly demonstrate that the SPPIFE solutions converge optimally in both the $L^2$ and the semi-$H^1$ norms to the exact solution $u$ which has the usual $PH^2(\Omega)\backslash PH^3(\Omega)$ regularity instead of the excessive $PH^3(\Omega)$ regularity in the space variable. On the other hand, the data in Table 7.1 indicate that the SPPIFE solutions converge only sub-optimally in the $L^\infty$ norm for this example. Similar behaviors have been observed for the NPPIFE methods.

| $\beta^+/\beta^-$ | $N$ | $\|u-u_h\|_{0,\infty,\Omega}$ | rate | $\|u-u_h\|_{0,\Omega}$ | rate | $\|u-u_h\|_{1,\Omega}$ | rate |
|---|---|---|---|---|---|---|---|
| 20 | 10 | 3.6118e-02 | NA | 1.7086e-02 | NA | 1.7581e-01 | NA |
| | 20 | 1.2235e-02 | 1.5617 | 4.1852e-03 | 2.0294 | 8.5439e-02 | 1.0410 |
| | 40 | 4.2133e-03 | 1.5380 | 9.8575e-04 | 2.0860 | 4.2826e-02 | 0.9964 |
| | 80 | 1.4966e-03 | 1.4933 | 2.3491e-04 | 2.0691 | 2.1337e-02 | 1.0051 |
| | 160 | 5.4176e-04 | 1.4660 | 6.1620e-05 | 1.9306 | 1.0670e-02 | 0.9998 |
| | 320 | 1.9582e-04 | 1.4681 | 1.5943e-05 | 1.9505 | 5.3278e-03 | 1.0019 |
| | 640 | 7.0744e-05 | 1.4689 | 4.2719e-06 | 1.9000 | 2.6620e-03 | 1.0010 |
| | 1280 | 2.5523e-05 | 1.4708 | 1.1748e-06 | 1.8625 | 1.3307e-03 | 1.0003 |
| 1000 | 10 | 4.5293e-02 | NA | 2.4431e-02 | NA | 1.9352e-01 | NA |
| | 20 | 1.5672e-02 | 1.5311 | 7.4969e-03 | 1.9415 | 1.0234e-01 | 1.5182 |
| | 40 | 6.4667e-03 | 1.2771 | 2.1756e-03 | 2.0436 | 5.2366e-02 | 1.0397 |
| | 80 | 1.8625e-03 | 1.7958 | 4.4670e-04 | 2.0230 | 2.3942e-02 | 1.0151 |
| | 160 | 9.9846e-04 | 0.8994 | 1.1160e-04 | 1.9908 | 1.1737e-02 | 1.0039 |
| | 320 | 2.4385e-04 | 2.0337 | 2.0782e-05 | 1.8822 | 5.5251e-03 | 1.0012 |
| | 640 | 7.1122e-05 | 1.7776 | 5.1545e-06 | 2.0114 | 2.7282e-03 | 1.0181 |
| | 1280 | 2.5569e-05 | 1.4759 | 1.3078e-06 | 1.9786 | 1.3471e-03 | 1.0181 |

Table 7.1: Errors of SPPIFE Crank-Nicolson solutions at $t = 1$ with $r_x = \pi/4.28, r_y = \pi/6.28$.

# Bibliography

[1] David S. Abraham, Alexandre Noll Marques, and Jean-Christophe Nave. A correction function method for the wave equation with interface jump conditions. *J. Comput. Phys.*, 353:281–299, 2018.

[2] Slimane Adjerid and Kihyo Moon. An immersed discontinuous Galerkin method for acoustic wave propagation in inhomogeneous media. *SIAM J. Sci. Comput.*, 41(1): A139–A162, 2018.

[3] Slimane Adjerid, Mohamed Ben-Romdhane, and Tao Lin. Higher degree immersed finite element methods for second-order elliptic interface problems. *Int. J. Numer. Anal. Model.*, 11(3):541–566, 2014. ISSN 1705-5105.

[4] Slimane Adjerid, Nabil Chaabane, and Tao Lin. An immersed discontinuous finite element method for stokes interface problems. *Comput. Methods Appl. Mech. Engrg.*, 293:170–190, 2015.

[5] Slimane Adjerid, Ruchi Guo, and Tao Lin. High degree immersed finite element spaces by a least squares method. *Int. J. Numer. Anal. Model.*, 14(4-5):604–626, 2017. ISSN 1705-5105.

[6] Slimane Adjerid, Mohamed Ben-Romdhane, and Tao Lin. Higher degree immersed finite element spaces constructed according to the actual interface. *Computers & Mathematics with Applications*, 75(6):1868–1881, 2018. ISSN 0898-1221. doi: https://doi.org/10.1016/j.camwa.2017.10.010. URL http://www.sciencedirect.com/science/article/pii/S0898122117306582.

[7] Slimane Adjerid, Nabil Chaabane, Tao Lin, and Pengtao Yue. An immersed discontinuous finite element method for the stokes problem with a moving interface. *J. Comput. Appl. Math.*, 362:540–559, 2019.

[8] Slimane Adjerid, Ivo Babuška, Ruchi Guo, and Tao Lin. An enriched immersed finite element method for interface problems with nonhomogeneous jump conditions. *arXiv:2004.13244v1*, 2020.

[9] Slimane Adjerid, Tao Lin, and Qiao Zhuang. Error estimates for an immersed finite element method for second order hyperbolic equations in inhomogeneous media. *Submitted*, 2020.

[10] Mark Ainsworth. Dispersive and dissipative behaviour of high order discontinuous galerkin finite element methods. *Journal of Computational Physics*, 198:106–130, April 2004.

[11] A. Al-Droubi and M. Renardy. Energy methods for a parabolic-hyperbolic interface problem arising in electromagnetism. *ZAMP*, 39:931–936, 1988.

[12] Douglas N. Arnold. An interior penalty finite element method with discontinuous elements. *SIAM J. Numer. Anal.*, 19(4):742–760, 1982. ISSN 0036-1429. doi: 10.1137/0719052. URL http://dx.doi.org/10.1137/0719052.

[13] Champike Attanayake and Deepthika Senaratne. Convergence of an immersed finite element method for semilinear parabolic interface problems. *Appl. Math. Sci. (Ruse)*, 5(1-4):135–147, 2011. ISSN 1312-885X.

[14] A.K. Aziz and A. Werschulz. On the numerical solutions of helmholtz's equation by the finite element method. *SIAM. J. Numer. Anal.*, 19(5):166–178, 1995.

[15] I. Babuška and J. M. Melenk. The partition of unity method. *Internat. J. Numer. Methods Engrg.*, 40(4):727–758, 1997. ISSN 0029-5981.

[16] Ivo Babuška. The finite element method for elliptic equations with discontinuous coefficients. *Computing (Arch. Elektron. Rechnen)*, 5:207–213, 1970.

[17] I. M. Babuška and S. A. Sauter. Is the pollution effect of the fem avoidable for the helmholtz equation considering high wave numbers? *Comput. Math. Appl.*, 34(6): 2392–2423, 1997.

[18] John W. Barrett and Charles M. Elliott. Fitted and unfitted finite-element methods for elliptic equations with smooth interfaces. *IMA J. Numer. Anal.*, 7(3):283–300, 1987. ISSN 0272-4979. doi: 10.1093/imanum/7.3.283. URL http://dx.doi.org/10.1093/imanum/7.3.283.

[19] B.Deka and R. Sinha. Finite element methods for second order linear hyperbolic interface problems. *Appl. Math. comput.*, 218:10922–10933, 2012.

[20] Hadrien Bériot, Albert Prinn, and Gwénaël Gabard. Efficient implementation of high-order finite elements for helmholtz problems. *Int. J. Numer. Meth. Engng.*, 106:213–240, 2016.

[21] B.Klenow, A Nisewonger, R.C. Batra, and A. Brown. Reflection and transmission of plane waves at an interface between two fluids. *Comput. Fluids*, 36:1298–1306, 2007.

[22] Dietrich Braess. *Finite elements*. Cambridge University Press, Cambridge, second edition, 2001. ISBN 0-521-01195-7. Theory, fast solvers, and applications in solid mechanics, Translated from the 1992 German edition by Larry L. Schumaker.

[23] James H. Bramble and J. Thomas King. A finite element method for interface problems in domains with smooth boundaries and interfaces. *Adv. Comput. Math.*, 6(2):109–

138, 1996. ISSN 1019-7168. doi: 10.1007/BF02127700. URL http://dx.doi.org/10.1007/BF02127700.

[24] Susanne Brenner. Poincaré-friedrichs inequalities for piecewise $h^1$ functions. *SIAM J. Numer. Anal.*, 41(1):306–324, 2003.

[25] D. Britt, S. Tsynkov, and E. Turkel. A high-order numerical method for the helmholtz equation with nonstandard boundary conditions. *SIAM. J. Sci. Comput.*, 35(5):A2255–A2292, 2013.

[26] David L. Brown. A note on the numerical solution of the wave equation with piecewise smooth coefficients. *Math. Comput*, 42(166):369–391, 1984.

[27] Martin Burger. A framework for the construction of level set methods for shape optimization and reconstruction. *Interfaces and Free Boundaries*, 5:301–329, 2002.

[28] Eric Burman, Haijun Wu, and Lingxue Zhu. Linear continuous interior penalty finite element method for Helmholtz equation with high wave number: one-dimensional analysis. *Numer. Methods Partial Differential Equations*, 32(5):1378–1410, 2016.

[29] Erik Burman, Susanne Claus, Peter Hansbo, Mats G. Larson, and André Massing. Cutfem: Discretizing geometry and partial differential equations. *International Journal for Numerical Methods in Engineering*, 104(7):472–501, 2015.

[30] Michele Caputo and Cesare Cametti. Fractional derivative in the diffusion process in heterogeneous systems: The case of transdermal patches. *Mathematical Biosciences*, 291:38–45, 2017.

[31] G.F. Carey and J.T. Oden. *Finite Elements, Vol. 3: Computational Aspects*. Prentice Hall, 1984.

[32] Nabil Chaabane. *Immersed and Discontinuous Finite Element Methods*. PhD thesis, Virginia Polytechnic Institute and State University, 2015.

[33] C.Y. Chan and P.C. Kong. Channel flow of a viscous fluid in the boundary layer. *Quart. Appl. Math.*, 55:51–56, 2015.

[34] Simon N. Chandler-wilde and Bo Zhang. Scattering of electromagnetic waves by rough interfaces and inhomogeneous layers. *SIAM J. Math. Anal.*, 30(3):559–583, 1989.

[35] T. Chaumont-Frelet. *Finite Element Approximation of Helmholtz Problems with Application to Seimsic Wave Propagation,*. PhD thesis, INSA Rouen, 2015.

[36] Zhangxin Chen. *Finite element methods and their applications*. Scientific Computation. Springer-Verlag, Berlin, 2005. ISBN 978-3-540-24078-5; 3-540-24078-0.

[37] Zhiming Chen and Jun Zou. Finite element methods and their convergence for elliptic and parabolic interface problems. *Numer. Math.*, 79(2):175–202, 1998. ISSN 0029-599X. doi: 10.1007/s002110050336. URL http://dx.doi.org/10.1007/s002110050336.

[38] P.S. Christiansen and S. Krenk. A recursive finite element technique for acoustic fields in pipes with absorption. *J Sound Vib.*, 122(1):107–118, 1988.

[39] C.-C. Chu, I. G. Graham, and T.-Y. Hou. A new multiscale finite element method for high-contrast elliptic interface problems. *Math. Comp.*, 79(272):1915–1955, 2010. ISSN 0025-5718. doi: 10.1090/S0025-5718-2010-02372-5. URL http://dx.doi.org/10.1090/S0025-5718-2010-02372-5.

[40] Yuchuan Chu, Daoru Han, Yong Cao, Xiaoming He, and Joseph Wang. An immersed-finite-element particle-in-cell sumulation tool for plasma surface interaction. *Int. J. Numer. Anal. Model.*, 14(2):175–200, 2017.

[41] Ray. W. Clough and James L. Tocher. Finite element stiffness matrices for analysis of plate bending. In J. S. Przemieniecki, R. M. Bader, W. F. Bozich, J. R. Johnson, and W. J. Mykytow, editors, *Matrix Methods in Structural Mechanics, The Proceedings of the Conference held at Wright-Parrterson Air Force Base, Ohio, 26-28, October, 1965*, pages 515–545, Washington, 1966. Air Force Flight Dynamics Laboratory.

[42] Bernardo Cockburn, George E. Karniadakis, and Chi-Wang Shu, editors. *Discontinuous Galerkin methods*, volume 11 of *Lecture Notes in Computational Science and Engineering*. Springer-Verlag, Berlin, 2000. ISBN 3-540-66787-3. doi: 10.1007/978-3-642-59721-3. URL http://dx.doi.org/10.1007/978-3-642-59721-3. Theory, computation and applications, Papers from the 1st International Symposium held in Newport, RI, May 24–26, 1999.

[43] John Crank. *The Mathematics of Diffusion, Second Edition.* Oxford Science Publications, 1975.

[44] A.S. Bonnet-Ben Dhia, P. Ciarlet Jr., and C.M. Zwölf. Time harmonic wave diffraction problems in materials with sign-shifting coefficients. *J. Comput. Appl. Math.*, 234: 1912–1919, 2010.

[45] D.Leguillon and E. Sanchez- Palencia. *Computation of singular solutions in elliptic problems and elasticity.* Wiley, Chichester[Chichestershire], 1987.

[46] V.I. Dmitriev and E.V. Saharov. *Integral Equations in Boundary Value Problems of Electrodynamics.* Nauka, Moscow (in Russian), 1987.

[47] Yu Du and Haijun Wu. Preasymptotic error analysis of higher order FEM and CIP-FEM for Helmholtz equation with high wave number. *SIAM J. Numer. Anal.*, 53(2): 782–804, 2015.

[48] T. Dupont. $L^2$-estimates for Galerkin methods for second order hyperbolic equations. *SIAM J. Numer. Anal.*, 10(5):880–889, 1973.

[49] Charbel Farhat, Issac Harari, and Ulrich Hetmaniuk. A discontinuous galerkin method with lagrange multipliers for the solution of helmholtz problems in the mid-frequency regime. *Comput.Methods Appl. Mech. Engrg.*, 192:1389–1419, 2003.

[50] Xiaobing Feng and Haijun Wu. Discontinuous Galerkin methods for the helmholtz equation with large wave number. *SIAM J. Numer. Anal.*, 47(4):2872–2896, 2009. doi: 10.1137/080737538. URL http://epubs.siam.org/doi/pdf/10.1137/080737538.

[51] Glaude Gittelson, Ralf Hiptmair, and Ilaria Perugia. Plane wave discontinuous galerkin methods : analysis of the h-version. *Esaim Math. Model. Numer. Anal.*, 43:297–331, 2009.

[52] Yan Gong. *Immersed-interface finite-element methods for elliptic and elasticity interface problems*. PhD thesis, North Carolina State University, 2007.

[53] Yan Gong and Zhilin Li. Immersed interface finite element methods for elasticity interface problems with non-homogeneous jump conditions. *Numer. Math. Theory Methods Appl.*, 3(1):23–39, 2010. ISSN 1004-8979. doi: 10.4208/nmtma.2009.m9001. URL http://dx.doi.org/10.4208/nmtma.2009.m9001.

[54] Yan Gong, Bo Li, and Zhilin Li. Immersed-interface finite-element methods for elliptic interface problems with nonhomogeneous jump conditions. *SIAM J. Numer. Anal.*, 46(1):472–495, 2007/08. ISSN 0036-1429. doi: 10.1137/060666482. URL http://dx.doi.org/10.1137/060666482.

[55] Vincent Guinot. *Wave propagation in fluids: models and numerical techniques, Second Edition*. John Wiley & Sons, Hoboken, 2010.

[56] Ruchi Guo. Solving parabolic moving interface problems with dynamical immersed spaces on unfitted meshes: Fully discrete analysis. *arXiv:2004.15005v1*, 2020.

[57] Ruchi Guo and Tao Lin. A group of immersed finite element spaces for elliptic interface problems. *IMA J.Numer. Anal.*, 39(1):482–511, 2019. doi: 10.1093/imanum/drx074.

[58] Ruchi Guo and Xu Zhang. Solving three-dimensional interface problems with immersed finite elements: A-priori error analysis. *arXiv:2004.08984v1*, 2020.

[59] Ruchi Guo, Tao Lin, and Xu Zhang. Nonconforming immersed finite element spaces for elliptic interface problems. *Comput. Math. Appl.*, 2017. doi: https://doi.org/10.1016/j.camwa.2017.10.040.

[60] Ruchi Guo, Tao Lin, and Yanping Lin. Approximation capabilities of immersed finite element spaces for elasticity interface problems. *Numer. Meth. Part. Diff. Eqn.*, 35(3):1243–1268, 2019.

[61] Ruchi Guo, Tao Lin, and Yanping Lin. A fixed mesh method with immersed finite elements for solving interface inverse problems. *J. Sci. Comput.*, 79:148–175, 2019.

[62] Ruchi Guo, Tao Lin, Yanping Lin, and Qiao Zhuang. Error analysis of symmetric linear/bilinear partially penalized immersed finite element methods for Helmholtz interface problems. *Submitted*, 2019.

[63] Ruchi Guo, Tao Lin, and Qiao Zhuang. An improved error estimation for partial penalized immersed finite element methods for elliptic interface problems. *Int. J. Numer. Anal. Model.*, 16:575–589, 2019.

[64] Ruchi Guo, Tao Lin, and Yanping Lin. Error estimates for a partially penalized immersed finite element method for elasticity interface problems. *ESAIM: M2AN*, 54(1):1–24, 2020.

[65] Ruchi Guo, Tao Lin, and Yanping Lin. A fixed mesh method with immersed finite elements for solving interface inverse problems. *J. Comput. Phys.*, 404:109123, 2020.

[66] Johnny Guzmán, Manuel A. Sánchez, and Marcus Sarkis. On the accuracy of finite element approximations to a class of interface problems. *Mathematics of Computation*, 85(301):2071–2098, 2015. doi: http://dx.doi.org/10.1090/mcom3051.

[67] Johnny Guzmán, Manuel A. Sánchez, and Marcus Sarkis. A finite element method for high-contrast interface problems with error estimates independent of contrast. *Journal of Scientific Computing*, 73(1):330–365, 2017. doi: arXiv:1507.03873v2.

[68] T. Chaumont-Frelet H. Barucq and C. Gout. Stability analysis of heterogeneous Helmholtz problems and finite element solution based on propagation media approximation. *Math. Comp.*, 86:2129–2157, 2016.

[69] Anita Hansbo and Peter Hansbo. A finite element method for the simulation of strong and weak discontinuities in solid mechanics. *Comput. Methods Appl. Mech. Engrg.*, 193(33-35):3523–3540, 2004. ISSN 0045-7825. doi: 10.1016/j.cma.2003.12.041. URL http://dx.doi.org/10.1016/j.cma.2003.12.041.

[70] Xiaoming He. *Bilinear immersed finite elements for interface problems*. PhD thesis, Virginia Polytechnic Institute and State University, 2009.

[71] Xiaoming He, Tao Lin, and Yanping Lin. Approximation capability of a bilinear immersed finite element space. *Numer. Methods Partial Differential Equations*, 24(5): 1265–1300, 2008. ISSN 0749-159X. doi: 10.1002/num.20318. URL http://dx.doi.org/10.1002/num.20318.

[72] Xiaoming He, Tao Lin, and Yanping Lin. A bilinear immersed finite volume element method for the diffusion equation with discontinuous coefficient. *Commun. Comput.*

*Phys.*, 6(1):185–202, 2009. ISSN 1815-2406. doi: 10.4208/cicp.2009.v6.p185. URL http://dx.doi.org/10.4208/cicp.2009.v6.p185.

[73] Xiaoming He, Tao Lin, and Yanping Lin. Interior penalty bilinear IFE discontinuous Galerkin methods for elliptic equations with discontinuous coefficient. *J. Syst. Sci. Complex.*, 23(3):467–483, 2010. ISSN 1009-6124. doi: 10.1007/s11424-010-0141-z. URL http://dx.doi.org/10.1007/s11424-010-0141-z.

[74] Xiaoming He, Tao Lin, and Yanping Lin. Immersed finite element methods for elliptic interface problems with non-homogeneous jump conditions. *Int. J. Numer. Anal. Model.*, 8(2):284–301, 2011. ISSN 1705-5105.

[75] Xiaoming He, Tao Lin, and Yanping Lin. The convergence of the bilinear and linear immersed finite element solutions to interface problems. *Numer. Methods Partial Differential Equations*, 28(1):312–330, 2012. ISSN 0749-159X. doi: 10.1002/num.20620. URL http://dx.doi.org/10.1002/num.20620.

[76] Xiaoming He, Tao Lin, Yanping Lin, and Xu Zhang. Immersed finite element methods for parabolic equations with moving interface. *Numer. Methods Partial Differential Equations*, 29(2):619–646, 2013. ISSN 0749-159X. doi: 10.1002/num.21722. URL http://dx.doi.org/10.1002/num.21722.

[77] Xiaoming He, Tao Lin, and Yanping Lin. A selective immersed discontinuous Galerkin method for elliptic interface problems. *Math. Methods Appl. Sci.*, 37(7):983–1002, 2014. ISSN 0170-4214. doi: 10.1002/mma.2856. URL http://dx.doi.org/10.1002/mma.2856.

[78] Jan S. Hesthaven and Tim Warburton. *Nodal discontinuous Galerkin methods*, volume 54 of *Texts in Applied Mathematics*. Springer, New York, 2008. ISBN 978-0-

387-72065-4. doi: 10.1007/978-0-387-72067-8. URL http://dx.doi.org/10.1007/978-0-387-72067-8. Algorithms, analysis, and applications.

[79] Songming Hou and Xu-Dong Liu. A numerical method for solving variable coefficient elliptic equation with interfaces. *Journal of Computational Physics*, 202(2):411–445, 2005.

[80] Thomas Y. Hou and Xiao-Hui Wu. A multiscale finite element method for elliptic problems in composite materials and porous media. *J. Comput. Phys.*, 134(1):169–189, 1997. ISSN 0021-9991. doi: 10.1006/jcph.1997.5682. URL http://dx.doi.org/10.1006/jcph.1997.5682.

[81] Y. Thomas Hou, Xiao-Hui Wu, and Zhiqiang Cai. Convergence of a multiscale finite element method for elliptic problems with rapidly oscillating coefficients. *Math. Comp.*, 68:913–943, 1999.

[82] F. Ihlenburg and I. Babuška. Finite element solution of the Helmholtz equation with high wave number. I. the h-version of the FEM. *Comput. Math. Appl.*, 30(9):9–37, 1995.

[83] Frank Ihlenburg and Ivo Babuška. Finite element solutions of the Helmholtz equation with high wave number part II: the h-p version of the FEM. *SIAM J.Numer.Anal*, 34 (1):315–358, 1997.

[84] Jr. J. Douglas, D. Sheen, and J.E. Santos. Approximation of scalar waves in the space-frequency domain. *Math. Models Methods Appl. Sci.*, 4(4):509–531, 1994.

[85] A. Parsania J. M. Melenk and D. Sauter. General DG-methods for highly indefinite Helmholtz problems. *J. Sci. Comput*, 57:536–581, 2013.

[86] Finn B. Jensen, William A. Kuperman, Michael B. Porter, and Henrik Schmidt. *Computational Ocean Acoustics*. Springer Publishing Company, 1995.

[87] R. Kafafy, J. Wang, and T. Lin. A hybrid-grid immersed-finite-element particle-in-cell simulation model of ion optics plasma dynamics. *Dyn. Contin. Discrete Impuls. Syst. Ser. B Appl. Algorithms*, 12(Suppl. Vol. 12b):1–16, 2005. ISSN 1492-8760.

[88] Raed Kafafy and Joseph Wang. Whole ion optics gridlet simulations using a hybrid-grid immersed-finite-element particle-in-cell code. *J. Propulsion Power*, 23(1):59–68, 2007.

[89] Juri D. Kandilarov and Lubin G.Vulkov. The immersed interface method for two-dimensional heat-diffusion equations with singular own sources. *Applied Numerical Mathematics*, 57:486–497, 2007.

[90] Tarek A. Kassim and Kenneth J. Williamson. *Environmental Impact Assessment of Recycled Wases on Surface and Ground Waters*. Springer-Verlag, Berlin, 2005.

[91] A. Kirsch and F. Hettlich. The mathematical theory of Maxwell's equations. *Lecture Notes, Karlsruhe Institute of Technology*, 2014.

[92] H. P. Knibble. *Reduction of computing time for seismic applications based on the Helmholtz equation by Graphics Processing Units*. PhD thesis, Delft University of Technology, 2015.

[93] Heinz-otto Kreiss and N.Anders Petersson. An embedded boundary method for the wave equation with discontinuous coefficients. *SIAM J. Sci. Comput*, 28(6):2054–2074, 2006.

[94] Do Y. Kwak, Kye T. Wee, and Kwang S. Chang. An analysis of a broken $P_1$-nonconforming finite element method for interface problems. *SIAM J. Numer.*

*Anal.*, 48(6):2117–2134, 2010. ISSN 0036-1429. doi: 10.1137/080728056. URL http://dx.doi.org/10.1137/080728056.

[95] Chi Yeung Lam and Chi-Wang Shu. A phase-based interior penalty discontinuous galerkin method for the helmholtz equation with spatially varying wavenumber. *Comput.Methods Appl. Mech. Engrg.*, 318:456–473, 2017.

[96] Mats. G. Larson and Fredrik. Bengzon. *The finite element method: theory, implementation and application*. Springer, 2013.

[97] Randall J. LeVeque and Zhi Lin Li. The immersed interface method for elliptic equations with discontinuous coefficients and singular sources. *SIAM J. Numer. Anal.*, 31(4):1019–1044, 1994. ISSN 0036-1429. doi: 10.1137/0731054. URL http://dx.doi.org/10.1137/0731054.

[98] Fengquan Li and Weiwei Sun. Hyperbolic boundary value problem with equivalued surface on a domain with thin layer. *Application of Mathematics*, 54:351–375, 2009.

[99] Jie Li, Yuriko Y. Renardy, and Michael Renardy. Numerical simulation of breakup of a viscous drop in simple shear flow through a volume-of-fluid method. *Physics of Fluids*, 12(2):269–282, 2000.

[100] Z. Li, T. Lin, Y. Lin, and R. C. Rogers. An immersed finite element space and its approximation capability. *Numer. Methods Partial Differential Equations*, 20(3):338–367, 2004. ISSN 0749-159X. doi: 10.1002/num.10092. URL http://dx.doi.org/10.1002/num.10092.

[101] Zhilin Li. The immersed interface method using a finite element formulation. *Appl. Numer. Math.*, 27(3):253–267, 1998. ISSN 0168-9274. doi: 10.1016/S0168-9274(98)00015-4. URL http://dx.doi.org/10.1016/S0168-9274(98)00015-4.

[102] Zhilin Li and Kazufumi Ito. *The immersed interface method*, volume 33 of *Frontiers in Applied Mathematics*. Society for Industrial and Applied Mathematics (SIAM), Philadelphia, PA, 2006. ISBN 0-89871-609-8. doi: 10.1137/1.9780898717464. URL http://dx.doi.org/10.1137/1.9780898717464. Numerical solutions of PDEs involving interfaces and irregular domains.

[103] Zhilin Li and Xingzhou Yang. An immersed finite element method for elasticity equations with interfaces. In *Recent advances in adaptive computation*, volume 383 of *Contemporary Mathematics*, pages 285–298. Amer. Math. Soc., Providence, RI, 2005. doi: 10.1090/conm/383/07171. URL http://dx.doi.org/10.1090/conm/383/07171.

[104] Zhilin Li, Tao Lin, and Xiaohui Wu. New Cartesian grid methods for interface problems using the finite element formulation. *Numer. Math.*, 96(1):61–98, 2003. ISSN 0029-599X. doi: 10.1007/s00211-003-0473-x. URL http://dx.doi.org/10.1007/s00211-003-0473-x.

[105] Tao Lin and Dongwoo Sheen. The immersed finite element method for parabolic problems using the Laplace transformation in time discretization. *Int. J. Numer. Anal. Model.*, 10(2):298–313, 2013. ISSN 1705-5105.

[106] Tao Lin and Xu Zhang. Linear and bilinear immersed finite elements for planar elasticity interface problems. *J. Comput. Appl. Math.*, 236(18):4681–4699, 2012. ISSN 0377-0427. doi: 10.1016/j.cam.2012.03.012. URL http://dx.doi.org/10.1016/j.cam.2012.03.012.

[107] Tao Lin, Yanping Lin, Robert Rogers, and M. Lynne Ryan. A rectangular immersed finite element space for interface problems. In *Scientific computing and applications (Kananaskis, AB, 2000)*, volume 7 of *Advances In Computation: Theory And Practice*, pages 107–114. Nova Sci. Publ., Huntington, NY, 2001.

[108] Tao Lin, Yanping Lin, and Xu Zhang. A method of lines based on immersed finite elements for parabolic moving interface problems. *Adv. Appl. Math. Mech.*, 5(4):548–568, 2013. ISSN 2070-0733.

[109] Tao Lin, Yanping Lin, and Xu Zhang. Immersed finite element method of lines for moving interface problems with nonhomogeneous flux jump. In *Recent advances in scientific computing and applications*, volume 586 of *Contemp. Math.*, pages 257–265. Amer. Math. Soc., Providence, RI, 2013. doi: 10.1090/conm/586/11633. URL http://dx.doi.org/10.1090/conm/586/11633.

[110] Tao Lin, Dongwoo Sheen, and Xu Zhang. A locking-free immersed finite element method for planar elasticity interface problems. *J. Comput. Phys.*, 247:228–247, 2013. ISSN 0021-9991.

[111] Tao Lin, Yanping Lin, and Xu Zhang. Partially penalized immersed finite element methods for elliptic interface problems. *SIAM J. Numer. Anal.*, 53(2):1121–1144, 2015. ISSN 0036-1429. doi: 10.1137/130912700. URL http://dx.doi.org/10.1137/130912700.

[112] Tao Lin, Qing Yang, and Xu Zhang. *A Priori* error estimates for some discontinuous Galerkin immersed finite element methods. *J. Sci. Comput.*, 2015.

[113] Tao Lin, Qing Yang, and Xu Zhang. Partially penalized immersed finite element methods for parabolic interface problems. *Numer Methods Partial Differential Eq*, 31: 749–763, 2015.

[114] Tao Lin, Yanping Lin, and Qiao Zhuang. Solving interface problems of the Helmholtz equation by immersed finite element methods. *Communications on Applied Mathematics and Computation*, 1(2), 2019.

[115] Bruno Lombard and Joël Piraux. Numerical treatment of two-dimensional interfaces for acoustic and elastic waves. *J. Comput. Phys.*, 195:90–116, 2004.

[116] Michael Mascagni and A. Simonov Nikolai. Monte carlo methods for calculating some physical properties of large molecules. *SIAM. J. Sci. Comput*, 26(1):339–357, 2004.

[117] Ralf Massjung. An unfitted discontinuous galerkin method applied to elliptic interface problems. *SIAM Journal on Numerical Analysis*, 50(6):3134–3162, 2012.

[118] Jens Markus Melenk. *On generalized finite element methods*. PhD thesis, University of Maryland, 1997.

[119] Andrea Moiola and Euan A. Spence. Acoustic transmission problems: Wavenumber-explicit bounds and resonance-free regions. *Mathematical Models and Methods in Applied Sciences*, 02 2017. doi: 10.1142/S0218202519500106.

[120] Kihyo Moon. *Immersed Discontinuous Galerkin Methods for Acoustic Wave Propagation in Inhomogeneous Media*. PhD thesis, Virginia Tech, 2016.

[121] Benoît Perthame. *Parabolic Equations in Biology*, pages 1–21. Springer International Publishing, Cham, 2015. ISBN 978-3-319-19500-1. doi: 10.1007/978-3-319-19500-1_1. URL https://doi.org/10.1007/978-3-319-19500-1_1.

[122] I. Perugia. A note on the discontinuous Galerkin approximation of the helmholtz equation. *Lecture Notes, ETH Zürich*, 2006.

[123] P.Monk and G.R. Richter. A discontinuous galerkin method for linear symmetric hyperbolic systems in inhoumogenous media. *J. Sci. comput.*, 22(1):443–477, 2005.

[124] Sankara K. Rao. *Introduction to partial differential equations, Third Edition*. Prentice-Hall of India Pvt.Ltd, 2011.

[125] Hans-Georg Raumer. *Shape Optimization for Interface Problems Using Unfitted Finite Elements*. PhD thesis, University of Göttingen, 2018.

[126] Xiaofeng Ren and Jucheng Wei. On a two-dimensional elliptic problem with large exponent in nonlinearity. *Trans. Amer. Math. Soc.*, 343(2):749–763, 2000.

[127] Béatrice Rivière. *Discontinuous Galerkin methods for solving elliptic and parabolic equations*, volume 35 of *Frontiers in Applied Mathematics*. Society for Industrial and Applied Mathematics (SIAM), Philadelphia, PA, 2008. ISBN 978-0-898716-56-6. doi: 10.1137/1.9780898717440. URL http://dx.doi.org/10.1137/1.9780898717440. Theory and implementation.

[128] Mohamed Ben Romdhane. *Higher-degree immersed finite elements for second-order elliptic interface problems*. PhD thesis, Virginia Polytechnic Institute and State University, 2011.

[129] V.S. Ryaben'kii, V.I. Turchaninov, and Ye.Yu. Epshteyn. Algorithm composition scheme for problems in composite domains based on the difference potential method. *Comput. Math. Math. Phys.*, 46(10):1768–1784, 2006.

[130] Fadil Santosa. A level-set approach for inverse problems involving obstacles. *ESAIM: Control, Optimisation and Calculus of Variations*, 1:17–33, 1996.

[131] A.H. Schatz. An observation concerning ritz-galerkin methods with indefinite bilinear forms. *Math. Comp.*, 28:959–962, 1974.

[132] J.F. Semblat and J.J.Brioist. Efficiency of higher order finite elements for the analysis of seismic wave propagation. *Journal of Sound and Vibration*, 231(2):460–467, 2000.

[133] Martin Siebenborn. A shape optimization algorithm for interface identification allowing topological changes. *J. Optim Theory Appl*, 177:306–328, 2018.

[134] F.O. Speck. Sommerfeld diffraction problems with first and second kind boundary conditions. *SIAM J. Math. Anal.*, 20(2):396–407, 1989.

[135] Luke James Swift. *Geometrically unfitted finite element methods for the Helmholtz equation*. PhD thesis, University of London, 2018.

[136] S.Yu, Y.C.Zhou, and G.W.Wei. A shape optimization algorithm for interface identification allowing topological changes. *J. Comput. Phys.*, 224(2):729–756, 2007.

[137] Tayfun E. Tezduyar. Finite element methods for flow problems with moving boundaries and interfaces. *Archives of Computational Methods in Engineering*, 8(2):83–130, 2001.

[138] Karl Larsson Tobia Jonsson, Mats G.Larson. Cut finite element methods for elliptic problems on multipatch parametric surfaces. *Comput. Methos Appl. Mech. Engrg.*, 324:366–394, 2017. ISSN 1705-5105.

[139] Kun Wang and Yaushu Wong. Pollution-free finite difference schemes for non-homogeneous helmholtz equation. *Int. J. Numer. Anal. Model.*, 11(4):787–815, 2014.

[140] E. Bruce Watson and Ethan F. Baxter. Diffusion in solid-earth systems. *Earth Planet Sci. Lett.*, 253:307–327, 2007.

[141] George Wypych. *Handbook of Plasticizer, 3rd Edition*. ChemTec Publishing, 2017.

[142] Jinchao Xu. Estimate of the convergence rate of the finite element solutions to elliptic equation of second order with discontinuous coefficients. *Natural Science Journal of Xiangtan University*, 1:1–5, 1982.

[143] Qing Yang. Numerical analysis of partially penalized immersed finite element methods for hyperbolic interface problems. *Numer. Math. Theor. Meth. Appl.*, 11:272–298, 2018.

[144] Qing Yang and Xu Zhang. Discontinuous Galerkin immersed finite element methods for parabolic interface problems. *J. Comput. Appl. Math*, 299:127–139, 2016.

[145] Xingzhou Yang. *Immersed interface method for elasticity problems with interfaces*. PhD thesis, North Carolina State University, 2004.

[146] Z.Belhachmi and H.Meftahi. Shape sensitivity analysis for an interface problem via minimax differentiability. *Applied Mathematics and Computation*, 219:6828–6842, 2013.

[147] Chaoming Zhang. *Immersed Interface Methods for Hyperbolic Systems of Partial Diferential Equations with Discontinuous Coefficients*. PhD thesis, University of Washington, 1996.

[148] Chaoming Zhang and Randall J. LeVeque. The immersed interface method for acoustic wave equations with discontinuous coefficients. *Wave Motion*, 25(4):237–263, 1997.

[149] Jianfeng Zhang. Wave propagation across fluid–solid interfaces: a grid method approach. *Geophys. J. Int.*, 159:240–252, 2004.

[150] Sidong M. Zhang and Zhilin Li. An augmented IIM for helmholtz/poisson equations on irregular domains in complex space. *Int. J. Numer. Anal. Mod.*, 13(1):166–178, 2016.

[151] Xu Zhang. *Nonconforming Immersed Finite Element Methods for Interface Problems*. PhD thesis, Virginia Polytechnic Institute and State University, 2013. URL http://gateway.proquest.com/openurl?url_ver=Z39.88-2004&rft_val_fmt=info:ofi/fmt:kev:mtx:dissertation&res_dat=xri:pqm&rft_dat=xri:pqdiss:3585879.

[152] Xu Zhang. *Nonconforming Immersed Finite Element Methods for Interface Problems*. PhD thesis, Virginia Polytechnic Institute and State University, 2013.

[153] Y. C. Zhou and G. W. Wei. On the fictitious-domain and interpolation formulations of the matched interface and boundary (MIB) method. *J. Comput. Phys.*, 219(1): 228–246, 2006. ISSN 0021-9991. doi: 10.1016/j.jcp.2006.03.027. URL http://dx.doi.org/10.1016/j.jcp.2006.03.027.

[154] Qiao Zhuang and Ruchi Guo. High degree discontinuous petrov-Galerkin immersed finite element methods using fictitious elements for elliptic interface problems. *J. Comput. Appl. Math.*, 362:560–573, 2019.

[155] Zilong Zou, Wilkins Aquino, and Isaac Harari. Nitsche's method for Helmholtz problems with embedded interfaces. *Int. J. Numer. Meth. Engng*, 110:618–636, 2017.